

Riku Hyytiäinen

# Evaluating Trajectories of Air-to-Ground Weapons using a Probability Map for Surface-to-Air Threats

**Aalto University**  
**School of Science**

Master's Thesis  
Espoo, January 20, 2017

**Thesis supervisor:** Prof. Kai Virtanen

**Thesis advisor:** M.Sc. (Tech.) Heikki Puustinen



The document can be stored and made available to the public on the open internet pages of Aalto University.  
All other rights are reserved.

Author: Riku Hyytiäinen

Title: Evaluating Trajectories of Air-to-Ground Weapons using a Probability Map for  
Surface-to-Air Threats

Date: January 20, 2017

Language: English

Number of pages: 6+94

Degree programme: Master's Programme in Mathematics and Operations Research

Major: Systems and Operations Research

Code: SCI3055

Supervisor: Prof. Kai Virtanen

Advisor: M.Sc. (Tech.) Heikki Puustinen

As a part of planning an air mission, the trajectory of an air-to-ground (A/G) weapon must be determined. In this thesis, the novel trajectory evaluation framework with which the best trajectory can be identified from a set of possible trajectories under uncertainty regarding the locations of surface-to-air (S/A) threats is presented. The best trajectory is the trajectory which has the highest survivability, i.e., the probability for the A/G weapon to traverse the trajectory without being intercepted.

The trajectory evaluation framework relies on two new models introduced in this thesis which together provide the survivability of a given trajectory. The spatial prediction model is used to build a probability map for the location of an S/A threat based on Bayesian reasoning with geographical data and knowledge about common tactical principles utilised in forming an air defence. The Markov survivability model describes the process of intercepting an A/G weapon with the air defence consisting of radar sensors and S/A weapons with an inhomogeneous continuous-time Markov chain. Using the probability maps produced by the spatial prediction model, the Markov survivability model produces the survivability of the trajectory, such that uncertainties regarding the locations of the S/A threats are taken into account.

The Markov survivability model presented in this thesis is compared with existing reference survivability models through numerical experiments by replacing it in the framework with each of the reference models. In the experiments, the survivabilities of different trajectories obtained with each model are evaluated and compared. The sensitivity of the models to uncertainty regarding the locations of S/A threats is studied by varying sizes of areas in which it is believed that the threats are located. The experiments imply that the novel framework gives intuitive results. In addition, the Markov survivability model is less affected by imprecise information regarding the locations of the S/A threats than the reference models.

Keywords: Air mission planning, inhomogeneous continuous-time Markov-chains,  
geographic information science, probability map, radar

Tekijä: Riku Hyytiäinen

Työn nimi: Ilmatorjunnan ilmasta-maahan -aseeseen aiheuttaman uhkan arviointi perustuen  
ilmatorjunnan ryhmitymisen todennäköisyysmalliin

Päivämäärä: 20. tammikuuta, 2017

Kieli: Englanti

Sivumäärä: 6+94

Koulutusohjelma: Matematiikan ja operaatiotutkimuksen maisteriohjelma

Pääaine: Systemi- ja operaatiotutkimus

Koodi: SCI3055

Valvoja: Prof. Kai Virtanen

Ohjaaja: DI Heikki Puustinen

Ilmaoperaation suunnitteluun sisältyy operaatiossa käytettävien ilmasta-maahan -aseiden reitien valinta siten, että aseisiin kohdistuu ilmatorjunnasta mahdollisimman vähän uhkaa. Tässä työssä esitellään uusi menetelmä, jolla arvioidaan ilmatorjunnan aiheuttamaa uhkaa annetulla lentoradalla lentävään ilmasta-maahan -aseeseen, kun ilmatorjunnan tarkkaa ryhmitystä ei tiedetä. Menetelmässä käytetään kahta tässä työssä kehitettyä mallia: ryhmitymisen sijaintijakauman tuottavaa mallia ja ilmasta-maahan -aseeseen annetulla lentoradalla kohdistuvan uhkan kertymistä kuvaavaa mallia.

Ilmatorjunnan ryhmitymisen sijaintijakauma määritetään Bayesiläisen päättelyn avulla käyttämällä maantieteellisiä tietolähteitä ja tiedustelutietoa todennäköisistä ryhmitysalueista. Ilmasta-maahan -aseeseen annetulla lentoradalla kohdistuva uhka arvioidaan jatkuva-aikaiseen Markov-ketjuun perustuvalla mallilla, joka kuvaa ilmatorjuntayksikön kykyä havaita ase, seurata asetta ja vaikuttaa aseeseen. Sijaintijakaumaa hyödyntämällä Markov-malli tuottaa todennäköisyyden sille, että yksi tai useampi ilmatorjunta-ase onnistuneesti torjuu ilmasta-maahan -aseen. Markov-mallin ja samalla koko menetelmän tuottama lopputulos huomioi ilmatorjunnan ryhmitykseen liittyvän epävarmuuden.

Tässä työssä esiteltyä Markov-mallia verrataan numeerisin kokein kahteen ilmatorjuntaa kuvaavaan referenssimalliin. Kokeissa verrataan kunkin mallin tuottamia ilmasta-maahan -aseeseen kohdistuvia uhkia eri lentoradoilla kahdessa skenaariossa. Mallien alttiutta epätarkkuuksille sijaintitiedossa tutkitaan varioimalla ilmatorjunnan ryhmitysalueen suuruutta ja tarkastelemalla, kuinka hyvin mallit säilyttävät lentoratojen keskinäisen uhkajärjestyksen. Kokeiden tuloksena voidaan todeta, että uuden menetelmän hyödyntämä Markov-malli yhtäältä tuottaa realistisia uhka-arvioita ja toisaalta se on vähemmän altis epätarkkuuksille ilmatorjunnan ryhmitymisen sijaintitiedossa verrattuna referenssimalleihin.

Avainsanat: Ilmaoperaation suunnittelu, jatkuva-aikaiset Markov-ketjut, geoinformatiikka, sijaintijakauma, tutka

## Acknowledgements

First and foremost I would like to thank my supervisor Professor Kai Virtanen, my advisor Heikki Puustinen and the Systems Analysis Laboratory at Aalto University for giving me the opportunity to work on this project, for guiding me through the whole process and for continuous support throughout this experience. A significant contribution to the completion of this thesis must also be attributed to my family, Ilkka, Raija, Sini and of course Anastasia. I am sure this thesis would not have been completed in such a timely manner, had not been for all of you. Last but not least, I must thank Retuperän WBK and Leevi Letkutsalo for ensuring Otaniemi is a fire hazard free campus and thus a suitable environment for working on this thesis, and for making my time in Otaniemi most pleasurable.

Otaniemi, January 20, 2017

Riku Hyytiäinen

# Contents

Abstract . . . . .	ii
Abstract (in Finnish) . . . . .	iii
Acknowledgements . . . . .	iv
Contents . . . . .	iv
<b>1 Introduction</b>	<b>1</b>
<b>2 Related research</b>	<b>7</b>
<b>3 Trajectory planning problem</b>	<b>11</b>
3.1 Real world problem setting . . . . .	11
3.2 Modelling assumptions and simplifications . . . . .	13
<b>4 Trajectory evaluation framework</b>	<b>17</b>
4.1 Spatial prediction model . . . . .	18
4.1.1 Indices . . . . .	19
4.1.2 Probability map reduction . . . . .	27
4.2 Markov survivability model . . . . .	30
<b>5 Reference survivability models</b>	<b>35</b>
5.1 Erlandsson model . . . . .	35
5.2 Technical model . . . . .	42
<b>6 Numerical experiments</b>	<b>48</b>
6.1 Illustration of spatial prediction model . . . . .	49
6.2 Verification of probability map reduction . . . . .	55
6.3 Comparison of survivability models . . . . .	58
6.3.1 Otaniemi scenario . . . . .	60
6.3.2 Hyvinkää scenario . . . . .	67
<b>7 Summary and discussion</b>	<b>72</b>

<b>References</b>	<b>76</b>
<b>A Probability of detection (<math>P_D</math>)</b>	<b>80</b>
<b>B Continuous-time Markov chains</b>	<b>89</b>
<b>C Slope coefficient (<math>C_{\text{slope}}</math>)</b>	<b>92</b>
<b>D Terrain coefficient (<math>C_{\text{terrain}}</math>)</b>	<b>94</b>

# Chapter 1

## Introduction

The identification of the best possible trajectory for an air-to-ground (A/G) weapon is an integral part of air mission planning (see, e.g., [6, 17]). The best trajectory is such that the probability for the A/G weapon to traverse the entire length of the trajectory without being intercepted by any surface-to-air (S/A) threats is greater than with any other plausible trajectories. The locations of the S/A threats play a central role in their capabilities to intercept the A/G weapon. Thus, knowledge regarding the locations of the possible S/A threats is of utmost importance when determining the best trajectory for the A/G weapon [6]. However, precise information regarding these locations is seldom available. Therefore, such location uncertainty should be treated when evaluating the alternative trajectories of the A/G weapon.

In this thesis, the novel trajectory evaluation framework for evaluating the trajectories of A/G weapons under uncertainty regarding the locations of the S/A threats is presented. The framework illustrated in Figure 1.1 consists of the spatial prediction model and the Markov survivability model which are developed in this thesis and used to produce a survivability measure for a given trajectory. The survivability measure is the probability for the A/G weapon to traverse the trajectory without being intercepted by S/A threats. Within the trajectory evaluation framework, the spatial prediction model produces a probability map for each S/A threat. These probability maps are then used by the Markov survivability model to provide the survivabilities of feasible trajectories. Thus, using the framework, the best trajectory is determined from the given set of the trajectories. The framework is used in the planning of air missions when a choice between the multiple A/G weapon trajectories is made to ensure the successful outcome of the air mission.

Threat inducing systems which are of interest when evaluating trajectories of A/G weapons include S/A missiles and anti-aircraft cannons as well as aircraft

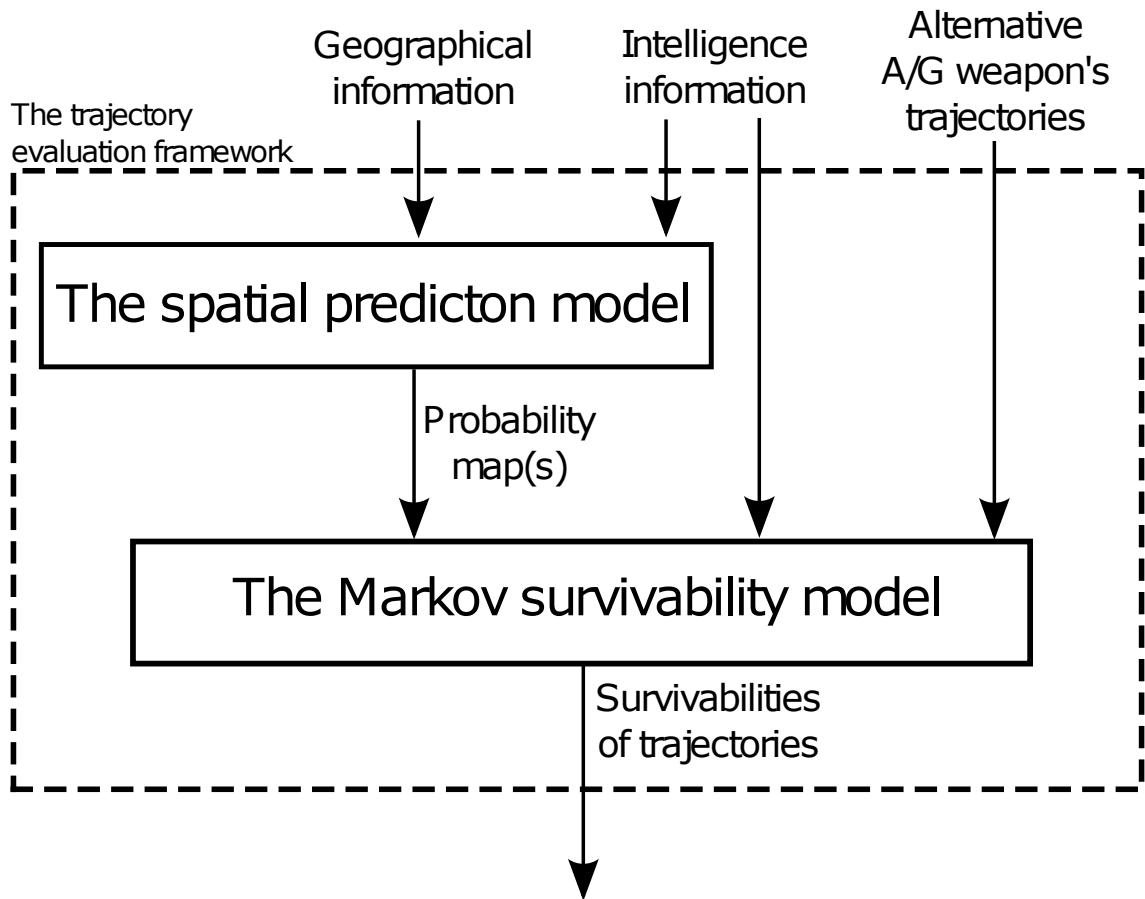


Figure 1.1: The trajectory evaluation framework presented in this thesis.

tracking radars which are used in accordance with guided S/A missiles. With a slight abuse of terminology, the term “S/A threat system” or simply “S/A threat” is used throughout this thesis to refer to all of these different types of threat causing systems. These S/A threats are assumed to consist of a radar sensor which is used as a part of the air defence and can be accompanied with an S/A weapon which is used together with the radar sensor to intercept the A/G weapon. That is, an aircraft tracking radar can exist by itself but an S/A weapon is always accompanied by the radar sensor.

In this thesis, the S/A defence is assumed to consist of independent S/A threat groups. An S/A threat group in turn comprises target acquisition radars, fire control radars, and S/A weapons. For the S/A threat group to successfully intercept an A/G weapon, the A/G weapon must first be detected and tracked by the S/A threat group’s target acquisition radars. These send their detection information to a joint radar tracker which attempts to form a track of the A/G weapon based on all of the detections achieved by the target acquisition radars. Once the tracker has

formed the track of the A/G weapon, it is passed over to the fire control radars. Each fire control radar is linked to a single S/A weapon. In order to use the S/A weapon to intercept the A/G weapon, the associated fire control radar must have acquired the track of the A/G weapon. It is assumed that the fire control radar and the S/A weapon are always co-located, and they are jointly referred to as an S/A threat unit. Each fire control radar independently attempts to form the track of the A/G weapon. These radars do not share detection information with each other. Thus, each fire control radar must be able to detect and track the A/G weapon independently in order for the associated S/A weapon to be used. When the fire control radar successfully forms the track, the associated S/A weapon thereafter attempts to intercept the A/G weapon, if the A/G weapon is in the range of the S/A weapon.

The spatial prediction model developed in this thesis combines geographical and intelligence information, and through Bayesian reasoning [32] it produces a probability map for an S/A threat, i.e., the probability for the S/A threat to be situated at any given location. The probability map gives a distinct probability for the event that the S/A threat system is located at any given location. In order to estimate the locations of the S/A threat systems, methods for analysing the passability of the terrain and the quality of alternative locations for S/A defence in terms of visibility are developed. Intelligence information and knowledge about strategic principles commonly used in planning air defence with different types of S/A threat systems are also taken into account. The intelligence information used by the spatial prediction model concerns the capabilities of the S/A threats and areas in which the S/A threats are believed to be located. Additionally, a novel method for reducing the probability map to a discrete number of possible locations is presented. The probability map reduction method is applied to reduce the computational requirements of the trajectory evaluation framework.

The Markov survivability model presented in this thesis is used to provide the probability that an A/G weapon is tracked and intercepted. The A/G weapon is being tracked if the air defence has sufficient information regarding the A/G weapon's movements for the use of the S/A weapons. The A/G weapon is intercepted if the S/A weapon has been successfully utilised and the A/G weapon has been destroyed. The Markov survivability model is based on a four state inhomogeneous continuous-time Markov chain [9] (see also Appendix B). Each Markov chain which is used while evaluating the survivability of a given trajectory describes a single S/A threat unit's capability to intercept the A/G weapon. The first state of the Markov chain

is means the target acquisition radars of the S/A threat unit's threat group have not yet been able to form the track of the A/G weapon. The target acquisition radars might have detected the A/G weapon but not with sufficient regularity to form the track. Once the S/A threat group's target acquisition radars successfully form the track of the A/G weapon, the Markov chain advances to the second state and the fire control radars commence trying to acquire a track. The third state of the Markov chain is reached when the fire control radar associated with the S/A threat unit which the Markov chain is describing successfully forms the track of the A/G weapon. Finally, the fourth state is reached when the threat unit's weapon intercepts the A/G weapon.

When evaluating a trajectory, all of the Markov chains of which each describes a single S/A threat's capabilities to intercept the A/G weapon are solved as described in Appendix B. The survivability of the trajectory is obtained by calculating the probability that none of the Markov chains corresponding with the S/A threat units are in the fourth state at the end of the trajectory. The transition rates between the states of the Markov chain depend on parameters which are determined through the expected time needed for a transition under optimal conditions. The optimal conditions are the best possible detection capability for transitions corresponding to the forming of a track and interception of the A/G weapon, and zero detection capability for transitions corresponding to the loss of the track. The transition rates also depend on the probability of detection by radar sensors.

If exact locations of S/A threats are known, the Markov survivability model provides the survivabilities of alternative trajectories traversed by the A/G weapon. Since the exact locations of the S/A threats are rarely known, the spatial prediction model is used to estimate probability maps for the S/A threats. By using these probability maps, the Markov survivability model generates the survivabilities of the trajectories by taking into account uncertainties regarding the locations of the S/A threats. These survivabilities are used to rank the trajectories into a priority order and identify the best trajectory.

The Markov survivability model is compared with two reference survivability models – the Erlandsson model [11] and the technical survivability model [34] – through numerical experiments conducted in this thesis. The comparison is carried out by evaluating trajectories with the trajectory evaluation framework and by replacing the Markov survivability model in the framework in turn with each of the reference models. Similar to the Markov survivability model, the Erlandsson model also relies on continuous-time Markov chains to estimate the survivability of an

A/G weapon traversing its trajectory. In the Erlandsson model, each Markov chain portrays a single S/A threat group's capability to intercept the A/G weapon. The Erlandsson model was originally developed to calculate the survivability of trajectories for aircraft and not A/G weapons as is the case with the Markov survivability model. The Erlandsson model differs from the Markov survivability model also in the manner in which state transition rates are defined. While the state transition rates in the Markov survivability model are directly affected by the probability of detection by radar sensors, the transition rates in the Erlandsson model are explicitly dependent on the location of the A/G weapon. The area around S/A threats is classified into sensor and weapon areas. Each target acquisition radar is assigned a sensor area in which the radar is able to detect and track the A/G weapon. Each S/A threat unit is associated with a weapon area in which the threat unit's fire control radar is able to detect and track the A/G weapon and the S/A threat unit's weapon is capable of intercepting the A/G weapon. The state transition rates are varied depending on the areas in which the A/G weapon is located at a given time. The survivability of a given trajectory is obtained by calculating the probability that none of the Markov chains corresponding with the S/A threat groups are in the final state representing the event that the A/G has been intercepted by the S/A threat units at the end of the trajectory. Similar to the Markov survivability model, the Erlandsson survivability model also uses the probability maps produced with the spatial prediction model to take into account uncertainty regarding the locations of the S/A threats.

The technical survivability model recognises that target acquisition radars operate in search mode and thus scan the surrounding airspace in an organised manner. It follows that a target acquisition radar is directed in a given direction only at given intervals. On the other hand, it is assumed that in order for a track to be formed, the target acquisition radar must achieve a given number of successful detections of an A/G weapon on consequent scans. Taking these two notions into account, the technical survivability model provides the probability of successfully forming the track of the A/G weapon by the target acquisition radar. After this, the model calculates the probability whereby the fire control radar is able to obtain the track of the A/G weapon and maintain this track for the duration required to aim, launch, and guide the S/A weapon in order to intercept the A/G weapon. Combining these probabilities, the technical survivability model gives the probability whereby an S/A threat unit is capable of intercepting the A/G weapon at a given time. The survivability of a given trajectory is determined by calculating the probability that none of

the S/A threat units are able to destroy the A/G weapon along the trajectory. The probability maps produced by the spatial prediction model are used by the technical survivability model to take into account uncertainty regarding the locations of the S/A threats.

The novel trajectory evaluation framework presented in this thesis takes into account geographical data and uncertainties regarding the locations of S/A threats in more depth than any previously constructed models. The developed spatial prediction model produces a probability map for the location of an S/A threat system and takes into consideration requirements for its surrounding terrain set by characteristics and principles governing the use of the S/A threat system. Existing spatial models [17] describing possible locations of S/A threat systems have not taken into account similar aspects and have been based on measurements from radar sensing sensors on board an aircraft. With the probability map reduction method introduced in this thesis, the processing of probability maps is performed significantly more efficiently than would otherwise be possible.

Unlike previous introduced survivability models based on Markov chains [11, 12], the Markov survivability model also takes into account the need to track an A/G weapon with radar sensors before it can be intercepted and the theoretical capabilities of the radars to detect the A/G weapon. These capabilities include the directionality of the radar cross section of the A/G weapon which describes the characteristics of the weapon in regard to the radar sensor's capability to detect it. The trajectory evaluation framework also treats the uncertainty of S/A threat systems' locations which is described by probability maps constructed with the spatial prediction model.

The rest of this thesis is structured as follows. Previous research related to spatial analysis and S/A survivability modelling is discussed in Chapter 2. The description of the problem of determining the best trajectory for an A/G weapon which is solved by the framework presented in this thesis is given in Chapter 3. The spatial prediction model and the Markov survivability model are introduced in Chapter 4 and are followed by the presentation of reference survivability models in Chapter 5. Chapter 6 provides the results of numerical experiments as well as the comparison of the Markov survivability and the reference models. Finally, the thesis is summarised and future research is discussed in Chapter 7.

# Chapter 2

## Related research

Research into the evaluation of trajectories traversed by aerial devices has yielded numerous different approaches to the modelling of the survivability of a trajectory for an aerial device and to the optimisation of the trajectory of the device to maximise its survivability. The survivability of the trajectory for the aerial device is represented with the probability that the device is able to traverse the trajectory unharmed. A proposed straightforward approach is to define high risk areas into which the device must not navigate [31]. These no-fly zones represent areas in which it is likely for the aerial device to be harmed, and it is assumed that outside these areas the device can navigate with relatively high survivability. Another approach to evaluate the threat caused to aerial devices is to define a cost function for the route of the device that is inversely proportional to the fourth power of the distance between the aerial device and the S/A threat system [2, 27]. The relation of the cost function to the fourth power of the distance is motivated by the relationship between the signal-to-noise ratio achieved by radar sensors and the range of the target which the radar is attempting to detect. A similar cost function has been proposed by Pachter and Hebert [26]. They optimise routes for the aerial device with respect to the integral of the cost function over the course of the trajectory and give an analytic solution through the calculus of variations [22].

Radar detection is a stochastic process [25] and thus it is natural to address radar tracking and ultimately the possible interception of the aerial device as stochastic processes. A possible approach to modelling the stochasticity of radar detection and aerial device survivability is to use Markov chains as the basis for the models [10]. Erlandsson [11] proposed a Markov chain model where the transition rates depend on whether the aerial device is within a threshold distance from the S/A threat system and takes into account the need for the threat system to detect and track the aerial

device before it can be engaged. Another approach proposed by Erlandsson [12] is the use of a simplified two-state Markov chain where the rates of transition decrease either linearly or quadratically with the distance from the S/A threat system. The new Markov survivability model used in the trajectory evaluation framework introduced in this thesis builds on the models described here. However, in addition to recognising the distinct stages of radar detection, the Markov survivability model also strives to take into account the technical capabilities of the S/A threats.

A radar sensor’s capability to detect and track an aerial device depends also on the terrain and the orientation of the aerial device. The topography plays a role since if the aerial device is shadowed by the terrain, the S/A threat system cannot detect or track the device. For example, Zheng et al. [35] have shown how an evolutionary algorithm can be used to plan a route that maximises the use of terrain masking while simultaneously minimising the length of the route and maximising the distance from known S/A threat system sites. The directionality of the radar’s capability to detect and track an aerial device, i.e., the radar cross section of the device plays a key role and has been taken into account for example by Kabamba et al. [21]. They recognised that the radar cross section of an aerial device is often irregular, but for modelling purposes they used an ellipsoidal model for the radar cross section. The radar cross sections used in the trajectory evaluation framework are the actual measured radar cross sections of the A/G weapons being considered. Thus, the route evaluations given by the framework are more accurate than those calculated using ellipsoidal radar cross sections.

Models studying the threat inflicted on aerial devices traversing trajectories in the vicinity of S/A threat systems often assume that the locations of the threat systems are known. However, this is usually not the case and there is almost always at least some uncertainty in the location of the S/A threat systems. Jun and D’Andrea [20] discuss how the path of an unmanned aerial vehicle can be optimised based on a probability map generated from radar sensing sensor readings and a Bayesian survivability model. The uncertainty involving the locations of the S/A threat systems has also been studied by Erlandsson [11] by assuming a two dimensional Gaussian probability density function for the threat systems’ locations and by utilising Monte Carlo simulation methods [23]. A different perspective to the modelling of uncertainty regarding the positions of S/A threat systems is to categorise each location in the area into a discrete number of classes, each representing a different degree of threat [4]. The probability of being intercepted in any given location depends on the degree of threat assigned to the location in question.

Hespanha et. al [17] demonstrate how a probability map of S/A threat systems' locations can be built with noisy radar sensing sensors. They use Bayesian reasoning to build the probability map for the radars. The spatial prediction model developed in this thesis is similar to Hespanha et. al's model in many ways. Both models strive to estimate the locations of S/A threat systems and both models apply Bayesian reasoning. However, the data utilised is different. Hespanha et. al use noisy data from radar sensing sensors while the spatial prediction model uses geographical and intelligence information to form the probability map. The probability map generated with the spatial prediction model could be used as the *a priori* probability distribution in methods such as Hespanha et. al's.

The spatial prediction model presented in this thesis can be described as spatial analysis. Spatial analysis, see e.g., [24], is the analysis and extraction of knowledge from spatial data. Spatial data is information where geographic location and time play a vital role. Spatial data links descriptive properties, attributes, or events to a geographical location or point in time [14]. In the spatial prediction model presented in this thesis, spatial data such as elevation, tree height and land cover data is used to calculate a probability map for the location of S/A threat systems.

Similar spatial analysis has been applied in many different fields of research, e.g., to predict the locations of future events or estimate characteristics of certain geographical areas by using geographical data. For instance, landslide hazard prediction by geographic analysis methods has been studied [7]. Spatial analysis has also been applied to predict the locations of archeological sites [13] and species distribution [1]. However, in all of these applications there is prior data available and as such they all apply inductive reasoning such as regression analysis to obtain results.

Turning to the analysis of S/A threat systems siting, studies concerning how one should place air defence missile batteries exist [3, 16]. The problem of finding the best possible location for an air defence missile battery, taking into account the terrain, visibility, and other tactical properties that affect the efficiency of the defence battery, is referred to as the *missile siting problem*. Even though the perspective into the problem is opposite between the missile siting problem and the task of estimating the locations of enemy S/A threat systems, these two problems are essentially quite similar. In both problems, it is necessary to obtain knowledge about whether it is possible for an S/A threat system to operate at a location and whether there is sufficient visibility from the location in question.

In addition to addressing the missile siting problem, Franklin et al. [16] take an extensive look at line of sight algorithms and their performance. In particular,

Franklin et al. study viewshed and visibility index algorithms. Viewshed is the surface area, which is visible from any certain vantage point and the visibility index is a value that can be calculated for any point on a surface, and tells how good the visibility is from that location [16]. In addition to exact algorithms, Franklin et al. also present many interesting approximative algorithms that can be used to speed up calculations. Methods inspired by the work of Franklin et. al. are used in the spatial prediction model to determine the visibility from a given location.

To summarise, the trajectory evaluation framework presented in this thesis builds on previous Markov chain models and takes into account the technical capabilities of S/A threats with more precision than earlier models. Unlike previous survivability models based on Markov chains, the new Markov survivability model presented in this thesis takes into account the directional radar cross-section and topological restrictions in the operation of S/A threats. Furthermore, the trajectory evaluation framework utilises methods from the realm of spatial analysis to estimate the unknown locations of the S/A threats. Earlier published models which strive to build a probability map for the S/A threats utilise data from radar detector sensors, while the new spatial prediction model introduced in this thesis uses geographical data to enhance existing intelligence information regarding the locations of the S/A threats.

# Chapter 3

## Trajectory planning problem

The trajectory planning problem discussed in this thesis is the problem faced in A/G air mission planning, when one must decide on a single trajectory out of many possible alternatives, to be used by an A/G weapon during the mission. The outcome which the spatial prediction model and the Markov survivability model together attempt to achieve is the successful identification of the best possible trajectories of A/G weapons with respect to the risk of being intercepted by an S/A threat. The best trajectory is the trajectory with the highest survivability, i.e., the highest probability for the A/G weapon to successfully traverse the entire trajectory unharmed. The survivability of the trajectory is dependent on the whereabouts of S/A threat systems and on the S/A threat systems' technical capabilities to detect and intercept the A/G weapon. The real world problem setting including the aforementioned dependencies and associated uncertainties, as well as the principles utilised in the spatial prediction and Markov survivability models to take into account these uncertainties, are discussed in this chapter.

### 3.1 Real world problem setting

In the trajectory planning problem, the ultimate objective is to deliver an A/G weapon through enemy defences to a given target location. A variety of different trajectories are given as alternatives and the task is to choose the trajectory along which the A/G weapon has the highest probability of reaching the target unharmed. The target is protected by a defence which consists of threat systems. Sometimes the exact locations of threat systems are known, but in many cases this is not the case. In such instances, all available intelligence information regarding the threat systems and the terrain should be taken into account to estimate the threat systems'

locations. Threat systems can be characterised as sensors and weapons [28]. Slightly simplifying, the role of the sensors is to instruct and aim the weapon so that the weapon can successfully intercept the A/G weapon.

Sensors are used in different roles as either target acquisition sensors or fire control sensors [34]. In some instances, a single sensor can have several of the mentioned roles simultaneously. The target acquisition sensors are sensors that search the surrounding airspace for targets. Once a target acquisition has detected a possible target it attempts to form a track, i.e., gather information regarding the location, velocity, and heading of the target. The track formed by the target acquisition sensor is not accurate enough to be used directly with an S/A weapon to intercept the weapon and a fire control sensor is used to form a more accurate track. The fire control sensor is a sensor which is dedicated to forming an accurate track of the target, which can be used by the S/A weapon to intercept the target.

The process during which threat is induced onto the A/G weapon can be described with a chain of events that begins from the first detection of the A/G weapon by the early warning sensors and terminates once an S/A threat unit has successfully intercepted the A/G weapon. The chain of events can be portrayed with six discrete phases [34]. In the first phase, the early warning sensors detect the A/G weapon and alert the S/A defence to intercept it. In the second phase, the target acquisition sensors acquire a track for the A/G weapon. After this in the third phase, the target acquisition sensors pass the track of the A/G weapon over to the fire control sensor. The fourth phase consists of the fire control sensor acquiring a track of the A/G weapon, and in the fifth phase the actual S/A weapon is fired. Finally, in phase six, the A/G weapon is intercepted by the S/A weapon.

Sensors might be able to communicate detection information to one another, and thus a track can be formed based on detections made by several different sensors. With such a sensor network, a track can be formed even though no single sensor is constantly capable of detecting the target. Such sensor networks are often used in air surveillance systems [34].

Sensors can be characterised based on the technique used to detect targets into optical, infrared, and radar sensors [28]. Optical sensors use visible light to detect and locate targets. Optical sensors include electro-optical sensors which utilise the visible spectrum of electromagnetic radiation and the human eye. Optical sensors are intuitive in a sense that the capability to detect a target by such a sensor is similar to a person's capability of seeing the target. As such, optical sensors' shortcomings include deteriorating capabilities when faced with limited visibility which can be

due to smoke, fog, or clouds, and limited detection capability in the lack of light, e.g., during the night. Infrared sensors are electro-optic sensors which rely on the infrared spectrum of electromagnetic radiation. Infrared sensors share some of the shortcomings of optical sensors but since an infrared sensor detects heat from the source, the infrared sensor might be able to spot a target more easily and does not depend on lighting conditions. Radar sensors depend on electromagnetic radiation with longer wavelengths to detect targets. The capabilities of radar sensors to detect targets are not as much affected by visibility limitations as optical and infrared sensors. However, radar sensors must be accompanied with an artificial radiation source, i.e., a transmitter.

Sensors and weapons can either be stationary or set on a mobile platform [28]. Mobile platforms are either wheel-, track-, or foot-based. Depending on the propulsion system of a platform, i.e., wheels, tracks, or foot, the platform can have different passability in different terrains. A platform on wheels, for instance, can travel quickly on roads but poorly in forests, whereas tracked vehicles cannot travel as fast on roads but can travel in a wider range of terrain including forests.

When considering the problem of evaluating A/G trajectories in a real world setting, there are numerous uncertainties which are difficult, and in some cases impossible to eliminate. These include uncertainties regarding the positioning of the S/A threats, the technical capabilities of the S/A threats, and weather conditions which can affect the S/A threats' abilities to detect and intercept the A/G weapon. In addition to these uncertainties, there are human aspects which can have an effect on an S/A threat's capability to operate efficiently as many S/A threat systems rely on a human operator.

## 3.2 Modelling assumptions and simplifications

In this thesis, the task of evaluating trajectories of an A/G weapon when faced with uncertainties mentioned above is tackled by combining two separate models. The spatial prediction model addresses the uncertainties regarding the positioning of S/A threats by forming a probability map for the threats, and the Markov survivability model with the help of the probability map determines the probability for an A/G weapon to successfully traverse a trajectory without being harmed by any S/A threats. The survivability model strives to take into account the uncertainties concerning the technical capabilities of the S/A threats by treating track formation and interception as Poisson processes, see e.g., [32]. The intensity parameters of the

Poisson process depend on technical parameters of the S/A threat, characteristics of the A/G weapon and the geometry between the S/A threat and the A/G weapon. Only radar sensors are considered.

In the spatial prediction model, it is argued that the location of an S/A threat system can be estimated based on three distinct observations. The first observation is based on the fact that different types of threat systems are regularly operated and situated with different principles [3]. Some systems might be used for close range air defence, while others might be situated further away from the actual target which they are defending. This and all available intelligence information is taken into account in the grouping index (*GI*). The grouping index describes how well a certain location is situated regarding the target which the air defence is protecting. The assumed threat bearing and the common tactical principles for how the specific threat system is used are also taken into account. This grouping index is used as the *a priori* distribution for the location of an S/A threat system.

Second, it is unlikely for a threat system to be located in an area from which it is impossible for it to operate. For example, wetlands are areas in which it may be impossible for a threat system to operate. Such impossible areas may account for a great portion of the entire area under observation. Further, if it is assumed that the adversary has a finite amount of time to form their air defence, and thus it might be impossible for the threat systems to reach certain locations. These observations are described with the passability index (*PI*). The passability index is used as the likelihood that a threat system is capable of navigating to and operating from a given location.

The third observation regards the visibility from possible threat systems' locations. For an S/A threat system to operate properly, it must have sufficient visibility to detect and engage the target. The visibility from each location is described with the visibility index (*VI*). It is argued that it is more likely for an air defence system to be located at a location with good visibility than at a location with bad visibility. The visibility index is used as the likelihood that there is sufficient visibility from a given location for an S/A threat system to operate efficiently. Combining these observations the spatial prediction model gives a probability map for an S/A threat from which the probability whereby the S/A threat is located a given location is read.

The spatial prediction model uses geographical data from three different sources: a digital elevation model provided by the National Land Survey of Finland, the CORINE Land Cover 2006 material generated by the Finnish Environment Institute,

and a dataset consisting of the height of the forest cover. All of the data is in raster form. This means that the datasets have been discretised into pixels and each pixel is given a certain value. The pixel size for all of the datasets is 25 metres.

The CORINE Land Cover 2006 (CLC2006) is a dataset that consists of information concerning the nature and usage of land areas. In the CLC2006, each pixel is categorised into one of the 44 different land cover categories supported by the CLC2006. The digital elevation model and the forest cover height data sets are simply rasters that contain one integer for each pixel indicating the average height above sea level or forest cover height, depending on the data set in question.

In the Markov survivability model, the basic unit in an air defence system is an S/A threat group. The S/A threat group consists of one or more target acquisition radars and S/A threat units. The target acquisition radars and the S/A threat units can be situated at any distance from each other or at the same location on the same platform. The S/A threat unit consists of an S/A weapon itself and a fire control sensor. The target acquisition radars are capable of acquiring a track that can be passed on to the threat unit, but the S/A threat unit cannot intercept the A/G weapon solely based on the track formed by the target acquisition radar, and it must track the target with its own fire control radar as well. The target acquisition radars in the S/A threat group share information about detections with each other. Thus, the track which is passed on to the S/A threat units can be acquired through information gathered from all the target acquisition radars within the group. However, the fire control radars do not share detection information and each fire control radar must track the target independently for the associated S/A threat to be able to intercept the A/G weapon. In reality, an air defence system would also include one or more early warning sensors, which are the first to detect an incoming threat and alert the rest of the air defence system to act on the threat. In the Markov survivability model discussed in this thesis, it is assumed that the early warning sensors have already detected the A/G weapon and the S/A threat groups are aware of the incoming A/G weapon.

The Markov survivability model uses the probability of detection as a measure of S/A threats' capability to detect the A/G weapon. Due to interference by stochastic noise, radar detection is a stochastic process and the probability that an S/A threat is able to detect an A/G weapon in a given location and orientation is calculated as shown in Appendix A.

The Markov survivability model strives to determine the survivability of an A/G weapon flying a given trajectory in an area influenced by short- and medium-range

S/A threats. The survivability of the A/G weapon on the given trajectory is defined to be the probability whereby the weapon is able to traverse the trajectory and reach its target unharmed. The model determines the kill-probability whereby the A/G weapon will not be able to traverse the trajectory and reach its target unharmed, and the survivability of the weapon is then calculated as the complement of the kill-probability.

# Chapter 4

## Trajectory evaluation framework

The trajectory evaluation framework proposed in this thesis is used to solve the trajectory planning problem. The trajectory evaluation framework takes as inputs intelligence information regarding the threat systems in the area, information about the terrain, characteristics of the A/G weapon and a set of trajectories which are to be evaluated. The framework then determines the survivability of each trajectory. The survivabilities of the trajectories can then be used to determine the trajectory with which the A/G weapon would have the highest probability of reaching its target. The framework can be separated into two distinct phases, each of which are completed by separate models. First, a probability map of each S/A threat is formed with the spatial prediction model. These probability maps are then used by the Markov survivability model to determine the survivability of each trajectory. In this chapter, the details of both the spatial prediction model and the Markov survivability model are discussed.

In the forthcoming text, the separate threat groups are referred to with superscript  $k = 1 \dots N$ , where  $N$  is the total amount of threat groups. The individual target acquisition radars are referred to with subscript  $i = 1 \dots n_k$ , where  $n_k$  is the amount of target acquisition radars in threat group  $k$ . Similarly, the threat units in a threat group are referred to using subscript  $j = 1 \dots m_k$ , where  $m_k$  is the amount of threat units in threat group  $k$ . In Chapter 4.1, the spatial prediction model is discussed by only referring to S/A threat systems with subscripts  $i$ , i.e., target acquisition radars. Exactly the same logic applies to S/A threat units which would be referred to with subscripts  $j$ . The term S/A threat system is a generic term and it is used to refer to both target acquisition radars and S/A threat units.

## 4.1 Spatial prediction model

In order to form the probability map of an S/A threat system, the Bayes' rule is used:

$$P(A|B) = \frac{P(B|A)P(A)}{P(B)}, \quad (4.1)$$

where  $A$  and  $B$  are events,  $P(A)$  is the *a priori* probability,  $P(B|A)$  is the likelihood function and  $P(A|B)$  is the *a posteriori* probability.

In the spatial prediction model, the *a priori* distribution for the location of the S/A threat system  $i$  of threat group  $k$  is represented by the grouping index, i.e.,  $P(X_i^k = x, Y_i^k = y) = GI_i^k(x, y)$ . The grouping index gives the *a priori* probability that the threat system is situated at a location with coordinates  $(x, y)$ . Here  $X_i^k = x$  and  $Y_i^k = y$  depict the events that the longitude and latitude coordinates of the S/A threat system  $i$  of threat group  $k$  are  $x$  and  $y$ .

The S/A threat system is not situated at a location from which it does not have sufficient visibility to operate efficiently or a location to which it is impossible for it to navigate in a given time frame. The likelihood that a given location can be reached by the threat system in a given time is described with the passability index denoted by  $PI_i^k(x, y)$ . The likelihood that there is sufficient visibility for the threat system to operate at a given location is described with the visibility index denoted by  $VI_i^k(x, y)$ . This is written as

$$P(Pass_i^k | X_i^k = x, Y_i^k = y) = PI_i^k(x, y),$$

$$P(Visib_i^k | X_i^k = x, Y_i^k = y) = VI_i^k(x, y),$$

for the S/A threat system  $i$  of threat group  $k$ , where  $Pass$  represents the event that the threat system is situated at a location to which it is possible for the threat system to navigate in the given time frame. In turn,  $Visib$  depicts the event that the threat system is situated at a location from which there is sufficient visibility for the threat system to operate efficiently.

Based on Bayes' rule (4.1), the posterior distribution for the location of the S/A threat system  $i$  of threat group  $k$  is

$$P(X_i^k = x, Y_i^k = y | Pass_i^k, Visib_i^k) \propto P(Pass_i^k, Visib_i^k | X_i^k = x, Y_i^k = y) P(X_i^k = x, Y_i^k = y), \quad (4.2)$$

where  $P(X_i^k = x, Y_i^k = y)$  is the *a priori* probability map of the S/A threat, i.e.,

the grouping index  $GI_i^k(x, y)$ . Equation (4.2) gives the probability for the threat system  $i$  to be located at coordinates  $(x, y)$ , given that it is possible for the threat system to navigate to the location and there is sufficient visibility from the location for a threat system to operate efficiently.

By making the assumption that the events  $Pass_i^k$  and  $Visib_i^k$  are conditionally independent when conditioned with the location of the threat system, the expression for the posterior distribution is simplified. Since the two events are conditionally independent, their joint conditional probability is calculated as the product of the two individual conditional probabilities. By substituting the individual conditional probabilities with the respective indices, the posterior distribution (4.2) is

$$\begin{aligned} & P(X_i^k = x, Y_i^k = y | Pass_i^k, Visib_i^k) \\ & \propto P(Pass_i^k | X_i^k = x, Y_i^k = y) P(Visib_i^k | X_i^k = x, Y_i^k = y) P(X_i^k = x, Y_i^k = y) \\ & = PI_i^k(x, y) VI_i^k(x, y) GI_i^k(x, y). \end{aligned}$$

This posterior distribution is the probability map for a single threat system, which is produced by the spatial prediction model. In short, the probability map for threat system  $i$  of threat group  $k$  is denoted with

$$P_{L,i}^k(x, y) = PI_i^k(x, y) VI_i^k(x, y) GI_i^k(x, y). \quad (4.3)$$

The probability map  $P_{L,i}^k(x, y)$  gives the probability for the threat system  $i$  of threat group  $k$  to be located at any given location  $(x, y)$ .

### 4.1.1 Indices

#### Passability index ( $PI$ )

In the spatial prediction model, terrain passability plays an important role in estimating the location of a threat system. If it is not possible for the threat system to operate at a certain location or it is impossible for a threat system to navigate to a location, there is zero probability for the threat system to be there. Also, if it is impossible for a threat system to travel to a certain location within a given time frame, the threat system will have zero probability of being located at the given site. Thus, the passability index is set to be one if the time needed to travel to the site

is less than or equal to the time constraint and zero otherwise, i.e.,

$$PI_i^k(x, y) = \begin{cases} 1 & \text{if } t_{\min,i}^k(x, y) \leq t_{\max} \\ 0 & \text{otherwise} \end{cases}, \quad (4.4)$$

where  $t_{\max}$  is the time constraint set for forming the air defence and  $t_{\min,i}^k(x, y)$  is the traversal time to location  $(x, y)$  for threat system  $i$  of threat group  $k$ .

In order to calculate the time needed to navigate from a known depot, i.e., the starting place from which S/A threat systems move to their positions, to any given location, a grid graph  $G(V, E)$  that consists of vertices  $V$  and edges  $E$  is built. Vertices  $V$  correspond to each possible location  $(x, y)$  and edges  $E$  resemble a transition from a certain location to another adjacent location  $((x_1, y_1), (x_2, y_2))$ . Each vertex is connected to all of its eight neighbors with an edge. By default, the graph coincides with the rasterisation of the digital elevation model and CLC2006 dataset. It is assumed that each vertex is located at the center of each pixel. The cost of each edge corresponds to the time consumed in the transition. Thus, the cost  $c$  of traversing the edge between the two vertices is calculated as follows:

$$c = \frac{\delta/2}{v} + \frac{\delta/2}{v'} = \frac{\delta(v + v')}{2vv'}, \quad (4.5)$$

where  $\delta$  refers to distance between the two neighbouring vertices  $(x_1, y_1)$  and  $(x_2, y_2)$ . The variables  $v$  and  $v'$  are the velocities at which a threat system is capable of navigating at locations  $(x_1, y_1)$  and  $(x_2, y_2)$ .

It is assumed that the threat systems spread out from a given number  $n > 0$  of depots for which the locations are known. The minimal time  $t_{\min}(x, y)$  needed for the traversal from the depot(s) to each location in the area is calculated with Dijkstra's algorithm [8] using the grid graph  $G(V, E)$  where the edge costs are determined with Equation (4.5).

One way of estimating the velocities  $v$ , by which the different systems can navigate in different terrains, is based on the use of the coefficients of deceleration as proposed by Hofmann et al. [18]. The coefficients of deceleration used in the model are coefficients corresponding to the slope and the nature of the terrain. These are referred to as the slope and terrain coefficients.

The slope coefficient is calculated by using the digital elevation model and the terrain coefficients are determined by using the CLC2006 data. The velocity  $v(x, y)$  at which a threat system is able to navigate is calculated as the product of the

maximum velocity of an S/A threat system and the two deceleration coefficients,

$$v(x, y) = v_{max} \times C_{slope}(x, y) \times C_{terrain}(x, y), \quad (4.6)$$

where  $v_{max}$  is the maximum velocity at which a threat system can navigate in any terrain,  $C_{slope}$  is the slope coefficient, and  $C_{terrain}$  is the terrain coefficient. Both the slope coefficient and the terrain coefficient have values in the range  $C \in [0, 1]$ . Thus, the velocity  $v(x, y)$  calculated for a threat system at each location  $(x, y)$  ultimately evaluates to the range  $[0, v_{max}]$ . If either coefficient is valued at  $C = 0$ , it is impossible for a threat system to function or navigate at that location. Velocities determined with Equation (4.6) are substituted in Equation (4.5) to determine the edge costs when building the grid graph whereby the minimal traversal times are to be calculated.

The logical premises for the slope coefficient are quite obvious – if the terrain has a sufficiently large gradient, it is hard or impossible for any threat system to operate or navigate there. The greater the gradient, the smaller the slope coefficient becomes, symbolising the terrain becoming harder and harder to traverse. Details regarding the calculation of the slope coefficient are given in Appendix C.

The evaluation of the terrain coefficient is simply a question of determining a single coefficient of deceleration for each of the different land cover categories in the CLC2006 dataset. This should be done separately for each different threat system type.

### **Visibility index (VI)**

One of the main factors in the terrain that affects an S/A threat systems' operating capabilities at any location is the visibility. An S/A threat system requires good visibility to operate. In order to engage targets, a threat system must have a direct line of sight to them. In the calculation of the line of sight, the curvature of the Earth, as well as the terrain and the tree height are taken into account. It is also assumed that light travels in a straight line.

In the spatial prediction model, it is assumed that S/A threat systems have a higher probability of being situated at locations from which they have good visibility than in locations with poor visibility. As a measure of visibility, the model uses the mean maximum distance from which an object moving at a given altitude can be sighted. The model is given the principal threat bearing and the width of the observation sector. This sector is then divided into a given amount of sub-sectors,

and the maximum distance to which there is visibility at a given height is calculated in each sub-sector. Finally, when this maximum distance has been calculated for each sub-sector, the arithmetic mean is calculated over all of these. This mean is finally used as the measure of visibility.

The mean of the maximum distances  $\mu_{\max}(x, y)$  to which there is visibility for a given altitude  $h_{\text{trgt}}$  in the  $S$  subsectors is computed as

$$\mu_{\max}(x, y) = \frac{\sum_{\theta \in \Theta} (\max_{l \in \{\mathbb{R} | h_{\min}((x, y), \theta, l) \leq h_{\text{trgt}}\}} l)}{S}, \quad (4.7)$$

where  $\Theta$  is the set of directions corresponding to all  $S$  subsectors for which the maximum distance with visibility is computed, and  $h_{\min}((x, y), \theta, l)$  is the minimum altitude to which there is visibility from coordinates  $(x, y)$  in direction  $\theta$  and distance  $l$ . Finally, the mean maximum distances are normalised to the range  $[0, 1]$ , which provides the visibility index for threat system  $i$  of threat group  $k$

$$VI_i^k(x, y) = \frac{\mu_{\max, i}^k(x, y)}{\max_{(x', y')} \mu_{\max, i}^k(x', y')}. \quad (4.8)$$

The minimum altitude  $h_{\min}((x, y), \theta, l)$  to which there is visibility from a given location  $(x, y)$ , direction  $\theta$  and distance  $l$  needs to be determined. The minimum altitude to which there is visibility depends on the elevation profile of the terrain in the direction  $\theta$  with distances less than or equal to  $l$ . Specifically, the minimum altitude to which there is visibility depends on the maximum value of the tangent of the angle between the horizontal axis and a straight line to the surface of the elevation profile with distances less than or equal to  $l$ , i.e.,

$$h_{\min}((x, y), \theta, l) = l\tau_{\max}((x, y), \theta, l), \quad (4.9)$$

where  $l$  is the distance under observation,  $\theta$  the direction in which the observer is observing,  $(x, y)$  the coordinates of the observer, and  $\tau_{\max}$  is the maximum value of the tangent  $\tau$  with all distances between 0 and  $l$ . Therefore,

$$\tau_{\max}((x, y), \theta, l) = \max_{r \in (0, l]} \left( \frac{h((x, y), \theta, r)}{r} \right), \quad (4.10)$$

where  $h((x, y), \theta, r)$  is the height of the elevation profile at distance  $r$  and direction  $\theta$  from the observer situated at location  $(x, y)$ .

In the terrain elevation profile, the horizontal axis is by default set to be the

sea level and thus due to the Earth's curvature the horizontal axis is curved instead of straight. Because of this, the terrain elevation profile cannot directly be used together with Equation (4.9) to determine the minimum altitude to which there is visibility, but the elevation profile first must be transformed to counteract the Earth's curvature. The line of sight from the observer to the horizon, which is a straight line, is chosen to be the horizontal axis. The height difference between the line of sight to the horizon and the terrain must be determined. To determine this, the distance of the horizon is first calculated. The geometric setup is portrayed in Figure 4.1. As seen in Figure 4.1, the line of sight from the observer to the horizon

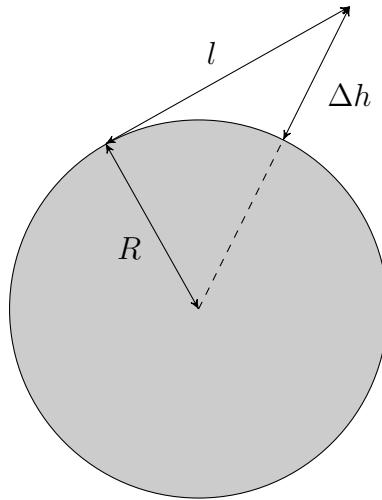


Figure 4.1: Geometry of calculating the distance of the horizon.

is actually a tangent of the Earth. Thus, there is a straight angle between the radius ( $R$ ) and the line of sight to the horizon ( $l_{\text{hor}}$ ) and Pythagoras' theorem is used to calculate the distance to the horizon, i.e.,

$$\begin{aligned}
 R^2 + l_{\text{hor}}^2 &= (\Delta h + R)^2 = \Delta h^2 + 2\Delta h R + R^2, \\
 l_{\text{hor}}^2 &= \Delta h^2 + 2\Delta h R, \\
 l_{\text{hor}} &= \sqrt{\Delta h^2 + 2\Delta h R}.
 \end{aligned} \tag{4.11}$$

On the other hand, the  $\Delta h$  in Figure 4.1 can also be interpreted as the change of elevation caused by the curvature of Earth. Solving  $\Delta h$  from Equation (4.11):

$$\Delta h(l^*) = \sqrt{R^2 + l^{*2}} - R, \tag{4.12}$$

where  $l^*$  is the distance from the horizon and  $R$  is the radius of the Earth. Equa-

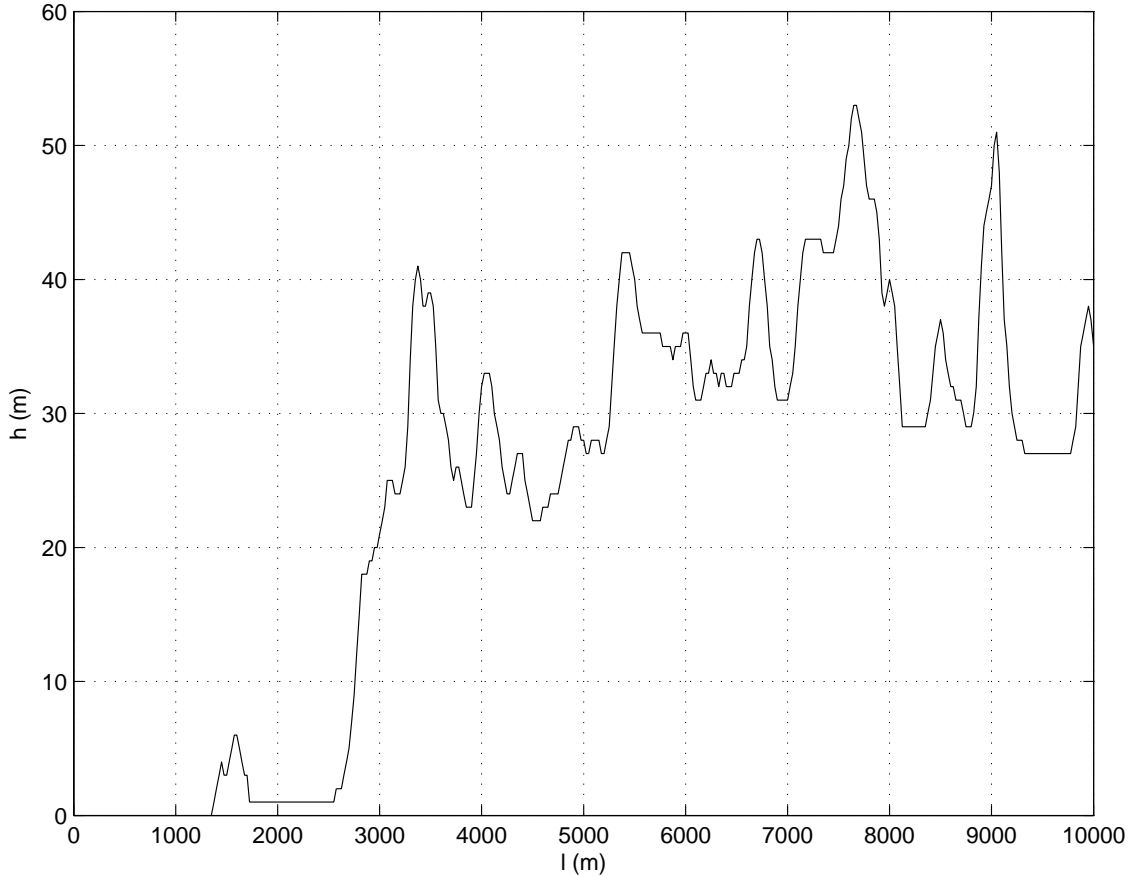


Figure 4.2: Elevation profile,  $h$  refers to elevation from sea level  $l$  refers to the distance from the observer.

tion (4.12) is written as the function of the distance from the observer as

$$\Delta h(l) = \sqrt{R^2 + (l - l_{\text{hor}})^2} - R, \quad (4.13)$$

where  $l_{\text{hor}}$  is the distance of the horizon from the observer assuming no obstructions and is calculated with Equation (4.11). By subtracting the height difference  $\Delta h$  given by Equation (4.13) from the original elevation profile the elevation profile is transformed to take into account the Earth's curvature. Together with this transformed elevation profile Equation (4.9) is used to determine the minimum altitude to which there is visibility from any given location, direction and distance. This result is then used to calculate the visibility index with Equations (4.7) and (4.8).

The process of transforming the elevation profile and determining the minimum altitude to which there is visibility is demonstrated through a short example. Figure 4.2 illustrates a possible elevation profile. In Figure 4.2, the horizontal axis is set to equal the sea level. Due to the curvature of the Earth, this axis is actually

curved. To counteract this, the horizontal axis is chosen to be the observer's line of sight to the horizon, which is a straight line. To do this, the distance to the horizon is first calculated. In the example, it is presumed that the observer is observing from a height of  $h_{\text{obv}} = 3$  m and that the Earth's radius is  $R = 6371$  km. With Equation (4.11), the distance to the horizon is calculated to be  $l_{\text{hor}} = 6183$  m. With Equation (4.13), all of the elevations in Figure 4.2 are transformed to be relative to the observer's line of sight to the horizon, instead of the sea level. The result is shown in Figure 4.3.

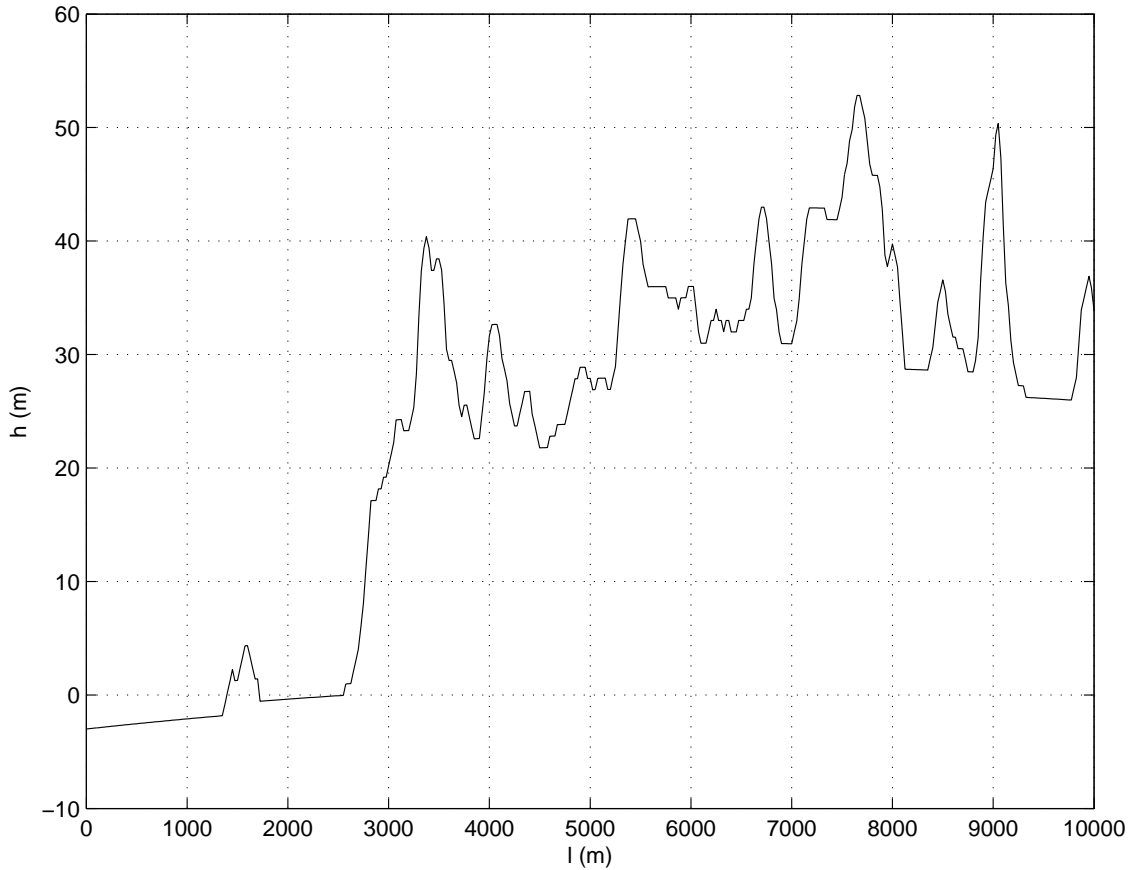


Figure 4.3: Elevation profile relative to the observer's line of sight to the horizon,  $h$  refers to elevation from to the observer's line of sight to the horizon and  $l$  refers to the distance from the observer.

The elevation profile relative to the observer's line of sight to the horizon (blue) and the minimum altitude ( $h_{\text{min}}$ ) required for the line of sight from the observer (red) are shown in Figure 4.4. From this figure, one can evaluate whether an object is visible to the observer – if the object is above the minimum altitude (red line), the object is visible. The black solid line in Figure 4.4 is a line marking the altitude of 80 metres above sea level. From the figure, one can read the maximum distance to

which the observer can see objects travelling at 80 metres above sea level by finding the intersection of the minimum altitude line and the 80 metres above sea level line. The observer can see objects travelling at an altitude of 80 metres from a distance of 6700 metres.

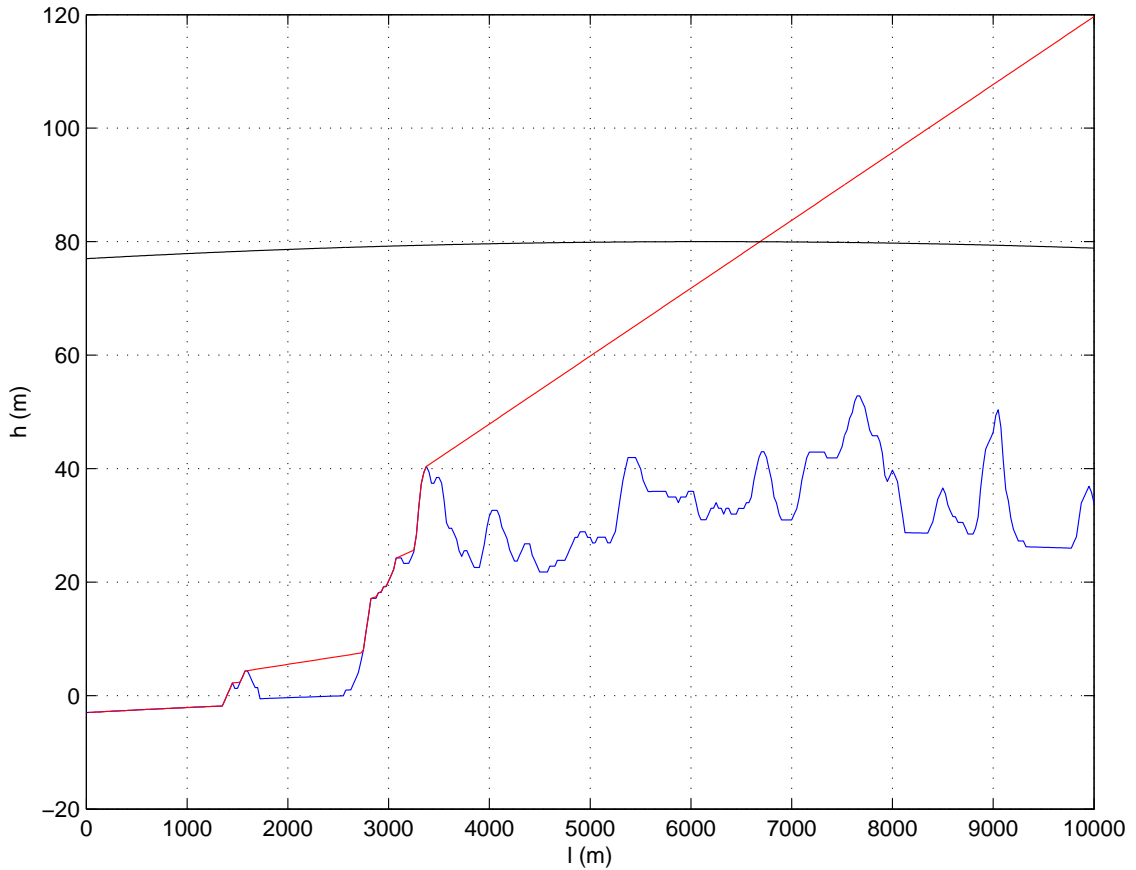


Figure 4.4: Minimum visible height from point  $l = 0, h = 0$ , where  $h$  refers to elevation from to the observer's line of sight to the horizon and  $l$  refers to the distance from the observer. The blue line corresponds to the elevation profile, the red line is the minimum altitude to which the observer has visibility and the black line represents the altitude of 80 metres above sea level.

### Grouping index ( $GI$ )

In the spatial prediction model, the grouping index is by default defined to be a two dimensional multivariate normal distribution in the polar coordinate system with the target which the air defence is protecting in the origin. One of the dimensions for the multivariate normal distribution is the distance  $r$  from the target and the other dimension is the bearing  $\omega$  from the target. The mean and variance of the distance from the target are defined by the common tactical principles used when forming an

air defence with the type of threat system in question. The mean of the bearing is defined by the direction from which an attack is being anticipated. The variance of the bearing corresponds with the width of the sector for which the defence is being formed. The polar coordinate multivariate normal distribution is then transformed to the Cartesian coordinate system, which gives the grouping index

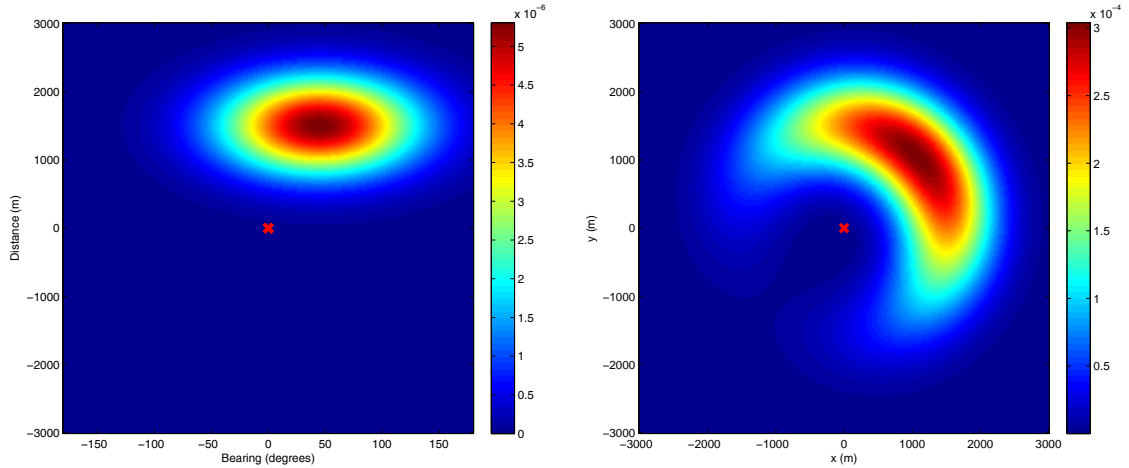
$$GI_i^k(x, y) = \frac{1}{2\pi\sigma_r\sigma_\omega} \exp\left(-\frac{1}{2}\left[\frac{(\sqrt{(x-x_0)^2+(y-y_0)^2}-\mu_r)^2}{\sigma_r^2} + \frac{(\arctan(\frac{x-x_0}{y-y_0})-\mu_\omega)^2}{\sigma_\omega^2}\right]\right), \quad (4.14)$$

where  $\mu_r$  and  $\sigma_r$  are the mean and standard deviation of the distance from the target,  $\mu_\omega$  and  $\sigma_\omega$  are the mean and standard deviation of the bearing from the target, and  $(x_0, y_0)$  are the coordinates of the target.

Figure 4.5 shows the multivariate normal distribution in the polar coordinate system (Fig. 4.5a) and the corresponding augmented multivariate normal distribution in Cartesian coordinates (Fig. 4.5b). In Figure 4.5, the mean of the distance from the target which is being defended is 1500 metres and the distance's standard deviation is 500 metres. The direction from which the attack is anticipated from is 45 degrees while the width of the sector for which the defence is formed is 120 degrees. The location of the target which is being protected is marked with a red cross in Figure 4.5b.

### 4.1.2 Probability map reduction

The probability map  $P_{L,i}^k(x, y)$  calculated with Equation (4.3) gives the probability for an S/A threat system to be located at coordinates  $(x, y)$ . Since the possible coordinates of the threat system are discretised, the probability map is in essence a two dimensional discrete probability distribution. In many applications, it may be necessary to study each possible location separately and perform different operations for each possible coordinate. Such operations and examinations can be done with reasonable computational resources for small probability maps, but as the number of possible locations grows this becomes increasingly difficult and costly. To overcome this, a method for choosing a reasonable amount of discrete locations and assigning probabilities for them in a manner that preserves with sufficient accuracy the characteristics of the original probability map is presented. The characteristic that is the most important to preserve with respect to survivability models described in this



(a) The multivariate normal distribution in polar coordinates. (b) The multivariate normal distribution in Cartesian coordinates.

Figure 4.5: Multivariate normal distributions from which the grouping index is formed. The target which is being protected is marked with a red cross in Figure 4.5b.

thesis is the expected probability of detection of an A/G weapon in the airspace near the area described by the probability map. The probability map reduction method presented here is based on a clustering algorithm called  $k$ -means clustering [33].

The probability map reduction method should organise all possible locations into a chosen amount  $\kappa$  of different sets  $\mathbf{S} = \{S_1, S_2, S_3, \dots, S_\kappa\}$  so that the reduced probability map includes a discrete location from each of these sets and preserves the expected probability of detection by the S/A threat system whose whereabouts the probability map describes. Without probability map reduction, each area would be given an equal amount of attention resourcewise although it would be smarter to spend more time studying areas in where it is more likely for the S/A threat system to be located and less time studying expanses where it is less likely for the S/A threat system to be located. The  $k$ -means clustering algorithm tends to produce equisized clusters, and thus the clusters and reduced locations will be more densely distributed in areas with highly probable locations for S/A threat systems and sparsely in areas which are unlikely to host an S/A threat system. Since each reduced location is given equal attention in regard to computational resources, the goal of allocating more resources to areas with a higher probability of having S/A threat systems present is achieved. On the other hand, the less likely areas are not completely forgotten but are merely taken into account more crudely.

At the beginning of the  $k$ -means probability map reduction method, the  $\kappa$  single

most probable locations  $\{(x_1, y_1), (x_2, y_2), \dots, (x_\kappa, y_\kappa)\}$  are chosen as the initial  $\kappa$  means and are referred to as the corresponding sets' prototypes. After this, the  $k$ -means probability map reduction method proceeds by repeating the following two steps until it converges on a collection of sets  $\mathbf{S} = \{S_1, S_2, \dots, S_\kappa\}$ .

### Assignment step

Each possible location  $(x, y)$  is assigned to such a set  $S_l$  that the euclidian distance between the location and the set's prototype is minimised, i.e.,

$$S_l = \{(x, y) : (x - x_l)^2 + (y - y_l)^2 \leq (x - x_j)^2 + (y - y_j)^2 \forall j, 1 \leq j \leq \kappa\}.$$

### Update step

The prototype of each set  $S_l$  is updated to be situated at the expected location  $(x_l, y_l)$  of an S/A threat system in the set, given that the threat system is in the set  $S_l$ , i.e.,

$$x_l = \left( \sum_{(x,y) \in S_l} P_{L,i}^k(x, y) \right)^{-1} \sum_{(x,y) \in S_l} x P_{L,i}^k(x, y)$$

$$y_l = \left( \sum_{(x,y) \in S_l} P_{L,i}^k(x, y) \right)^{-1} \sum_{(x,y) \in S_l} y P_{L,i}^k(x, y),$$

where  $P_{L,i}^k(x, y)$  is the probability map which is being reduced.

Once the collection of sets  $\mathbf{S}$  has converged and the sets do not change between iterations, the repetition of the steps is ceased, and the sets  $S_l$  are set as the final clusters. The most probable location is chosen from each set to be the reduced location corresponding to that set. The event that a certain location in a set is chosen as the reduced location, i.e., it is the most probable location in the set, implies that the location in question is the best case location regarding the capabilities of an S/A threat system located there. This is because for a location to be given a high probability by the spatial prediction model, the location must be reachable in terms of the terrain, there must be good visibility from the location, and the location must be in unison with common tactical principles linked with the threat system in question.

Each reduced location is given a probability which is equal to the probability for the S/A threat system being located in any of the associated set's locations. This

is calculated as

$$P_{L,\text{reduced},i}^k(x_l, y_l) = \sum_{(x,y) \in \mathcal{S}_l} P_{L,i}^k(x, y). \quad (4.15)$$

To summarise, before the probability map reduction the probability map  $P_{L,i}^k$  of threat system  $i$  in threat group  $k$  was two dimensional discrete probability distribution and thus any numerical computations would have been laboursome. By reducing the probability map to  $\kappa$  distinct possible locations, any computations have been eased significantly while preserving the characteristics of the probability map.

## 4.2 Markov survivability model

The survivability model presented in this thesis is called the Markov survivability model, which is based on an inhomogenous continuous-time Markov chain that has four possible states. Markov chains are described in more detail in Appendix B. The Markov chain used in the model is portrayed in Figure 4.6. The model strives to determine the probability by which each threat unit  $j$  is capable of intercepting the A/G weapon before it reaches its target. In the Markov survivability model, each Markov chain represents the capability of a single threat unit  $j$  to detect, track and engage the A/G weapon. The transition rates of a single Markov chain depend on the particular S/A threat group's  $k$  target acquisition radars'  $i = 1 \dots n_k$  capability to detect and track the A/G weapon, the capability to detect and track the A/G weapon by the fire control radar of the specific threat unit  $j$ , and the kinematic capabilities of the S/A threat unit's  $j$  weapon. The model takes into account the directional radar cross section of the A/G weapon and any possible shadows cast by the terrain.

The Markov chain upon which the Markov survivability model is based has four states: "Undetected", "Tracked", "Locked", and "Hit". The state probabilities, i.e., the probabilities with which the Markov chain is in each state at time  $t$  are depicted with  $P_{\text{undetected},j}^k(t)$ ,  $P_{\text{track},j}^k(t)$ ,  $P_{\text{lock},j}^k(t)$  and  $P_{\text{hit},j}^k(t)$ , respectively. When the threat unit  $j$  is in the "Undetected" state, the target acquisition radars  $i = 1 \dots n_k$  in the threat unit's S/A threat group  $k$  have not detected the A/G weapon with sufficient accuracy to form a track. The target acquisition radars  $i = 1 \dots n_k$  might have achieved isolated detections of the A/G weapon but not enough to infer any valuable knowledge about the A/G weapon. Once the state transitions to "Tracked", the group's target acquisition radars have obtained enough detections of the A/G weapon to form a track. In the Markov survivability model, the track is passed over

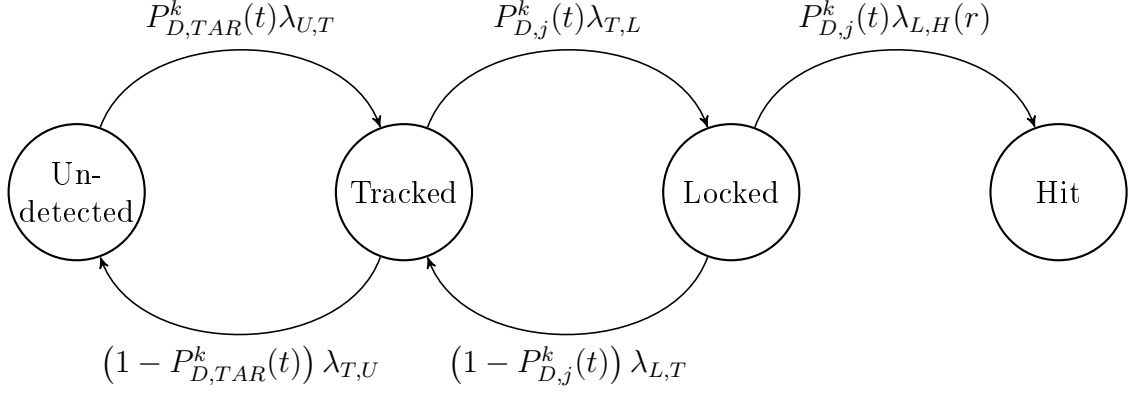


Figure 4.6: The continuous-time Markov chain used in the Markov survivability model where  $P_{D,TAR}^k$  depicts the probability that one or numerous target acquisition radars  $i = 1 \dots n_k$  in threat group  $k$  are capable of detecting the A/G weapon at time  $t$  and  $P_{D,j}^k$  is the probability that threat unit  $j$  of threat group  $k$  is capable of detecting the A/G weapon at time  $t$ .

to the threat units instantaneously once it has been formed. Once the “Locked” state has been reached, the fire control radar of the threat unit has achieved a track on the A/G weapon. Only this track obtained by the fire control radar can be used to guide the S/A threat’s weapon, and thus it is a requirement for the interception of the A/G weapon. Once the fire control track has been acquired, the weapon of the S/A threat unit in question instantaneously begins attempting to intercept the A/G weapon. The final state “Hit” is such that once it has been reached the S/A threat unit has successfully intercepted the A/G weapon. This state is an absorbing state and thus once it is reached, the system will never leave the state. Note, that each Markov chain describes a single S/A threat unit  $j$  and thus  $m_k$  separate chains are used to describe each S/A threat group  $k$ .

As can be seen in Figure 4.6, in addition to the constant state transition rate parameters  $\lambda_{U,T}$ ,  $\lambda_{T,U}$ ,  $\lambda_{T,L}$ ,  $\lambda_{L,T}$ , the transition rates also depend on the range dependent transition rate parameter  $\lambda_{L,H}(r)$  and time dependent variables. Thus, the Markov chains are inhomogeneous continuous-time Markov chains. The time dependent variables which the Markov chain depends upon are the combined expected probability of detection of the  $k$ th S/A threat group’s target acquisition radars  $i = 1 \dots n_k$   $P_{D,TAR}^k(t)$ , and the probability of detection of the  $j$ th threat unit’s fire control radar  $P_{D,j}^k(t)$ . The constant state transition parameters  $\lambda_{U,T}$  and  $\lambda_{T,L}$  can be interpreted as the reciprocals of the average time needed by a target acquisition radar  $i$  and S/A threat unit  $j$  to form a track for the A/G weapon assuming each are capable of detecting the A/G weapon with probability  $P_D = 1$ . Similarly,

the constant parameters  $\lambda_{T,U}$  and  $\lambda_{L,T}$  can be interpreted as the reciprocals of the average time it takes for a track to be lost by a target acquisition radar  $i$  and S/A threat unit  $j$  assuming they cannot detect the A/G weapon, i.e.,  $P_D = 0$ . With the range dependent transition rate parameter  $\lambda_{L,H}(r)$ , the model strives to take into account the range and kinematic capabilities of the weapon of the S/A threat unit  $j$ . The range dependent parameter is defined

$$\lambda_{L,H}(r) = \begin{cases} \lambda_{L,H}^{\text{const}} & \text{if } r \leq R_{\text{max}} \\ 0 & \text{otherwise} \end{cases}, \quad (4.16)$$

where  $\lambda_{L,H}^{\text{const}}$  is the average time needed for the S/A threat unit  $j$  to intercept the A/G weapon while it is in the effective slant range of the threat unit's weapon, and  $R_{\text{max}}$  is the maximum range at which the threat unit's weapon can engage targets. The target acquisition radars'  $i = 1 \dots n_k$  combined expected probability of detection  $P_{D,TAR}^k(t)$  and the S/A threat unit's  $j$  probability of detection  $P_{D,j}^k(t)$  are determined based on probabilities calculated as described in Appendix A.

The combined expected probability of detection of the S/A threat group's  $k$  target acquisition radars  $P_{D,TAR}^k(t)$  gives the probability that one or more of the S/A threat group's target acquisition radars  $i = 1 \dots n_k$  are able to detect the A/G weapon at a given time  $t$ . The probability that a single S/A threat system at a given location  $(x', y')$  can detect an A/G weapon located at coordinates  $(x, y, z)$  and with heading  $\phi$ , pitch angle  $\theta$ , and roll angle  $\psi$  is  $P_D^{(x',y')}(x, y, z, \phi, \theta, \psi)$  and is calculated with Equation (A.18). The probability of detection is dependent also on the orientation of the A/G weapon as the radar cross section changes depending on which part of the A/G weapon is facing the radar. Given a known probability map  $P_{L,i}^k(x', y')$  determined with Equation (4.3) for the  $i$ th target acquisition radar in S/A threat group  $k$ , the expected probability of detection for the  $i$ th radar is

$$\text{E} [P_{D,i}^k(x, y, z, \phi, \theta, \psi)] = \sum_{(x',y')} P_{L,i}^k(x', y') P_D^{(x',y')}(x, y, z, \phi, \theta, \psi). \quad (4.17)$$

Further, the combined expected probability of detection for the S/A threat group's  $k$  target acquisition radars  $i = 1 \dots n_k$  is calculated as

$$P_{D,TAR}^k(t) = P_{D,TAR}^k(x, y, z, \phi, \theta, \psi) = 1 - \prod_{i=1}^{n_k} (1 - \text{E} [P_{D,i}^k(x, y, z, \phi, \theta, \psi)]), \quad (4.18)$$

where subscript  $i$  refers to the target acquisition radars in S/A threat group  $k$ , and

$(x, y, z, \phi, \theta, \psi)$  are the A/G weapon's coordinates and orientation at time  $t$ .

In order to take into account the uncertainty regarding the location of the S/A threat unit  $j$ , the probability of successful interception of the A/G weapon by the S/A threat unit  $j$ , i.e.,  $P_{\text{hit},j}^k$ , must be determined from every possible threat unit's location  $(x', y')$ . When evaluating the probability of interception from a certain location  $(x', y')$ , the  $j$ th S/A threat unit's probability of detection  $P_{D,j}^k(t)$  is simply the probability that the S/A threat unit  $j$  is capable of detecting the A/G weapon which is at coordinates  $(x, y, z)$  with orientation  $(\phi, \theta, \psi)$  at time  $t$ , i.e.,

$$P_{D,j}^k(t) = P_{D,j}^k(x, y, z, \phi, \theta, \psi) = P_D^{(x',y')}(x, y, z, \phi, \theta, \psi), \quad (4.19)$$

in which  $(x', y')$  are the coordinates of the S/A threat unit under inspection. This is calculated with Equation (A.18).

The probability of S/A threat unit  $j$  located at a certain location  $(x, y)$  successfully intercepting the A/G weapon at some point during the trajectory  $)P_{\text{hit},j}^k(x, y)$  is determined by solving the differential equation given by Equation (B.3). The differential equation is numerically solved by using MATLAB's ode45 solver. The probability of successful interception is the probability that the Markov chain is in state "Hit" at the end of the trajectory. Note, that the probability of being in state "Hit" or any other state at a given time  $t$  can also be determined from Equation (B.3). The probabilities of successful interception by S/A threat unit  $j$  in alternative locations are combined to form an expected probability of interception for the threat unit  $j$  as

$$\text{E} [P_{\text{hit},j}^k] = \sum_{(x,y)} P_{L,j}^k(x, y) P_{\text{hit},j}^k(x, y), \quad (4.20)$$

where  $P_{L,j}^k(x, y)$  is determined with Equation (4.3) and gives the probability for the  $j$ th threat unit in the S/A threat group  $k$  to be located at location  $(x, y)$ . The final probability whereby the A/G weapon is intercepted by any S/A threat unit  $j$  in any threat group  $k$  is determined by calculating the probability that one or more threat units are capable of intercepting the A/G weapon, i.e.,

$$P_{\text{kill}} = 1 - \prod_{k=1}^N \prod_{j=1}^{m_k} (1 - \text{E} [P_{\text{hit},j}^k]). \quad (4.21)$$

Recall that  $N$  is the amount of S/A threat groups the air defence consists of and  $m_k$  is the number of S/A threat units in threat group  $k$ . Furthermore, the survivability

of the trajectory is determined with

$$P_{\text{surv}} = 1 - P_{\text{kill}}, \quad (4.22)$$

where  $P_{\text{kill}}$  is calculated with Equation (4.21).

As noted earlier, the probabilities of being in any state of a single Markov chain at time  $t$  is determined in an identical manner. The expected probability of being in the given state is calculated by modifying Equation (4.20) appropriately by exchanging the probabilities  $P_{\text{hit},j}^k$  with  $P_{\text{undetected},j}^k$  or  $P_{\text{track},j}^k$  etc. These expected state probabilities can for instance be used to determine the probabilities that no S/A threat unit has been able to intercept the A/G weapon but one or more threat units have been able to track the A/G with their independent radars.

In the situation in which the exact positions of the S/A threat systems are known the trajectory evaluation framework is used in the same manner as presented above. Then the probability maps of the S/A threat systems are reduced to maps that have value 1 in the location at which the S/A threat system is located and 0 elsewhere.

The Markov survivability model takes into account the topographical features of the surrounding terrain as well as the height of possible tree cover. These are taken into consideration during the evaluation of the probabilities of detection  $P_D$  used in Equations 4.17 and 4.19. If there is a visual obstruction between the S/A threat system and the A/G weapon, the S/A threat system cannot detect the A/G weapon and the probability of detection is zero.

To summarise, the first step in the trajectory evaluation is to determine a probability map for each S/A threat system, see Equation (4.3). Next, the expected probabilities of detection by target acquisition radars  $i = 1 \dots n_k$  are determined at every point of the trajectory for each S/A threat group  $k$  with Equation (4.17). Then, the Markov chain is evaluated by solving the differential Equation (B.3) for each possible location of each S/A threat unit  $j$ . The expected probabilities of successful interception are then determined with Equation (4.20) for each S/A threat unit  $j$ , and then the probability of one or more S/A threat units successfully intercepting the A/G weapon is calculated with Equation (4.21). Finally, the survivability of each trajectory is determined with Equation (4.22). The survivabilities of the trajectories are then compared and the trajectory with the highest survivability is identified as the best trajectory regarding the A/G weapon's survivability.

# Chapter 5

## Reference survivability models

The Markov survivability model introduced in Chapter 4 is verified to ensure that the model indeed portrays the accumulation of risk while an A/G weapon is traversing a given trajectory. This is done by comparing the survivability along the trajectories based on the Markov model with the survivabilities based on two reference models. The first of the reference models is a survivability model introduced by Erlandson and Niklasson [11]. The model relies on Markov chains to determine the survivability of A/G weapons. This model is referred to as the Erlandsson model. The second model aspires to capture the technical aspects of how a radar system acquires and maintains a track of a target [34]. The second model is referred to as the technical survivability model.

### 5.1 Erlandsson model

The Erlandsson model relies on five state continuous-time Markov chains to determine the likelihood of an A/G weapon being able to safely traverse the trajectory and reach its target, i.e., its survivability. The capabilities of the S/A threat groups are studied with  $N$  separate Markov chains. The Erlandsson model assigns a sensor area for each target acquisition radar  $i$  and a threat area for each threat unit  $j$  in S/A threat group  $k$ . The sensor areas represent areas in which the target acquisition radars  $i = 1..n_k$  are capable of detecting and tracking the A/G weapon, and the threat areas represent areas in which the S/A threat units  $j = 1..m_k$  can detect and track the A/G weapon with their fire control radars and are also capable of engaging the A/G weapon with their weapons. The Erlandsson model does not take into account the directional dependency of the A/G weapon's radar cross section or the possible shadows caused by the terrain, as the radars' and weapons' capabilities

to detect, track, and engage the A/G weapon are assumed to be constant within each sensor and threat area.

The Erlandsson model uses continuous-time Markov chains with five states to describe the capabilities of S/A threat groups  $k = 1 \dots N$ . It is assumed that the transitions between states are Poisson processes. Markov chains are described in more detail in Appendix B. The states are “Undetected”, “Detected”, “Tracked”, “Engaged”, and “Hit”. The transition rates between the states depend on which sensor and/or threat areas the A/G weapon is located in, if any. The Markov chain which is used is shown in Figure 5.1, with the positive non-zero transition rates in each different area depicted with arrows between the states.

While being in the “Undetected” state the S/A threat group  $k$  has not yet detected the A/G weapon. The “Detected” state is a state where the threat group’s target acquisition radars  $i = 1 \dots n_k$  have detected the A/G weapon but not with sufficient accuracy to form a track. Once in the “Tracked” state the S/A threat group’s target acquisition radars  $i = 1 \dots n_k$  have acquired sufficient knowledge on the whereabouts of the A/G weapon to form a track. The track can then be handed over to the threat units  $j = 1 \dots m_k$ . After the track formed by the target acquisition radars  $i = 1 \dots n_k$  has been forwarded to the threat units  $j = 1 \dots m_k$ , the fire control radars of the threat units try to obtain their own tracks of the A/G weapon which could be used by their weapons. Once this track has been formed by a threat unit  $j$  in the S/A threat group, the state of the S/A threat group  $k$  advances to “Engaged”. Finally, the state of the threat group  $k$  is changed to “Hit” once a threat unit  $j$  from the group has succeeded in engaging the A/G weapon and the A/G weapon has been intercepted.

The transition rates between states depend in what area or which different areas the A/G weapon is located in at any given time. Examples of transition rates between different states when the A/G weapon is outside all of the sensor and threat areas and when the A/G weapon is in exactly one sensor or threat area are given in Table 5.1. The values of state transition rates are calculated by first determining the mean time needed for a given transition and then calculating the reciprocal of these mean times. The mean time needed for a given transition is determined with the help of experts.

In many cases, the A/G weapon is in the sensor or threat areas of several different target acquisition radars  $i$  and threat units  $j$  of the same S/A threat group  $k$  simultaneously. In such cases, the state transition rates are calculated based on the transition rates of the individual sensor and threat areas. The combined transition

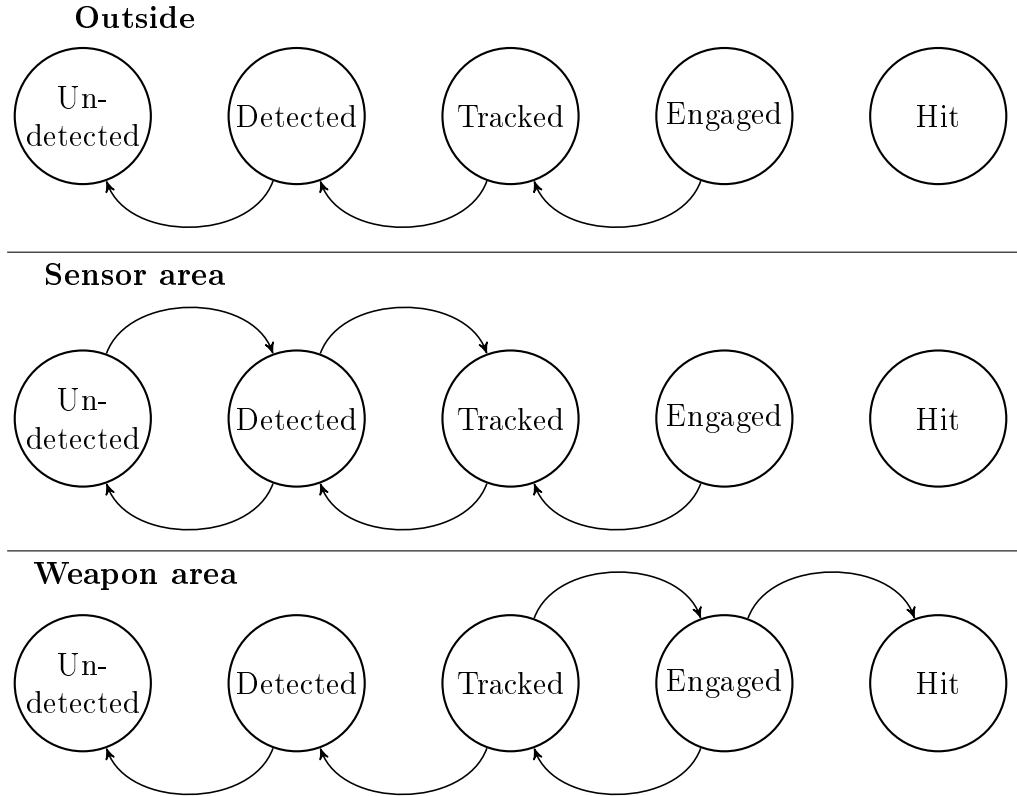


Figure 5.1: The Markov chain used in the Erlandsson model, with arrows depicting positive non-zero transition rates between states in given areas.

Table 5.1: State transition rates used by Erlandsson [11].

	$\lambda_{U,D}$	$\lambda_{D,U}$	$\lambda_{D,T}$	$\lambda_{T,D}$	$\lambda_{T,E}$	$\lambda_{E,T}$	$\lambda_{E,H}$
Outside	0	0.2	0	0.2	0	1	0
Sensor area	0.4	0.1	0.3	0.1	0	1	0
Threat area	0	0.2	0	0.2	0.2	0.1	0.3

rates are calculated in a slightly different manner depending on the transition in question. In the case that two or more sensor areas are overlapping, the Erlandsson model assumes that each radar independently strives to detect and track the A/G weapon, and the Markov chain transitions to the next state once the first sensor has detected the A/G weapon or acquired a track, depending on the state transition under inspection. Thus, the transitions from “Undetected” to “Detected” and from “Detected” to “Tracked” are viewed as sums of multiple independent Poisson processes. The transition rate of the combined Poisson process is calculated as the

sum of the transition rates of the independent Poisson processes, i.e.,

$$\lambda_{U,D}^{\text{Comb}} = \sum_{i=1}^{n_k} \lambda_{U,D}^i \quad (5.1)$$

$$\lambda_{D,T}^{\text{Comb}} = \sum_{i=1}^{n_k} \lambda_{D,T}^i, \quad (5.2)$$

where  $\lambda_{U,D}^i$  and  $\lambda_{D,T}^i$  are the transition rates from states “Undetected” to “Detected” and “Detected” to “Tracked” in the  $i$ th individual sensor area respectively. The derivation of transition rates for the opposite transitions, i.e., transitions from states “Detected” to “Undetected” and from “Tracked” to “Detected”, is inspired by reliability theory and the overlapping areas are described as parallel components such that each component has an exponentially distributed life time. In other words, in order for a state transition to happen each of the target acquisition radars  $i = 1 \dots n_k$  and threat units  $j = 1 \dots m_k$  in the vicinity must have lost track of the A/G weapon. From reliability theory it is known that with two parallel components the Poisson process parameter  $\lambda$  describing the reliability of the complete system is determined with

$$\frac{1}{\lambda^{1,2}} = \frac{1}{\lambda^1} + \frac{1}{\lambda^2} - \frac{1}{\lambda^1 + \lambda^2}, \quad (5.3)$$

where  $\lambda^1$  and  $\lambda^2$  are the Poisson process parameters of each individual component. As there are often more than two sensor or threat areas overlapped, Equation (5.3) is inadequate for determining the final transition rate. If there are more than two overlapped areas, the final transition rates are calculated by starting with the transition rate due to one sensor or threat area, and adding areas and sensors which are taken into account one at a time. Given a set  $S$  of sensor and threat areas for which the transition rates  $\lambda_{D,U}^S$  and  $\lambda_{T,D}^S$  are known, the transition rates for the set of areas  $S \cup \{i\}$ , which is achieved by adding a sensor area  $i$  to the set  $S$ , are determined with

$$\frac{1}{\lambda_{D,U}^{S \cup \{i\}}} = \frac{1}{\lambda_{D,U}^S} + \frac{1}{\lambda_{D,U}^i} - \frac{1}{\lambda_{D,U}^S + \lambda_{D,U}^i} \quad (5.4)$$

$$\frac{1}{\lambda_{T,D}^{S \cup \{i\}}} = \frac{1}{\lambda_{T,D}^S} + \frac{1}{\lambda_{T,D}^i} - \frac{1}{\lambda_{T,D}^S + \lambda_{T,D}^i}. \quad (5.5)$$

Threat areas  $j = 1 \dots m_k$  are treated in exactly the same manner as sensor areas  $i = 1 \dots n_k$  in Equations (5.4) and (5.5) when taking them into account in the transition

rates  $\lambda_{D,U}^{\text{Comb}}$  and  $\lambda_{T,D}^{\text{Comb}}$ .

Overlapping threat areas and corresponding transition rates from state “Tracked” to “Engaged”, from “Engaged” to “Hit”, and from “Engaged” to “Tracked” are determined in a different manner than the transition rates discussed earlier. Erlandsson argues that the decision of engaging the A/G weapon is made by the enemy commander. Thus, the number of threat areas that overlap on the given location does not explicitly have any effect on the decision. In the Erlandsson model, the transition rates used for the aforementioned transitions are chosen to be the worst case rates chosen from all overlapping areas, i.e.,

$$\lambda_{T,E}^{\text{Comb}} = \max_{j=1\dots m_k} \lambda_{T,E}^j \quad (5.6)$$

$$\lambda_{E,H}^{\text{Comb}} = \max_{j=1\dots m_k} \lambda_{E,H}^j \quad (5.7)$$

$$\lambda_{E,T}^{\text{Comb}} = \min_{j=1\dots m_k} \lambda_{E,T}^j, \quad (5.8)$$

where  $\lambda_{T,E}^j$ ,  $\lambda_{E,H}^j$ , and  $\lambda_{E,T}^j$  are the transition rates between states “Tracked”, “Engaged”, and “Hit” in each individual overlapping threat area. The transition rate away from the state “Hit” is always zero and this is an absorbing state.

It remains to determine the size of the sensor and threat areas. Erlandsson does not specify any method on how the sizes of the different areas should be determined. In this thesis, the size of the sensor and threat areas are determined by the radar’s capability to detect the A/G weapon and the range  $R_{\max}$  of the weapon of the S/A threat unit  $j$ . The maximum range at which a radar can detect the A/G weapon is solved from Equation (A.8):

$$\rho_{\max} = \sqrt[4]{\frac{P_t G_t G_r \lambda^2 \sigma \tau n_p}{(4\pi)^3 L_s k T_0 F \text{SNR}_{\min}}}, \quad (5.9)$$

where  $\text{SNR}_{\min}$  is the minimum signal-to-noise ratio at which it has been determined the radar can with a given certainty detect the A/G weapon. To calculate this, a threshold probability of detection  $P_{D,\min}$  must be chosen. With the chosen threshold probability of detection, the minimum detectable signal-to-noise ratio is determined by using Equation (A.18). The maximum range  $\rho_{\max}$  calculated for a target acquisition radar  $i$  with Equation (5.9) is used as the radius of the corresponding sensor area. The radius of a threat area is chosen to be either the range  $R_{\max}$  of the S/A threat’s weapon or the maximum range  $\rho_{\max}$  of the associated fire control radar, which ever is smaller.

When uncertainty concerning the location of the sensors and weapons is taken into consideration, the expected values of the state transition rates for individual sensor and weapon areas are used to determine the combined state transition rates  $\lambda_{U,D}^{\text{Comb}}$ ,  $\lambda_{D,T}^{\text{Comb}}$ , etc. For example, consider a target acquisition radar  $i$  for which based on the probability map calculated for the radar it is determined that with probability  $p$  the A/G weapon is in the target acquisition radar's sensor area. Then, the resulting transition rate is calculated as

$$\lambda = p\lambda_{\text{sensor}} + (1 - p)\lambda_{\text{out}}, \quad (5.10)$$

where  $\lambda_{\text{sensor}}$  is the transition rate for the single target acquisition radar  $i$  when the A/G weapon is inside the sensor area and  $\lambda_{\text{out}}$  is the transition rate when the A/G weapon is outside the sensor area.

This method for determining the transition rate  $\lambda$  under uncertainty regarding the locations of S/A threats is illustrated with an example portrayed in Figure 5.2. In the example, the probability map consists of three alternative locations for the S/A threat  $(x_1, y_1)$ ,  $(x_2, y_2)$  and  $(x_3, y_3)$ . The S/A threat is located at each of the locations with probabilities  $P_L(x_1, y_1) = 1/4$ ,  $P_L(x_2, y_2) = 1/4$  and  $P_L(x_3, y_3) = 1/2$ . Three separate positions are considered for the A/G weapon, these are denoted with A, B and C. The maximum range of the S/A threat is denoted with  $\rho_{\text{max}}$ . In position A, the probability whereby the A/G weapon is inside the threat's sensor area is  $p(A) = 0$ , thus based on Equation (5.10) the transition rate is  $\lambda = \lambda_{\text{out}}$ . In position B, the probability of being inside the sensor area is  $p(B) = 3/4$ . Thus, in this case the transition rate would be  $\lambda = 3/4 \lambda_{\text{sensor}} + 1/4 \lambda_{\text{out}}$ . Finally, in position C, the probability  $p(C)$  is  $1/4$ , and thus the transition rate is  $\lambda = 1/4 \lambda_{\text{sensor}} + 3/4 \lambda_{\text{out}}$ .

When evaluating the possible trajectories of an A/G weapon, a continuous-time Markov chain is evaluated over the course of the trajectory for each S/A threat group  $k$  by solving the differential equation given by Equation (B.3). Solving the differential equation results in probabilities for being in each of the states "Undetected", "Detected", "Tracked", "Engaged", and "Hit" at any given time  $t$ . For each of these S/A threat groups  $k$ , the final probability of successful interception  $P_{\text{hit}}^k$  is determined by reading the probability of being in state "Hit" at the end of the trajectory. The probability that one or more S/A threat groups are successful in intercepting the A/G weapon is calculated as

$$P_{\text{kill}} = 1 - \prod_{k=1}^N (1 - P_{\text{hit}}^k), \quad (5.11)$$

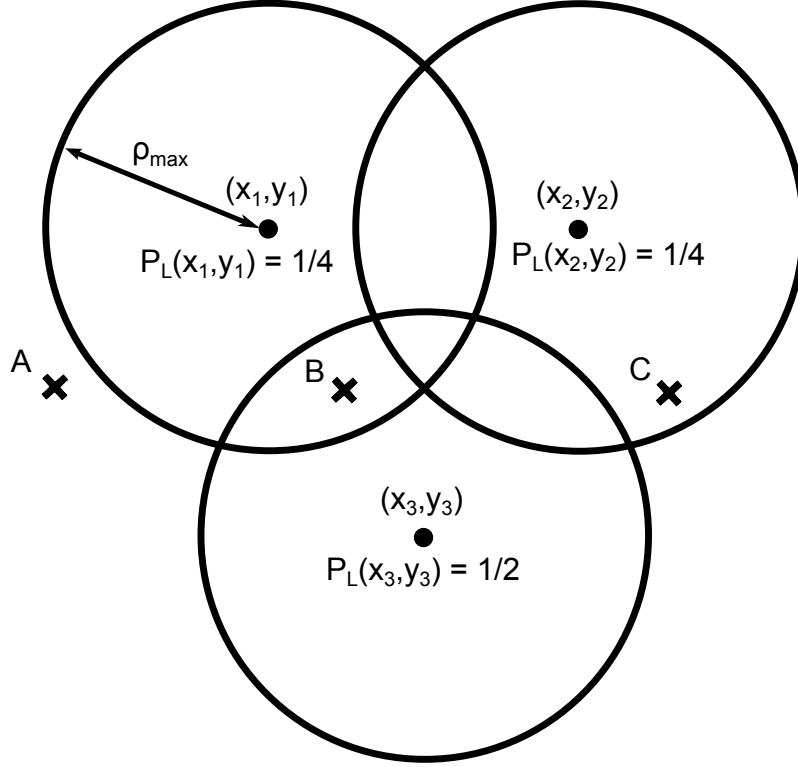


Figure 5.2: The example with which the calculation of transition rate  $\lambda$  under uncertainty is demonstrated.

in which  $P_{\text{hit}}^k$  is the probability whereby the  $k$ th S/A threat group successfully intercepts the A/G weapon, i.e., the probability that the group  $k$  is in state “Hit” at the end of the A/G weapon’s trajectory.

The final survivability  $P_{\text{surv}}$  of the A/G weapon is determined by calculating the complement probability of the event that one or more of the S/A threat groups successfully intercept the A/G weapon, i.e.,

$$P_{\text{surv}} = 1 - P_{\text{kill}}, \quad (5.12)$$

As mentioned earlier, solving the differential equation (B.3) produces the probabilities for the S/A threat group  $k$  to be in each of the states at any given time  $t$ , i.e., the state probabilities. The state probabilities of each of the  $k = 1 \dots N$  S/A threat groups are combined to determine the probabilities that one or more threat groups  $k$  have successfully intercepted the A/G weapon, i.e.,  $P_{\text{kill}}(t)$ . Additionally probabilities that, for instance, one or more S/A threat groups  $k$  have advanced to state “Engaged” but no S/A threat group  $k$  has yet successfully intercepted the A/G weapon can be calculated.

In the special case that exact locations for the S/A threat systems are known, the probability maps used to determine the state transition rates of single S/A threat systems in Equation (5.10) are simplified to equal one in the location where the S/A is located and zero elsewhere.

With the exception of probability maps used with the Erlandsson survivability model, it does not take into account any topological features of the surrounding terrain or the tree cover height. Due to this feature, the Erlandsson model might give relatively small survivabilities for trajectories which use shadows cast by the terrain to evade the S/A threat systems.

## 5.2 Technical model

The technical survivability model strives to take into account the technical aspects and requirements for detections needed to form and maintain a track of an A/G weapon by a radar sensor [34]. Similar to the other models discussed in this thesis, the technical survivability model also distinguishes target acquisition, fire control track formation and track maintenance while intercepting the A/G weapon as the distinct stages of the process leading from the first detection of the A/G weapon to its successful interception. Unlike in the other models discussed in this thesis, track formation is not assumed to be a Poisson process but instead a Bernoulli process which lasts a predetermined length of time and for which the outcome probabilities depend on the probabilities of detection by the radars under consideration. As the outcome probabilities of the successful track formation processes depend on the detection probabilities of the radars, the model takes into account the directional dependencies of the A/G weapon's radar cross section as well as any possible shadows cast by the terrain. Unlike the other survivability models studied in this thesis which are time-continuous, the technical survivability model addresses time in discrete time steps. The time discretisation step size is denoted by  $\Delta t$ .

In order to determine the probability of the A/G weapon's successful interception by the S/A defence, the technical survivability model separately calculates two distinct probabilities each of whom describes the probability of success in different stages of the process of intercepting the A/G weapon. The probabilities which are calculated are the probability of a track successfully being formed by the target acquisition radars  $i = 1 \dots n_k$  of each threat group  $k$  denoted by  $(P_{TA}^k)$  and the probability that the fire control radar of each threat unit  $j = 1 \dots m_k$  is capable of maintaining the track long enough to successfully intercept the A/G weapon with

the S/A threat unit's weapon denoted by  $(P_{\text{TM},j}^k)$ . The probability that a single chain of events which begins from the first detection by the target acquisition radars  $i = 1 \dots n_k$  of threat group  $k$  leads to the S/A threat unit  $j$  successfully intercepting the A/G weapon is calculated as

$$P_{\text{intrept},j}^k = P_{TA}^k \times P_{\text{TM},j}^k \times P_{\text{missile}}, \quad (5.13)$$

where  $P_{\text{missile}}$  is the probability that an S/A threat successfully intercepts the A/G weapon, given that the A/G weapon has been successfully tracked by the target acquisition radars and the fire control radar of the S/A threat unit is capable of maintaining the track for a sufficient length of time.

The technical survivability model assumes that when in search mode, the radar sensors scan the airspace around them in an organised fashion. The scan time  $T_{\text{scan}}$  is the time in which the searching radar scans the entire search area. Thus, the interval at which the radar is capable of detecting the A/G weapon is  $T_{\text{scan}}$ . It is assumed that in order for the target acquisition radar  $i$  to achieve a track of the A/G weapon, it must detect the A/G weapon on  $N_{\text{track}}$  subsequent scans. The probability that the radar sensor successfully detects the A/G weapon on any single attempt is determined as described in Appendix A. The process of forming a track of the A/G weapon by a searching target acquisition radar  $i$  is portrayed in Figure 5.3. In order for the target acquisition radar  $i$  to obtain a track of the A/G weapon at time  $t$ , the first detection of the A/G weapon must be achieved at time  $t - (N_{\text{track}} - 1)T_{\text{scan}}$ .

In order to take into consideration the uncertainty regarding the locations of the target acquisition radar  $i$ , the probability of successfully forming a track of the A/G weapon at time  $t$  is first determined for every possible location  $(x, y)$  of the target acquisition radar  $i$ . The probability that the target acquisition radar  $i$  at location  $(x, y)$  achieves a track of the A/G weapon at time  $t$ , i.e., it detects the A/G weapon for the first time at time  $t - (N_{\text{track}} - 1)T_{\text{scan}}$  and is consequently able to successfully detect the A/G weapon on  $N$  subsequent scans, is calculated with

$$P_{\text{track}}^{(x,y)}(t) = \frac{\Delta t}{T_{\text{scan}}} \prod_{n=1}^{N_{\text{track}}} P_D^{(x,y)}(t_n), \quad (5.14)$$

in which  $\Delta t$  is the time discretisation step and  $P_D^{(x,y)}(t_n)$  is the probability that the target acquisition radar located at  $(x, y)$  is able to detect the A/G weapon at time  $t_n$  (see Equation (A.18)). The probability that the searching target acquisition radar is scanning in the direction of the A/G weapon at times  $t - (n - 1)T_{\text{scan}}$  is  $\Delta t/T_{\text{scan}}$ .

Given the time  $t$  when the track is successfully formed, the times  $t_n$  at which the target acquisition radar must have detected the A/G weapon to form the track are

$$t_n = t - (N_{\text{track}} - n)T_{\text{scan}}, \quad (5.15)$$

where  $N_{\text{track}}$  is the amount of number of detections needed to form a track. The

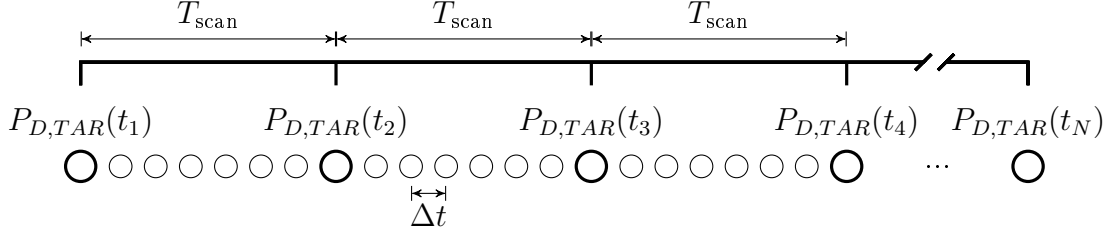


Figure 5.3: The process of forming a track of the A/G weapon by a target acquisition radar.

probabilities of successfully forming a track from the different possible locations are then combined with the probability map  $P_{L,i}^k(x, y)$  calculated with Equation (4.3) to form the expected probability of successfully forming a track for the target acquisition radar  $i$  at time  $t$ :

$$\text{E} [P_{\text{track},i}^k(t)] = \sum_{(x,y)} P_{L,i}^k(x, y) P_{\text{track}}^{(x,y)}(t), \quad (5.16)$$

where the superscript  $i$  refers to the  $i$ th target acquisition radar in a given S/A threat group  $k$ . Further, the probability that one or more target acquisition radars in the S/A threat group  $k$  successfully achieve a track of the A/G weapon at time  $t$  is determined by

$$P_{TA}^k(t) = 1 - \prod_{i=1}^{n_k} (1 - \text{E} [P_{\text{track},i}^k(t)]), \quad (5.17)$$

in which  $n_k$  is the number of target acquisition radars in the given S/A threat group  $k$ .

Once the target acquisition radars have achieved the track of the A/G weapon, the track is handed over to the threat units  $j = 1 \dots m_k$  of the S/A threat group  $k$ . The fire control radars of the threat units operate with a different principle than the searching target acquisition radars. Once the track has been handed over to an S/A threat unit  $j$ , the threat unit's fire control radar proceeds to concentrate all of its efforts to detect the A/G weapon at the location determined by the track it was given. The frequency at which the fire control radar attempts to detect the A/G

weapon is referred to as the pulse repetition frequency  $PRF$ . The interval between two detection attempts is referred to as the pulse repetition time  $PRT = PRF^{-1}$ . In order to maintain the track, the fire control radar must successfully detect the A/G weapon at least once during each track maintenance period  $T_{\text{maint}}$ . Thus, the fire control radar has  $M = PRF \times T_{\text{maint}}$  attempts during each maintenance period to detect the A/G weapon before the track is lost. Furthermore, the track must often be maintained for a period longer than the maintenance period  $T_{\text{maint}}$  in order to successfully intercept the A/G weapon. This period during which the A/G weapon must be tracked corresponds to the time taken to acquire the track by the fire control radar, the time needed to aim the S/A threat's weapon, and the flight time of the missile or other A/G weapon used to intercept the A/G weapon, all combined. This time period is denoted by  $T_{\text{track}}$ .

To take in consideration uncertainties concerning the location of an S/A threat unit  $j$ , the probability of successfully maintaining the track for the complete required period of  $T_{\text{track}}$  is calculated for every possible location  $(x, y)$  of the S/A threat unit  $j$ . First, the probability of successfully maintaining the track for a single track maintenance period  $T_{\text{maint}}$  is determined. The probability that a track is maintained for the duration of the track maintenance period beginning at time  $t$  by a fire control radar located at coordinates  $(x, y)$  is calculated as

$$P_{\text{maint}}^{(x,y)}(t) = 1 - \prod_{m=1}^M \left(1 - P_D^{(x,y)}(t_m)\right), \quad (5.18)$$

in which  $t_m$  is the time of the  $m$ th attempt to detect the A/G weapon, i.e.,  $t_m = t + (m - 1)PRT$ , and  $P_D^{(x,y)}(t_m)$  is calculated with Equation (A.18). Furthermore, the probability that a fire control radar at location  $(x, y)$  is able to maintain the track for the whole period of length  $T_{\text{track}}$  starting at time  $t$  is determined by

$$P_{TM}^{(x,y)}(t) = \prod_{\kappa=1}^K P_{\text{maint}}^{(x,y)}(t_\kappa), \quad (5.19)$$

where  $P_{\text{maint}}$  is calculated with Equation (5.18),  $K$  is the number of track maintenance periods that are included in the time period  $T_{\text{track}}$ , and  $t_\kappa$  refers to the time at which the  $\kappa$ th track maintenance period begins, i.e.,  $t_\kappa = t + (\kappa - 1)T_{\text{maint}}$ . Now the expected probability of S/A threat unit  $j$  of S/A threat group  $k$  successfully

maintaining the track of the A/G weapon is calculated with

$$\mathbb{E} [P_{\text{TM},j}^k(t)] = \sum_{(x,y)} P_{L,j}^k(x,y) P_{\text{TM}}^{(x,y)}(t), \quad (5.20)$$

where probability map  $P_{L,j}^k(x,y)$  gives the probability that S/A threat unit  $j$  is located at location  $(x,y)$  and is calculated with Equation (4.3).

By substituting Equations (5.17) and (5.20) into Equation (5.13), the probability that the single chain of events leads to the S/A threat unit  $j$  successfully intercepting the A/G weapon at time  $t$  is

$$P_{\text{intrcpt},j}^k(t) = P_{TA}^k(t - T_{\text{track}}) \times \mathbb{E} [P_{\text{TM},j}^k(t - T_{\text{track}})] \times P_{\text{missile}}, \quad (5.21)$$

where  $P_{\text{missile}}$  is the probability that the S/A weapon is successful in intercepting the A/G weapon assuming that the target acquisition radars  $i = 1 \dots n_k$  have successfully formed the track of the A/G weapon and the fire control radar of the fire control unit  $j$  has been able to maintain the track for the time needed for the S/A weapon to intercept the A/G weapon. Equation (5.21) describes the probability that the given threat unit  $j$  succeeds in intercepting the A/G weapon at time  $t$  assuming that the threat unit has not intercepted the A/G weapon at an earlier point in time. The probability for the given threat unit  $j$  to intercept the A/G weapon specifically at time  $t$  is calculated by

$$P_{\text{hit},j}^k(t) = P_{\text{intrcpt},j}^k(t) \times \prod_{n=1}^{t-1} (1 - P_{\text{intrcpt},j}^k(n)). \quad (5.22)$$

Using Equation (5.22), the probability that the A/G weapon is intercepted by S/A threat unit  $j$  of S/A threat group  $k$  at any point on the trajectory is determined with

$$P_{\text{hit},j}^k = 1 - \prod_{t=1}^{N_{\text{trajectory}}} P_{\text{hit},j}^k(t), \quad (5.23)$$

where  $N_{\text{trajectory}}$  is the number of time discretisation steps needed to traverse the entire trajectory.

With Equation (5.23), the probability that the A/G weapon is intercepted on the given trajectory by any of the S/A threat units  $j = 1 \dots m_k$  of any of the S/A

threat groups  $k = 1 \dots N$  is determined with

$$P_{\text{kill}} = 1 - \prod_{k=1}^N \prod_{j=1}^{m_k} (1 - P_{\text{hit},j}^k), \quad (5.24)$$

where  $N$  is the number of S/A threat groups and  $m_k$  is the quantity of S/A threat units in threat group  $k$ . Finally, the survivability of the trajectory is determined with

$$P_{\text{surv}} = 1 - P_{\text{kill}}, \quad (5.25)$$

where  $P_{\text{kill}}$  is calculated with Equation (5.24).

In case the exact locations of S/A threat systems are known, the technical survivability model is used in a similar fashion, only the probability maps  $P_{L,i}^k$  and  $P_{L,j}^k$  differ. If the exact locations of the S/A threat systems are known, the probability maps used in Equations (5.16) and (5.20) are simplified so that the probability map equals one at the location in which the S/A threat system is located and zero elsewhere.

The technical survivability model takes into account the topological features of terrain and possible tree cover in a similar way as the Markov survivability model. In addition to the probability map, any possible topological features and tree cover are taken into account in the calculation of the probabilities of detection  $P_D^{(x,y)}(t)$  used in Equations (5.18) and (5.14) so that if there are visual obstructions due to the terrain or the trees, the probability of detection is zero.

# Chapter 6

## Numerical experiments

In this chapter, the trajectory evaluation framework introduced in Chapter 4 is tested to ensure results given by the framework in whole and its parts alone produce reasonable outcomes. In Chapter 6.1, the spatial prediction model is tested with a case set in the area surrounding Otaniemi in Espoo, Finland. A probability map is produced for a single S/A threat system and the probability map is inspected to ensure that it is reasonable and coincides with reality. Next, the probability map reduction method presented in Chapter 4.1.2 is inspected with two test cases in Chapter 6.2. The aim is to prove that the probability map reduction method preserves the characteristics which are important related to the survivability of trajectories reflected by the original probability map, i.e., the expected probabilities of detection. In Chapters 6.3.1 and 6.3.2, the Markov survivability model is compared with the reference survivability models. The models are compared with respect to the consistency of their results versus the results of other models, and the results are also evaluated with intuition and common sense. In Chapter 6.3.1, the robustness of the models in respect to uncertainty regarding the locations of S/A threat systems is inspected with the aim to show that the Markov model handles uncertainty well. Here the robustness of the models portrays the models' ability to preserve the threat ordering of trajectories based while degree of uncertainty regarding the locations of S/A threats is varied. The survivabilities of drastically different trajectories provided by the Markov survivability model and the reference models are studied in Chapter 6.3.2. The purpose of Chapter 6.3.2 is to show that the Markov survivability model gives reasonable results even with extreme trajectories.

## 6.1 Illustration of spatial prediction model

The usage of the spatial prediction model is demonstrated with an example scenario, for which data sets are shown in Figure 6.1. The direction from which an attack is anticipated is north. In order to form the probability map, the passability, visibility,

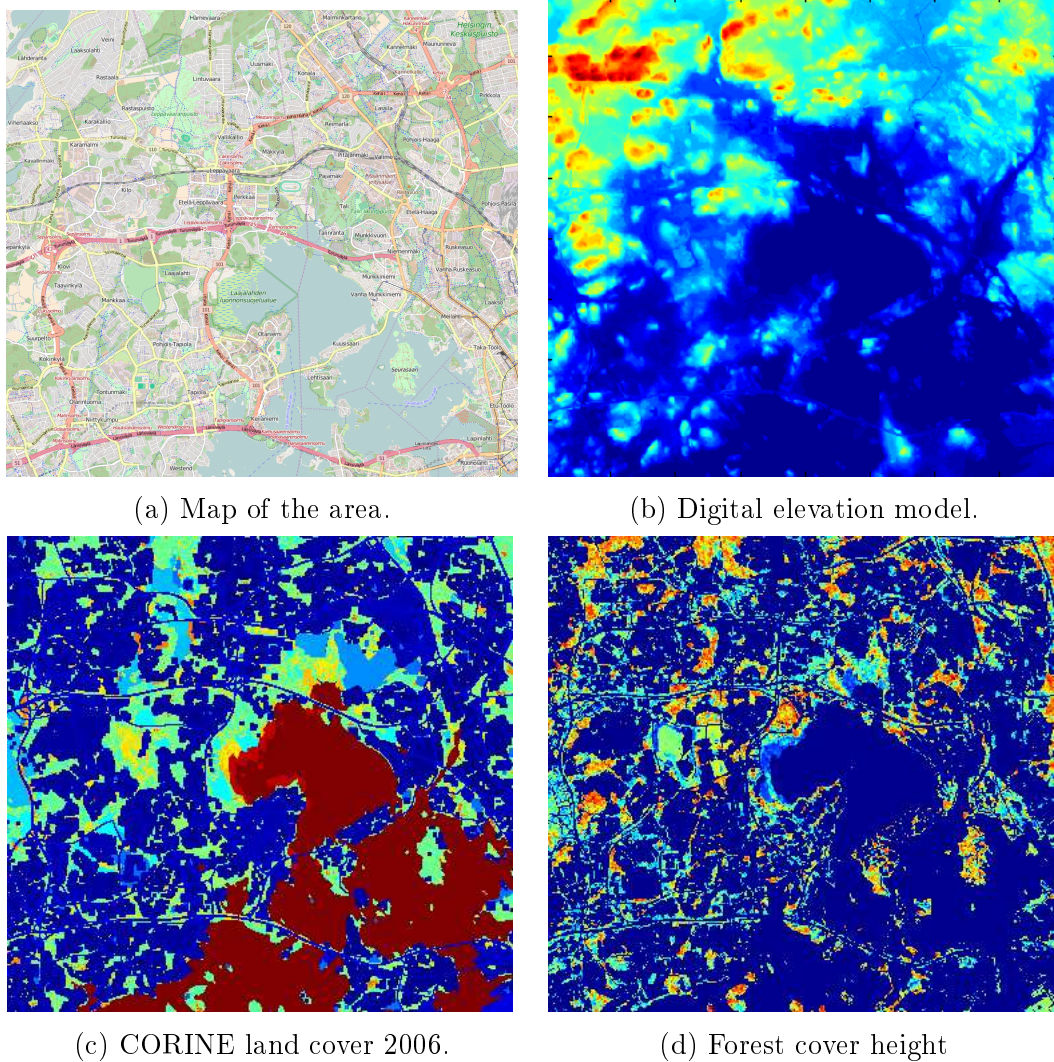
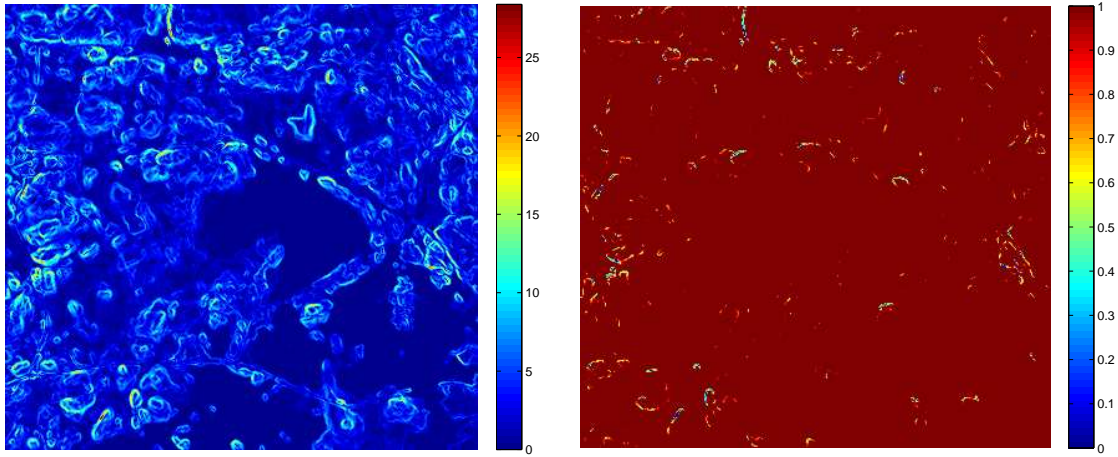


Figure 6.1: Data sets used in the spatial prediction model.

and grouping indices are calculated for each location. These indices are calculated with Equations (4.4), (4.8) and (4.14), respectively. The intermediate results needed to determine the indices, i.e., the slope angle and coefficient, the velocity at which an S/A threat can traverse the terrain, the time needed to reach any given location, and average visibility from any given location are shown in Figures 6.2, 6.3, 6.4, and 6.5.

The passability, visibility, and grouping indices are shown in Figure 6.6. The



(a) Slope angle in degrees ( $\phi$ ).

(b) Slope coefficient ( $C_{\text{slope}}$ ).

Figure 6.2: Slope angle and coefficient for the area of the example scenario with parameters  $\Phi_{\text{low}} = 10^\circ$  and  $\Phi_{\text{high}} = 20^\circ$ .

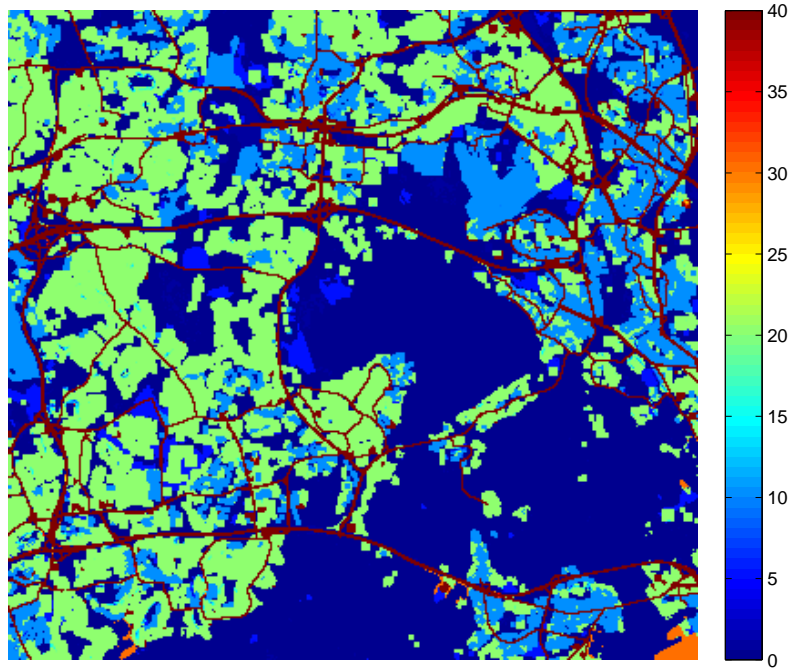


Figure 6.3: Velocity at which it is possible to traverse the terrain (km/h).

passability index (Fig. 6.6a) is given the value 1 for all locations that can be reached without crossing water. This is because all such locations in the area of the example scenario can be reached in a reasonable amount of time. If the area was larger, some areas might possibly be discarded, i.e., the passability index would be zero, since it would be impossible for threat systems to reach them in the given time frame.

Looking at the visibility index (Fig. 6.6b), one notices that the visibility index is

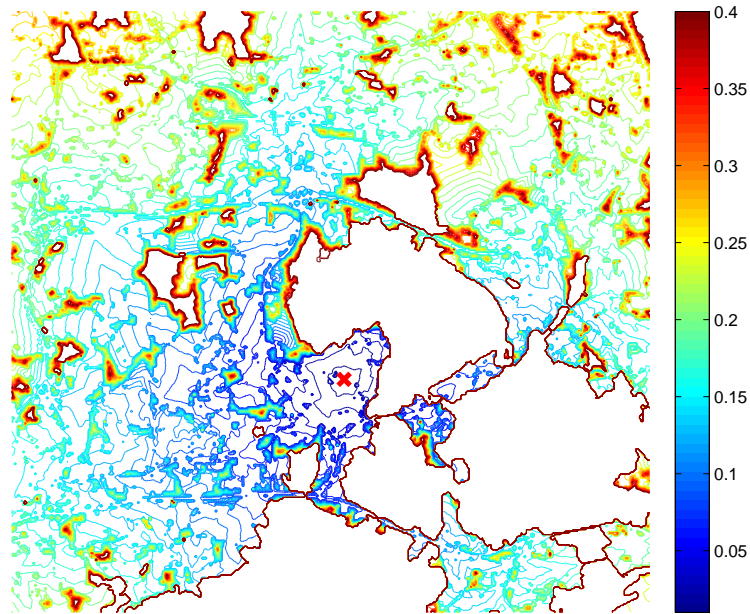


Figure 6.4: Time needed to navigate to any certain location in hours. The depot from which the threat systems spread out is marked with a red cross.

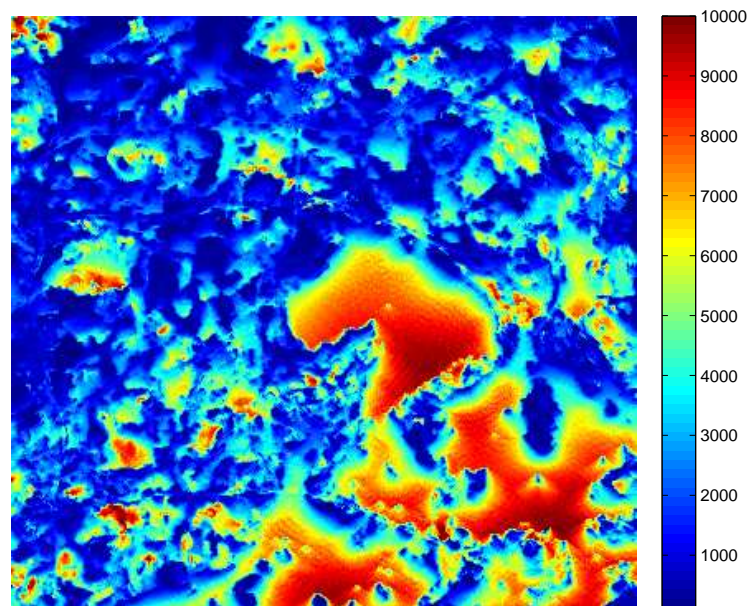
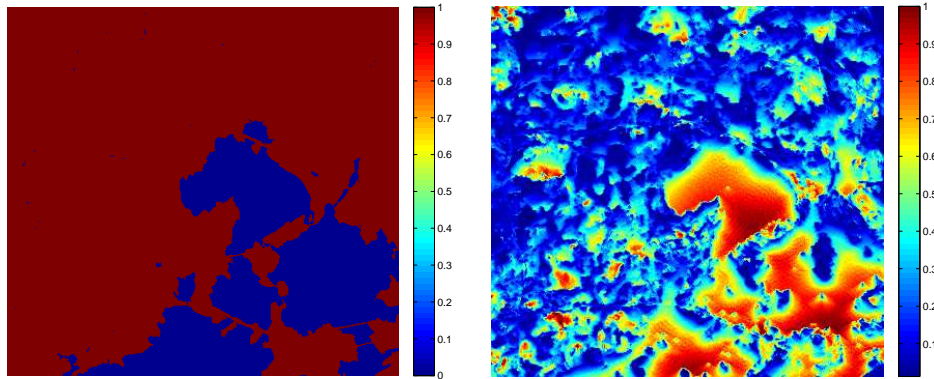


Figure 6.5: Average visibility in metres to an altitude of 150 metres above sea level when facing north in a 120 degree wide sector.

close to 1 at large expanses such as the bay in the area of the example scenario. The visibility index value decreases when the northern shore of the bay is approached. This is because in the example scenario the direction from which an attack is being anticipated is north and as the northern shore is approached the visibility north

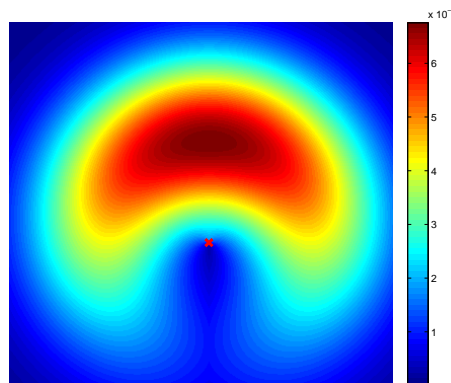
deteriorates. The visibility index is also greater in areas that are higher than the surrounding terrain and which do not have a lot of tree coverage. This is logical since from such locations the visibility is generally good.

The grouping index is portrayed in Figure 6.6c. The target which is being defended is marked with a red cross.



(a) The passability index.

(b) The visibility index.



(c) The grouping index.

Figure 6.6: Different indices from which the probability map is formed.

The resulting probability map is shown in Figure 6.7. Again, the target which is being defended is marked with a red cross. Reflecting on the actual terrain, the resulting probability map seems plausible. The locations where a high probability is given for the threat system to be situated are mostly locations with little or no tree coverage and often on top of hills.

An actual view from a location where the probability map gives a relatively high probability for a threat system to be located is shown in Figure 6.8. The view is facing north from the location marked with a red circle in Figure 6.7. As the photograph in Figure 6.8 is taken from a car, it is safe to say that the location is easily accessible. The visibility from the given location is also excellent, which is

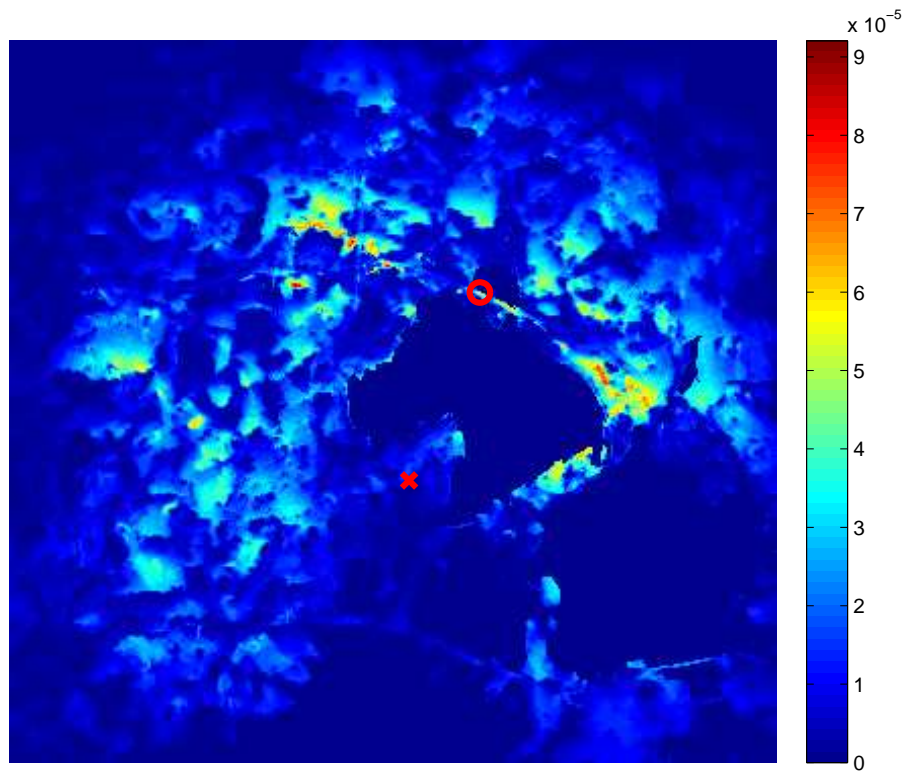


Figure 6.7: The probability map.



Figure 6.8: View from a highly probable location (source: Google Maps).

seen from Figure 6.8. The location in question should be a good location for the S/A threat system to operate, and thus it should be a location where it should be expected that such a threat system could be stationed.

Further, the probability map reduction method is used to reduce the probability

map shown in Figure 6.7 to 20 discrete locations. The first six repetitions of the *Assignment* and *Update* steps in the execution of the probability map reduction method described in Chapter 4.1.2 with the probability map from the example scenario are shown in Figure 6.9. The black dots indicate the positions of the set prototypes at the beginning of each repetition and the red crosses mark the new positions of the set prototypes into which they are moved in the *Update* step.

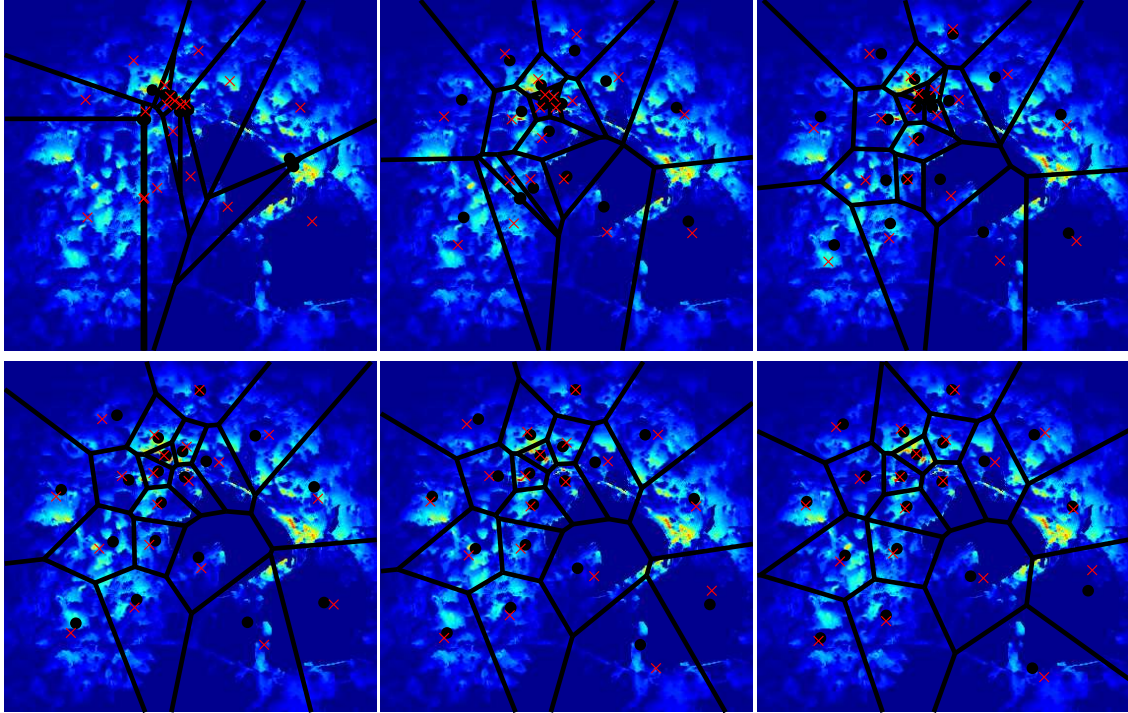


Figure 6.9: The first six repetitions of the *Assignment* and *Update* steps in the execution of the probability map reduction method.

The final converged collection of sets, corresponding set prototypes and final reduced locations for the example execution of the algorithm are shown in Figure 6.10. The black dots in Figure 6.10 represent the final set prototypes of the converged sets, and the red crosses mark the reduced locations used as the reduced probability map. Figure 6.10 implies that the resulting probability map is reasonable. The areas in which the probability map gives a zero probability for an S/A threat unit to be located are areas which are covered by water, i.e., in this case part of the Baltic Sea. Thus, it would be impossible for the S/A threat systems in question to operate there. As noted earlier with Figures 6.7 and 6.8, the areas which are highlighted as likely locations are mostly locations with higher altitude than the surrounding terrain and little or no tree cover. The reduced probability map highlights these same areas with the final reduced probability map locations.

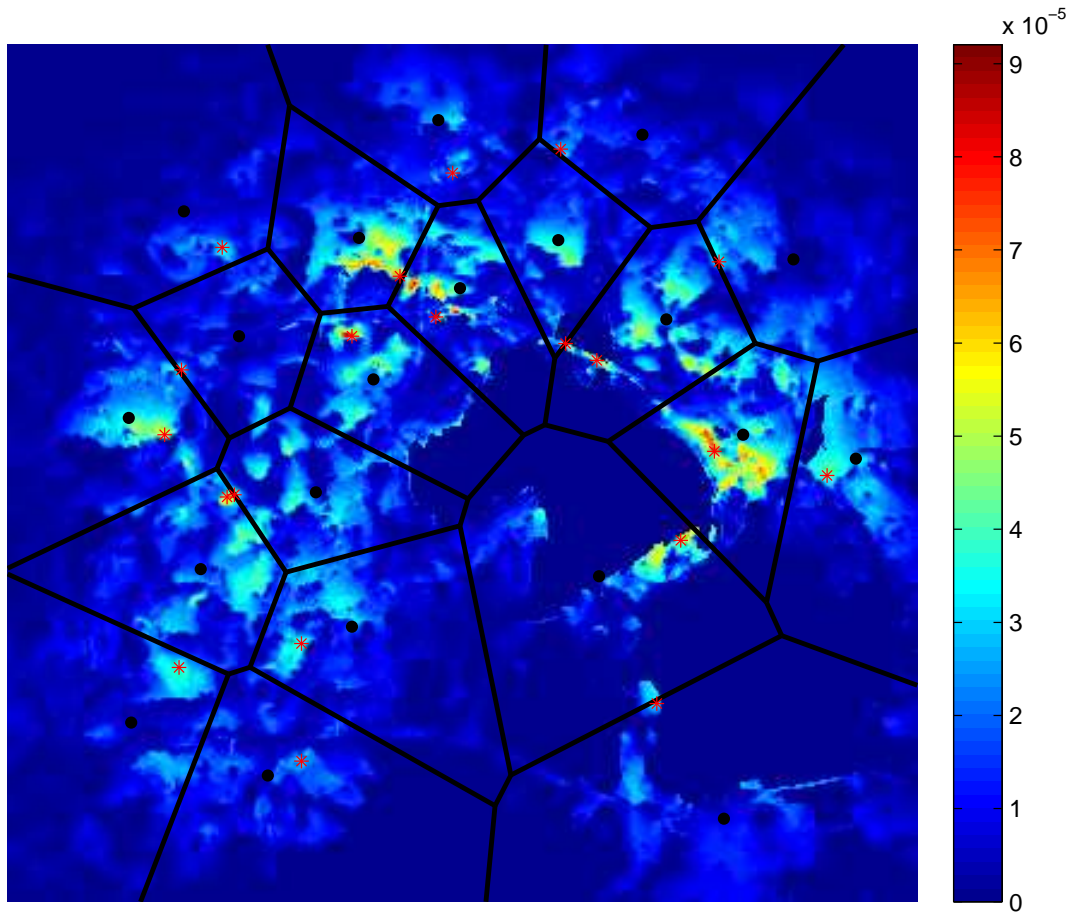


Figure 6.10: The final converged locations sets, corresponding set prototypes and final reduced probability map locations.

## 6.2 Verification of probability map reduction

Reduced probability maps produced by the probability map reduction method presented in Chapter 4.1.2 must be verified to make sure that they still approximate the original probability maps regarding S/A threat systems' capabilities to detect an A/G weapon with sufficient accuracy. To carry this out, the airspace around the area described by the probability map is divided into a grid with horizontal edges roughly one nautical mile and vertical edges roughly half a nautical mile long, and the expected probability of detection is determined for an A/G weapon with different orientations in each grid based on the reduced probability maps with different cluster quantities. The cluster quantity corresponds with the number of possible discrete locations into which the probability map is reduced. These expected detection probabilities are compared with the expected probabilities of detection calculated based on the original probability map.

The expected probability of detection of an A/G weapon located at coordinates  $(x, y, z)$ , heading in direction  $\phi$  with yaw angle  $\theta$  and roll angle  $\psi$  is calculated with

$$E [P_D(x, y, z, \phi, \theta, \psi)] = \sum_{(x', y')} \left( P_L(x', y') P_D^{(x', y')}(x, y, z, \phi, \theta, \psi) \right), \quad (6.1)$$

where  $P_D^{(x', y')}$  is the probability of detection for the A/G weapon by a sensor located at coordinates  $(x', y')$  and is calculated with Equation (A.18) and  $P_L(x', y')$  is the probability map which is calculated with Equation (4.3). The probability of detection  $P_D$  is dependent on all of the A/G weapon's six degrees of freedom because the radar cross section of the A/G weapon changes depending on which part of the weapon is facing the radar.

The different orientations of the A/G weapon for which the probabilities of detection are calculated at each grid location are shown in Figure 6.11. Different grid locations are marked in Figure 6.11 with dots, the left subfigure views the grid from above and the right subfigure gives a horizontal view of the grid. The arrows in the left subfigure of Figure 6.11 depict the different heading angles  $\phi$  for which the expected probabilities of detection are calculated. The right subfigure of Figure 6.11 shows the different pitch angles  $\theta$  with which the expected detection probabilities calculated based on the original and reduced probability map are compared. The roll angle  $\psi$  is always set to be zero in the comparisons.

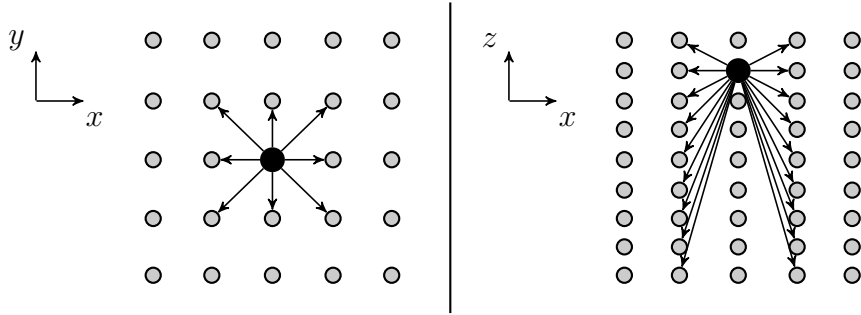


Figure 6.11: Different orientations of the A/G weapon for which the probabilities of detection are calculated in each grid.

The expected probability of detection (6.1) is calculated at each grid location with each orientation of the A/G weapon based on the original probability map and the reduced probability maps with alternative cluster quantities. The residuals of the expected probability of detection caused by the use of the reduced probability map are calculated as the difference between the expected probability of detection based on the original probability map and the expected probability of detection

based on the reduced probability maps. Different metrics are calculated based on the residuals, and these are shown in Figure 6.12 as a function of the cluster quantity used in the probability map reduction. The cluster quantity is the number of areas the original probability map is divided into, and thus also the amount of final reduced probability map locations produced by the probability map reduction method. The metrics are the mean of the residuals and the standard deviation of the residuals.

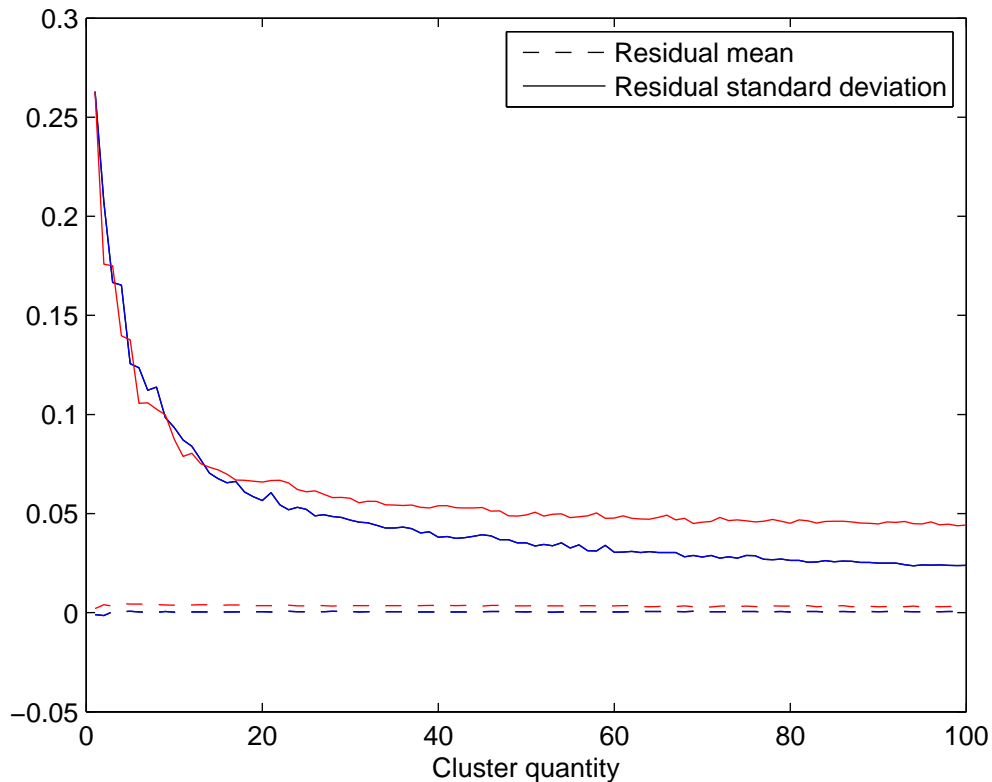


Figure 6.12: Residual means and standard deviations of the expected probabilities of detection based on the reduced probability map.

As seen from Figure 6.12, the mean of the residuals is close to zero even with very small cluster quantities used in the probability map reduction. Thus, it can be said that the approximated expected probabilities of detection are on average consistent with the detection probabilities based on the original probability map even with very few clusters being used in the reduction. However, with small cluster quantities there is quite a lot of variance in the residuals, i.e., even though the approximated expected detection probabilities are on average correct, individual approximated expected probabilities deviate quite a lot from the expected probabilities of detection based on the original probability map. As the number of clusters is increased, the variance

and thus also the standard deviation of the residuals decreases rapidly. Based on these observations, it is reasonable to conclude that the probability map reduction method presented in this thesis approximates the probability map sufficiently in respect to the expected probabilities of detection when the cluster quantity is set to be high enough.

### 6.3 Comparison of survivability models

The Markov survivability model presented in this thesis is verified and compared against the reference survivability models, i.e., the Erlandsson model and the technical survivability model. The models are compared by evaluating trajectories with each of the survivability models in two different scenarios and inspecting the accumulation of risk in different models. The survivabilities of the trajectories are set in priority order, with the best trajectory corresponding to the trajectory with the greatest survivability. These orderings of the trajectories based on the survivability models are then compared with each other. The models are compared with each other regarding the consistency of the results between the models and also in regard to common sense and reality. Also, the models' robustness is tested in respect to the amount of uncertainty regarding the locations of S/A threat systems in the area, i.e., how well the model retains the ordering of trajectories based on the trajectories' survivabilities when location uncertainty is varied. The first scenario is set around Otaniemi in Espoo, Finland while the second scenario is set in the country around and to the west of Hyvinkää, Finland.

In both scenarios, the S/A air defence strives to defend a single target. The S/A air defence in each scenario consists of multiple S/A threat groups, each of which in turn consists of four different types of S/A threat systems: medium range S/A missile systems, short range S/A missile systems, anti-aircraft guns and target acquisition radars. The medium range S/A missile systems, the short range S/A missile systems and the anti-aircraft guns are threat units and thus include in addition to the actual S/A weapon a fire control radar. The ranges  $R_{\max}$  of the medium range S/A missile systems, the short range S/A missile systems and the anti-aircraft guns are 15 km, 5 km and 7 km, respectively. In the example scenarios, the S/A threat units differ from each other only by the effective range of their weapons. In each of the radars, the height of the radar  $h_{\text{obv}}$  is 15 metres. The radio cross-section model used in the example scenarios is a realistic model for an A/G weapon, with a mean radar cross-section of about 5 m<sup>2</sup> but a median radar cross-section of only about 0.1 m<sup>2</sup>.

Thus, the radar cross-section of the A/G weapon is generally quite small. However, it also has significant “spikes”, corresponding to directions from which it is easy to detect the A/G weapon.

A thorough listing of the parameters used in the example scenarios is given in Tables 6.1, 6.2, and 6.3. The values of the state transition rates  $\lambda$  in Tables 6.1 and 6.2 can be thought of as the reciprocals of the actual times needed for the state transfer in question. For example, if the time needed to form a track is on average 12 seconds, the state transition rate  $\lambda_{U,T}$  in the Markov survivability model is  $1/12$ . This corresponds to the parameters of the technical survivability model for which the scan time  $T_{\text{scan}}$  is 6 seconds and the track criteria  $N_{\text{track}}$  is 2. Thus, the time needed to form a track is  $6 \text{ s} \times 2 = 12 \text{ s}$ . Similarly, the average time taken to advance from state “Undetected” to “Tracked” via the state “Detected” in the Erlandsson survivability model is  $6 \text{ s} + 6 \text{ s} = 12 \text{ s}$ . The threshold probability of detection  $P_{D,\text{min}}$  is set to be 0.8 for the Erlandsson survivability model. This threshold is used in calculating the radii  $\rho_{\text{max}}$  of the sensor and threat areas with Equation (5.9).

Table 6.1: Parameters of the Markov survivability model used in the example scenarios.

$\lambda_{U,T}$	$\lambda_{T,U}$	$\lambda_{T,L}$	$\lambda_{L,T}$	$\lambda_{L,H}^{\text{const}}$
1/12	1/5	1/6	1	1/10

Table 6.2: Parameters of the Erlandsson model used in the example scenarios.

	$\lambda_{U,D}$	$\lambda_{D,U}$	$\lambda_{D,T}$	$\lambda_{T,D}$	$\lambda_{T,E}$	$\lambda_{E,T}$	$\lambda_{E,H}$
Outside	0	1	0	1	0	1	0
Sensor area	1/6	0	1/6	0	0	1	0
Threat area	0	1	0	1	1/6	0	1/3

Table 6.3: Parameters of the technical model used in the example scenarios.

Time discretisation step ( $\Delta t$ )	1 s
Scan time ( $T_{\text{scan}}$ )	6 s
Track criteria ( $N_{\text{track}}$ )	2
Pulse repetition time ( $PRT$ )	0.1 s
Maintenance period ( $T_{\text{maint}}$ )	1 s

The accumulation of risk obtained with the survivability models is studied by qualitative comparison of the threat profiles of trajectories, i.e., the state probabilities at given time  $t$  achieved when solving the differential equation (B.3). The

trajectories are ordered based on the survivabilities determined with each survivability model. Then, these orderings are compared. Also, each model's sensitivity to uncertainty regarding the position of the S/A threat systems, i.e., how well each model preserves the ordering of the trajectories based on each trajectory's survivability, is inspected by first evaluating the trajectories based on exact locations and gradually increasing the uncertainty of the S/A threat systems' positions while evaluating each trajectory after every increment of the position uncertainty. The uncertainty is increased by increasing the size of the area in which it is believed that each S/A threat system is located. All of the trajectories studied in Chapters 6.3.1 and 6.3.2 are parabolic, i.e., air resistance is not taken into consideration. The horizontal velocity of the A/G weapon is constant 350 m/s in every trajectory, and the A/G weapon is initially in a purely horizontal motion.

### 6.3.1 Otaniemi scenario

The first example scenario is set around Otaniemi in Espoo, Finland. The air defence consists of four S/A threat groups, all of whom include a target acquisition radar. Additionally, two of the S/A threat groups include four anti-aircraft guns and one of the groups contains four short range S/A missile systems. One S/A threat group contains a medium range S/A missile system. The grouping areas of the different S/A threat systems in each threat group are portrayed in Figure 6.13. The grouping area of an S/A threat is a geographic area in which it is thought that the S/A threat system is located. In the examples, the grouping index of the spatial prediction model is set to be two-dimensional normal distributions defined by the grouping areas. The center of the grouping area corresponds to the expected value of the *a priori* probability map, i.e., the grouping index in the spatial prediction model. Similarly, the distance of the edges from the center of the grouping area corresponds to one standard deviation in the grouping index of the spatial prediction model. The relation between the grouping area of the S/A threat system, the expected location of the S/A threat system and the standard deviations of the S/A threat system's location are portrayed in Figure 6.14.

Three different trajectories are evaluated with the Markov survivability model and each of the reference models. The trajectories originate from an altitude of about 10 kilometres and ultimately reach the target which is set in the middle of Otaniemi in Espoo, Finland. The trajectories differentiate from each other only by the direction from which they originate from. The first trajectory begins north-west from Otaniemi, the second begins north from Otaniemi while the third begins from

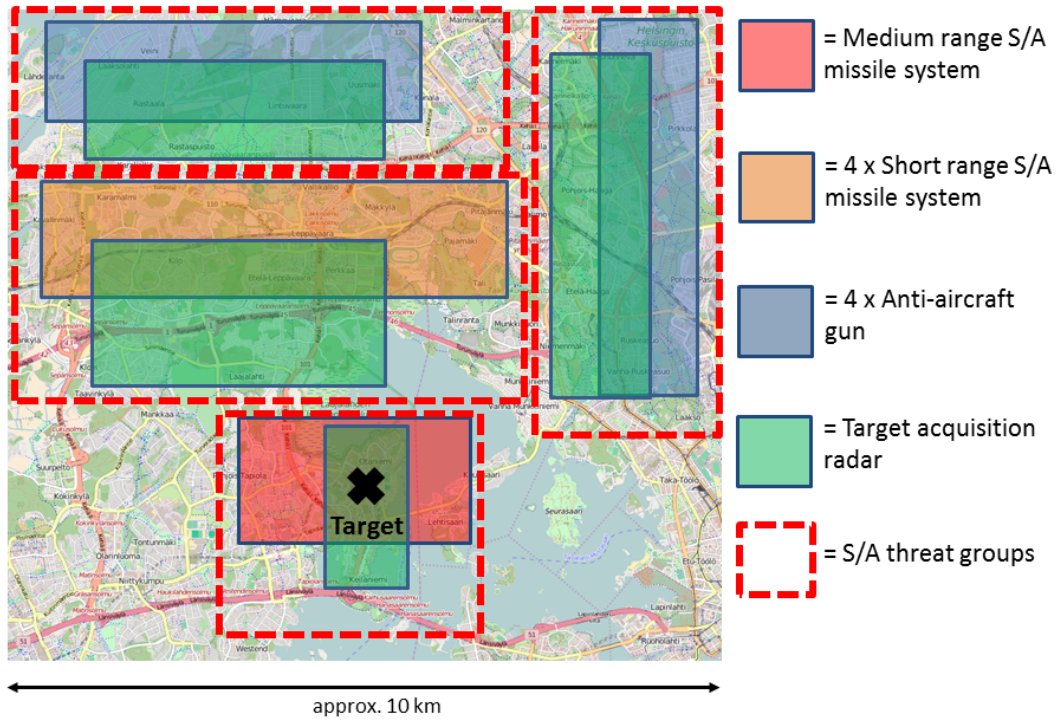


Figure 6.13: The grouping areas of the S/A threat systems.

the north-east of Otaniemi. The trajectories are shown in Figure 6.15.

The locations of the S/A threat systems are assumed unknown and thus probability maps determined with the spatial prediction model are used to determine the survivabilities over each trajectory. The resulting probability maps and resemble that of the probability map shown in Figure 6.7. The survivabilities of the trajectories are given in Table 6.4.

Table 6.4: Survivabilities ( $P_{\text{surv}}$ ) of the trajectories in the Otaniemi scenario.

	Trajectory 1	Trajectory 2	Trajectory 3
Markov model	0.33	0.20	0.28
Erlandsson model	0.79	0.74	0.79
Technical model	0.18	0.16	0.02

As seen in Table 6.4, all models evaluate trajectory 1 to be the best trajectory, i.e., the trajectory with the highest survivability. Both the Markov survivability model and the Erlandsson model evaluate trajectory 3 to be the second safest trajectory but the technical model evaluates trajectory 2 to be the second safest. All of

The grouping area of an S/A threat system

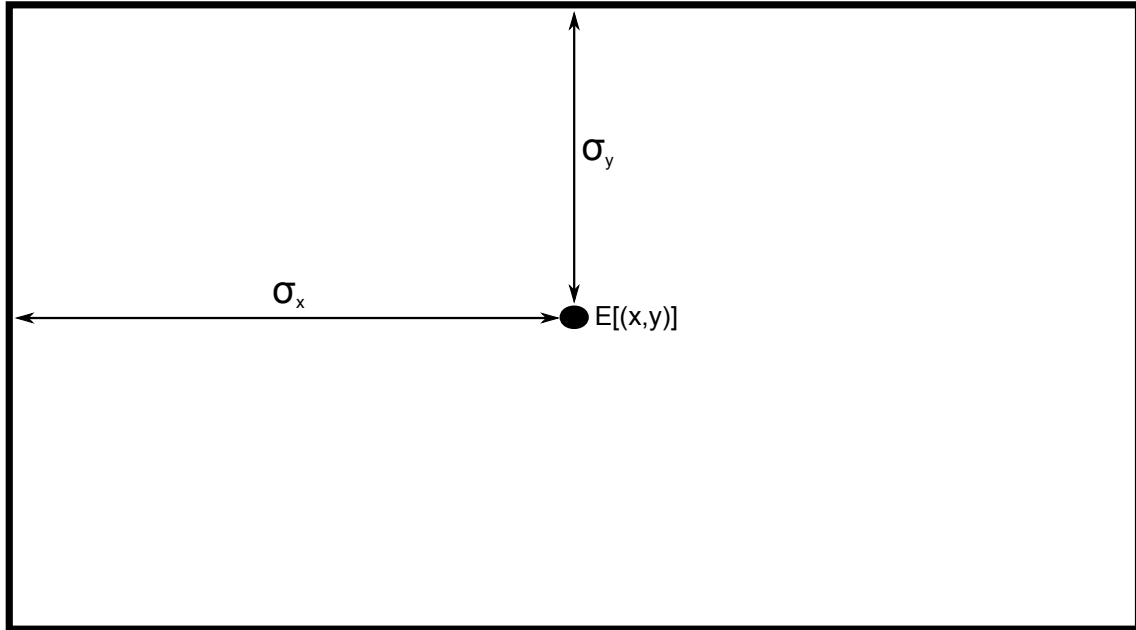


Figure 6.14: The expected location of an S/A threat system, the standard deviations of the S/A threat system's location and the grouping area of the S/A threat system.

the models give consistent results concerning which trajectory is the best, i.e., has the highest survivability.

In order to study the accumulation of risk while traversing a trajectory, stacked area graphs are drawn to illustrate the state probabilities at any given point in time. Such stacked area graphs are shown for trajectory 1 in Figure 6.16. The areas in Figure 6.16 correspond to the probability that at least one Markov chain has reached the state resembled by the area while no Markov chains have reached a "worse" state, i.e., a state further on in the chain. Each Markov chain corresponds to either an S/A threat unit in the Markov survivability model and an S/A threat group in the Erlandsson survivability model. Thus, the area corresponding to the state "Hit" in Figure 6.16 corresponds to the probability that one or more S/A threat units have been able to successfully intercept the A/G weapon, i.e.,  $P_{kill}$ . The probability of the A/G weapon being successfully intercepted at a given time based on the technical survivability model is portrayed by the  $P_{kill}$  curve in the bottommost plot of Figure 6.16.

As is seen from Figure 6.16, the Markov survivability model is quickest to react to the threat and the survivability, i.e., the complement probability of the probability of at least one Markov chain being in state "Hit", begins to decrease after  $t = 10$  s. The reference models are slower to react to the S/A threat and both of them predict

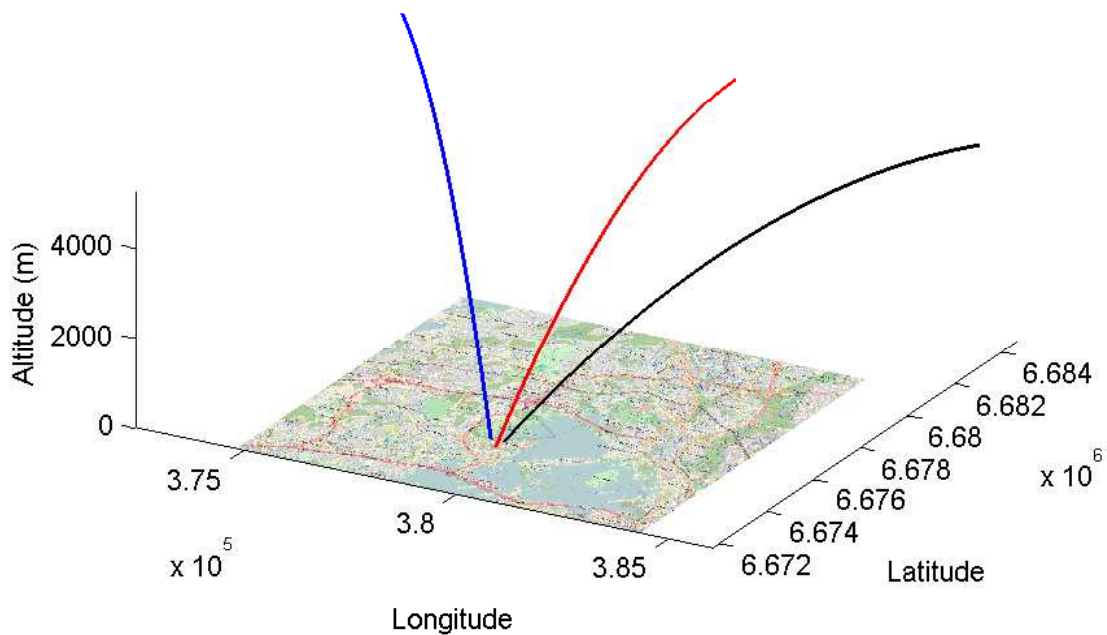


Figure 6.15: The trajectories under consideration. Trajectory 1 is marked with a blue curve, trajectory 2 is marked with a red curve, and trajectory 3 is marked with a black curve.

the survivability to begin decreasing after  $t = 20$  s. Again, each of the models seems to be consistent with each other in this example scenario. In each of the models the probability of being intercepted by an S/A threat increases gradually towards the end of the trajectory.

The models' sensitivity to uncertainty regarding the locations of the S/A threat systems is studied by first evaluating the survivabilities of the trajectories based on the known locations of the S/A threat systems. Then, the locations' uncertainties are gradually increased until the *a priori* knowledge of the threat systems' whereabouts is described by the grouping areas given in Figure 6.13. The uncertainty increased by increasing the size of the grouping areas in which the threat systems are believed to reside, starting from grouping areas of only the known exact locations and ending in the grouping areas depicted in Figure 6.13. The uncertainty regarding the location is characterised with location uncertainty  $\eta$ . The grouping area with location uncertainty  $\eta$  is determined with the known location of the S/A

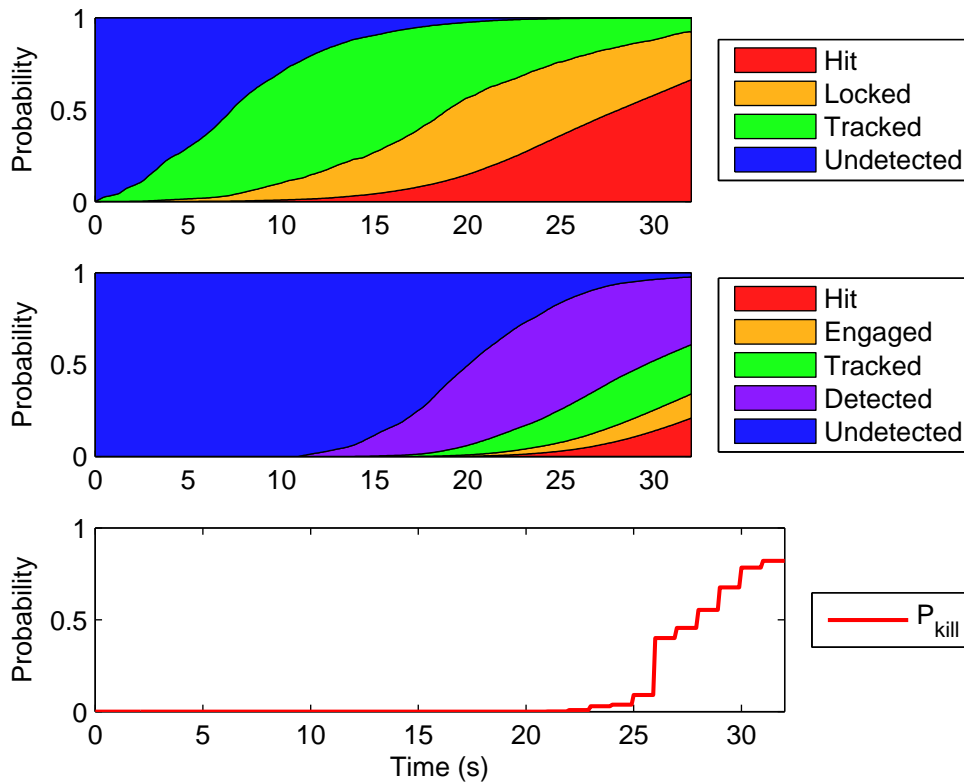


Figure 6.16: Graphs of the state probabilities along trajectory 1 based on the Markov survivability model, the Erlandsson model, and the technical model (top to bottom).

threat system and the original grouping area as shown in Figure 6.17. The location uncertainty  $\eta = 0$  depicts knowledge of exact locations and location uncertainty  $\eta = 1$  depicts grouping areas equal to those shown in Figure 6.13.

The known locations of the S/A threat systems are given in Figure 6.18. The known locations are plausible locations in a sense that there is good visibility from each location, each site is accessible by the threat systems and the locations are in or very near to the grouping areas given in Figure 6.13.

The probability of the A/G weapon being intercepted on each trajectory  $P_{kill}$ , i.e.,  $1 - P_{surv}$ , related to each trajectory is evaluated with location uncertainties  $\eta$  ranging from 0 to 1. The survivabilities of the trajectories with different location uncertainties  $\eta$  are given in Figure 6.19. The Markov survivability model and the Erlandsson model give relatively stable results even though the uncertainty regarding the S/A threat systems' locations is increased, i.e., the ordering of the trajectories based on their survivability does not often change. The results provided by the technical model vary more than the results of the other models. The priority of the

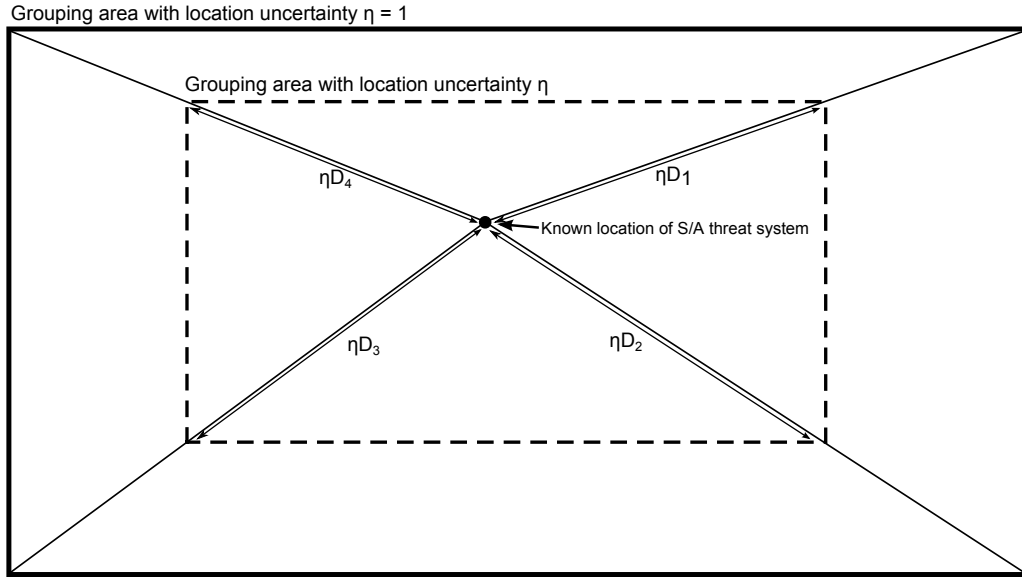


Figure 6.17: The grouping area with location uncertainty  $\eta$ , where  $D_1$ ,  $D_2$ ,  $D_3$ , and  $D_4$  depict the distances from the known location of the S/A threat system to the top right, bottom right, bottom left, and top left corners of the original grouping area, respectively.

trajectories regarding their survivability changes multiple times during the course of increasing the uncertainty when evaluating with the technical model while with the Markov survivability model trajectory 1 remains the safest trajectory throughout the process. Both the Markov survivability model and the Erlandsson model prove to be robust regarding the amount of uncertainty as the ordering of trajectories seldom change while the uncertainty is increased.

Based on the Otaniemi example scenario, the survivability models seem to behave consistently, i.e., all models evaluate trajectory 1 as the best, when uncertainty regarding the locations of S/A threat systems is constant. However, once the uncertainty is varied, differences between the two Markov chain based survivability models and the technical survivability model become clear. The results of the technical survivability model prove to be unstable when the location uncertainty is varied and thus the model would give different results depending on how accurate information regarding the locations of the S/A threat systems is available. Meanwhile, the Markov chain based survivability models both produce relatively consistent survivabilities for the trajectories, which is seen in Figure 6.19. Based on the Otaniemi example scenario not much can be said regarding the differences between the Markov survivability model and the Erlandsson model. Both give similar results and are robust with respect to uncertainty regarding the locations of S/A threat units.

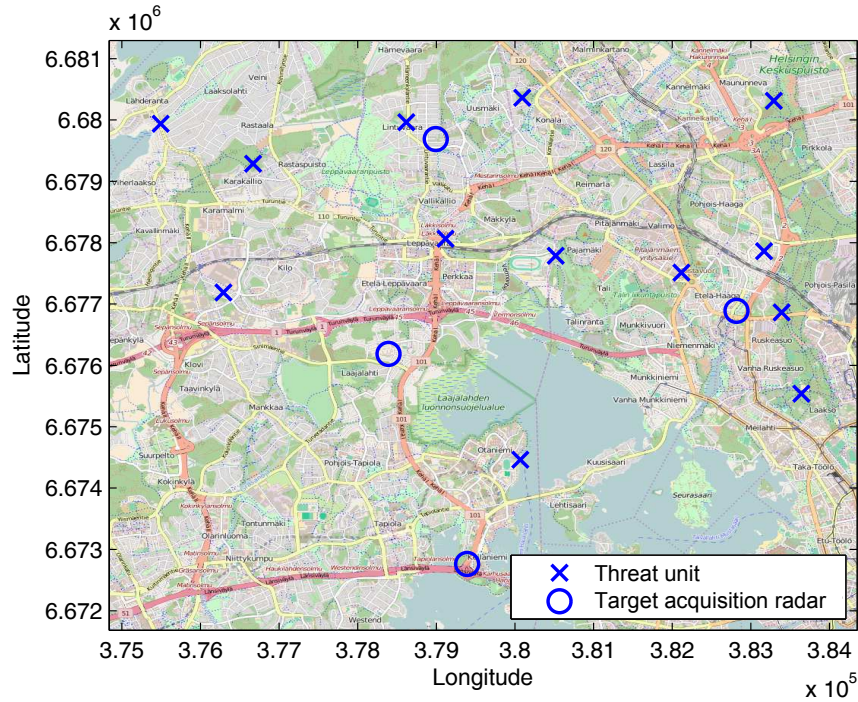


Figure 6.18: The known locations with which the robustness of the survivability models to uncertainty regarding the S/A threat systems' locations is studied.

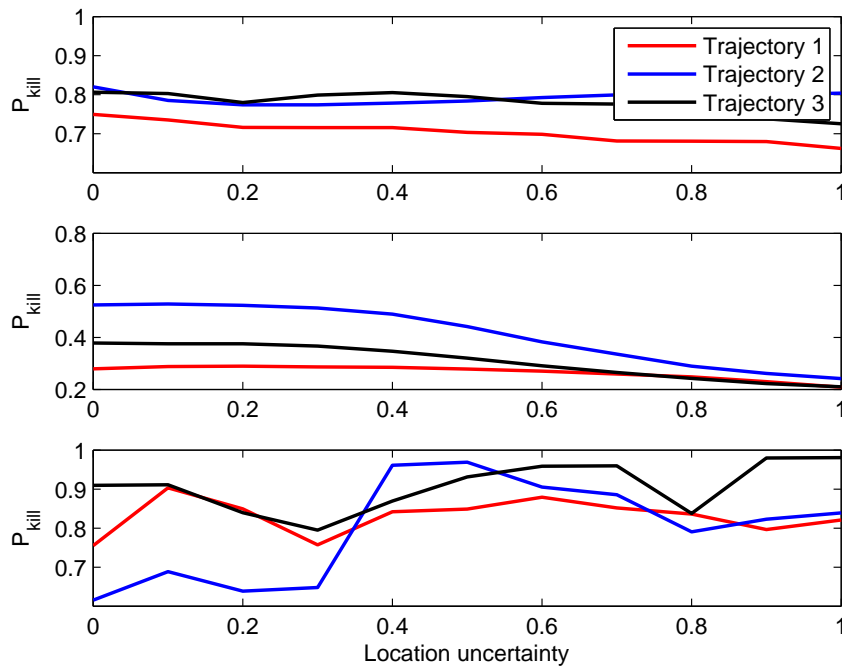


Figure 6.19: The probabilities  $P_{kill}$  of the trajectories with increasing uncertainty regarding the locations of the S/A threat systems evaluated with the Markov survivability model, the Erlandsson model, and the technical model (top to bottom).

### 6.3.2 Hyvinkää scenario

The second scenario in which the Markov survivability model is verified is set in and to the west of Hyvinkää, Finland. The air defence is set up in three tiers, each of which is designated as an independent S/A threat group. The westernmost S/A threat group consists of a target acquisition radar and four anti-aircraft guns. The middle S/A threat group contains a target acquisition radar and four short range S/A missile systems. The easternmost S/A threat group consists of a target acquisition radar and two medium range S/A missile systems. The assumed grouping areas of the S/A threat systems are portrayed in Figure 6.20.

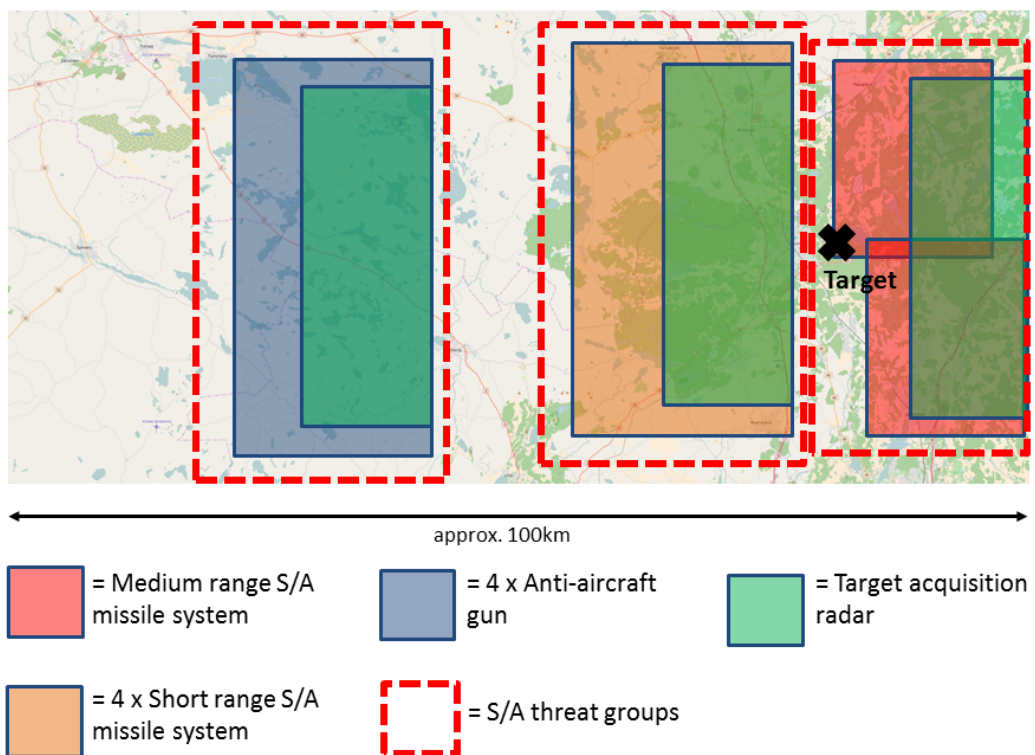


Figure 6.20: The grouping areas of the S/A threat systems.

Trajectories under consideration travel from west to east but start from different altitudes. The first trajectory originates from an altitude of 15 kilometres, the second starts from an altitude of 5 kilometres and the third begins from an altitude of 500 metres. All of the trajectories originate from approximately 100 kilometres west of the target.

Each trajectory is evaluated using the Markov survivability model and the reference models. Once again, the locations of the S/A threat systems are assumed

to be unknown, and thus probability maps are determined for each threat system. These probability maps are used as a basis for the trajectory evaluation. A combined probability map similar to that related to the Hyvinkää scenario is given in Figure 6.21. This map is a probability map which gives the probability that at least one of many S/A threat systems in the area is located at any given location.

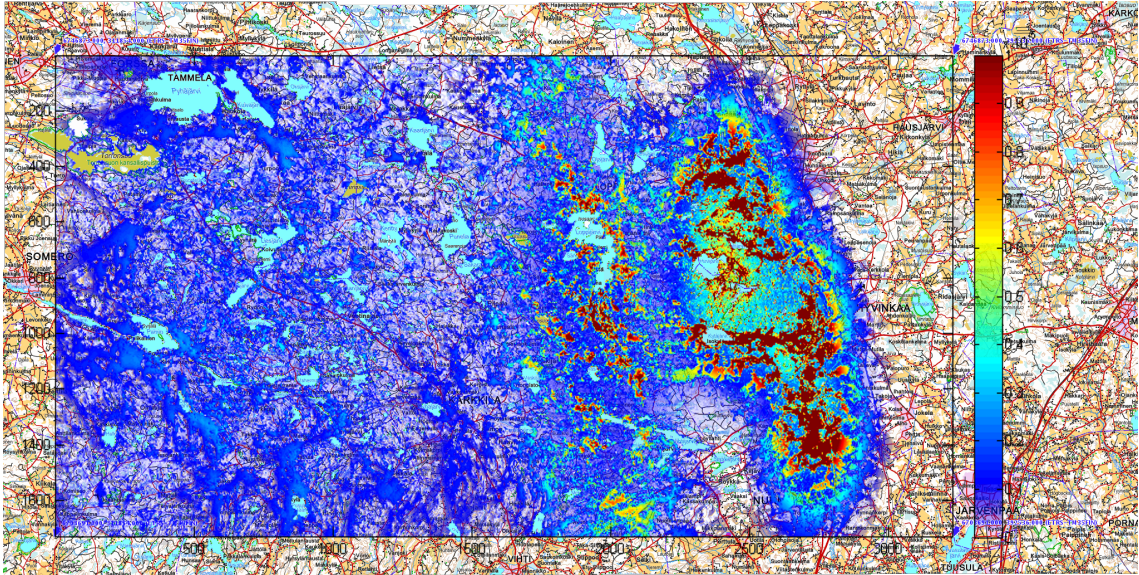


Figure 6.21: A combined probability map for S/A threat systems similar to that used in the Hyvinkää scenario.

The survivabilities of the trajectories are given in Table 6.5. The Markov survivability model estimates a high survivability for all trajectories while based the reference models the survivabilities of each trajectory are low. Based on the Markov model trajectory 1 is the best, while the technical model evaluates trajectory 3 to be preferable. The Erlandsson model evaluates equal survivabilities for each trajectory.

Table 6.5: Survivabilities ( $P_{\text{surv}}$ ) of the trajectories in the Hyvinkää scenario.

	Trajectory 1	Trajectory 2	Trajectory 3
Markov model	0.98	0.82	0.88
Erlandsson model	0.00	0.00	0.00
Technical model	0.04	0.00	0.07

The survivabilities determined for the trajectories in the Hyvinkää scenario demonstrate the shortcomings of the implementation of the Erlandsson model used in the example scenarios. The sensor and threat areas used in the Erlandsson model are cylinders with radius  $\rho_{\text{max}}$  in 3-dimensional space. Thus, the implementation

of the Erlandsson model gives low survivabilities for trajectories at high altitudes, even though the trajectories are at the very limits of the S/A weapons' capabilities, i.e., the S/A weapons' range  $R_{\max}$ . Similarly, the implementation of the Erlandsson model used in this thesis also provides low survivabilities for the trajectories at very low altitudes as the Erlandsson model does not take into account any shadows cast by the terrain. Thus, the implementation of the Erlandsson model assumes the S/A threat systems are able to detect, track and engage the A/G weapon even though the systems would not have been able to detect the A/G weapon or the S/A weapon would not be able to engage the A/G weapon in reality. The technical survivability model gives lower survivabilities than the Markov survivability model, but distinguishes between the trajectories at extreme altitudes and the trajectory within the range of the S/A threat systems. Trajectory 2, which is at an altitude at which the S/A threats can intercept it throughout the trajectory is evaluated the lowest survivability by both the Markov model and the technical model.

The accumulation of risk is studied using a stacked area graph in which the areas correspond to state probabilities at any given time. Such a stacked area graph is provided in Figure 6.22 for trajectory 2. The risk caused by the different S/A threat groups is seen in the graphs. The first S/A threat group is encountered around time  $t = 100$  s. At this point the Erlandsson model forecasts that the A/G weapon will be intercepted almost certainly while the other models give a smaller probability of interception at this point. The second S/A threat group is encountered at about  $t = 200$  s. The third S/A threat group can not be distinguished as clearly from Figure 6.22, however the slight rise in probability of being in "Locked" state based on the Markov model at time  $t = 250$  s is due to this third threat group.

Unlike the Erlandsson model, the Markov survivability model and the technical survivability model handle the range  $R_{\max}$  of the S/A weapons as the slant range between the S/A weapon and the A/G weapon, i.e., the models takes into account also the altitude difference. The Markov survivability model evaluates trajectory 1 to be the safest trajectory (see, Table 6.5). This is due to the maximum slant range defined within the model for the S/A weapons (the largest possible range is  $R_{\max} = 15$  km) and the fact that the trajectory is at such a high altitude (starting at 15 km). Therefore, almost all of the S/A weapons are out of the range throughout the trajectory. The survivability based on the technical survivability model differs from the Markov survivability model's survivability mainly on how likely it determines for the A/G weapon to be intercepted towards the end of its trajectory as is seen from the steep rise of  $P_{\text{kill}}$  based on the technical model towards the end of the trajectory

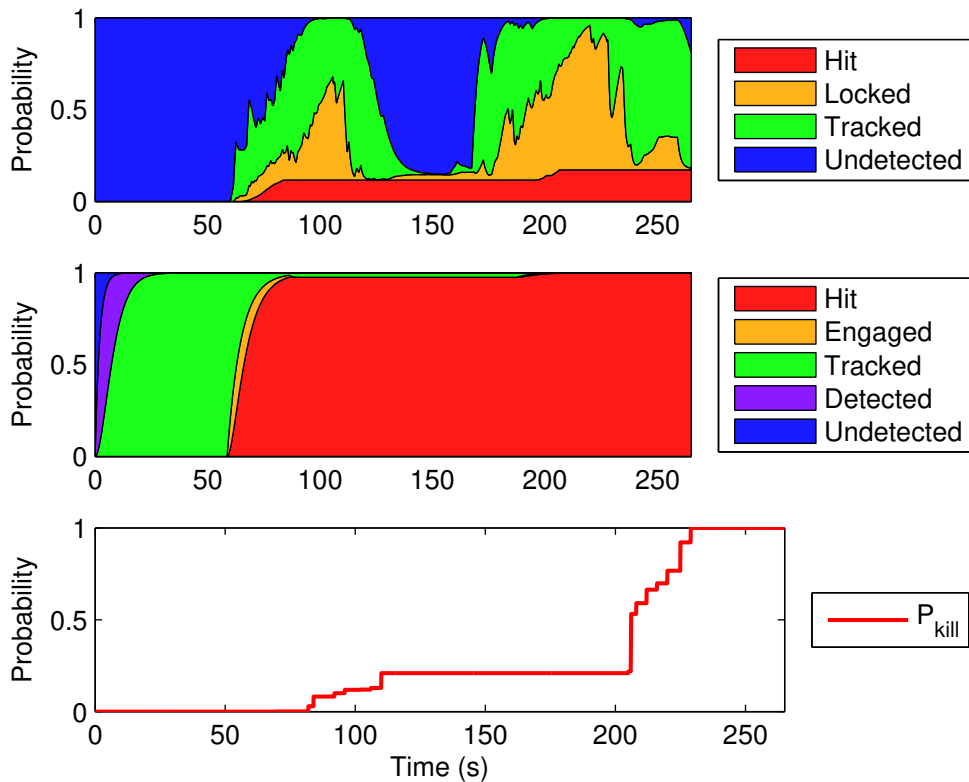


Figure 6.22: Graphs of the state probabilities along trajectory 2 based on the Markov survivability model, the Erlandsson model, and the technical model (top to bottom).

in the bottommost plot of Figure 6.22. Based on the Markov survivability model the A/G weapon is not as likely to be intercepted, even towards the end of its trajectory.

Based on the Hyvinkää scenario, the Markov survivability model is quite consistent with the technical survivability model because we were able to identify trajectory 2 as the worst trajectory, i.e., the trajectory with the lowest survivability. Trajectory 1 travels most of the distance at a high altitude and out of reach of all or most of the S/A weapons. Only at the final stages of trajectory 1 the A/G weapon descends to altitudes at which more S/A weapons can engage it. The technical survivability model seems to emphasise the last stages of the trajectory when the A/G weapon descends towards its target more than the Markov survivability model. Thus, the technical survivability model gives trajectory 3 a lower survivability than trajectory 1. Compared with trajectory 2, both the Markov survivability model and the technical survivability model evaluate trajectory 3 to be safer. This is consistent with common sense, as A/G weapons on low-flying trajectories should be harder to detect and engage due to shadows cast by the terrain. The implementation of

the Erlandsson survivability model used in this thesis fails to detect any differences between any of the trajectories in the Hyvinkää example scenario.

The following concludes the numerical experiments section of this thesis. The spatial prediction model was seen to produce reasonable probability maps for S/A threats in Chapter 6.1, and the probability map reduction method was seen to preserve the characteristics which are important related to the survivability of trajectories in Chapter 6.2. In Chapter 6.3, the Markov survivability model was compared with the reference survivability models in regard to the consistency of survivabilities and the robustness of the models with respect to the amount of uncertainty regarding the locations of the S/A threat systems. The Markov survivability model both gives intuitive results and is robust with respect to the amount of location uncertainty. The robustness of the Markov model was shown in Chapter 6.3.1, where both the Markov survivability model and the Erlandsson survivability model were noted to be robust while the technical survivability model changed the ordering of trajectories based on the survivability numerous times as the location uncertainty was varied. In Chapter 6.3.2, the Erlandsson survivability model was found to produce results inconsistent with reality in extreme cases, and the implementation of the Erlandsson model which was used was unable to distinguish between any of the trajectories evaluated. The Markov survivability model and the technical survivability model both produced results consistent with common sense and intuition. To summarise, the trajectory evaluation framework is capable of evaluating trajectories under uncertainty regarding the locations of S/A threat systems of which the air defence consists of. Based on intelligence information regarding the locations and capabilities of S/A threat systems, the trajectory evaluation framework is used to determine the best trajectory from a set of alternative trajectories.

# Chapter 7

## Summary and discussion

This thesis introduces the novel trajectory evaluation framework for comparing trajectories of A/G weapons based on the risk of being intercepted with an S/A threat system. The risk is due to adverse S/A threats which try to intercept the A/G weapon. The framework is used to facilitate decision making regarding route planning for A/G missions by identifying the trajectory on which the probability for the A/G weapon to be intercepted with the S/A threats is the smallest. The framework consists of the spatial prediction model and the Markov survivability model developed in this thesis.

The spatial prediction model is used to build a probability map for an S/A threat system. Such a system is a target acquisition radar or an S/A threat unit which consists of a radar and an S/A weapon. The probability map is constructed by using geographical data and knowledge about common tactical principles applied in forming air defence. The model is based on sound observations on the requirements of the terrain where the S/A threat system is capable of operating effectively. It also takes into account available intelligence information on the grouping of the S/A threat systems and their capabilities. Thus, the resulting probability map concisely describes the available information concerning the positioning of the S/A threat system in any region. To the knowledge of the author, no similar spatial models have been published prior to this thesis.

Probability maps produced by the spatial prediction model are used for estimating threat induced by a known amount of S/A threat systems in a given area onto an A/G weapon which is the approach applied in the trajectory evaluation framework. Results obtained with the model can also be used as an *a priori* estimate for the locations of the S/A threat systems when building a probability map with data from noisy radar sensing sensors [17].

It should be noted that due to lack of data, the spatial prediction model does not take into account buildings and their effect on the capability of S/A threat systems to operate. Especially in populated areas, buildings can account for a great amount of visual obstructions. Since the populated areas also often have less tree growth, the model gives unrealistically great probabilities for S/A threat systems to be located in the built areas. In reality, it might be impossible for the S/A threat systems to operate with buildings in the immediate vicinity. Nevertheless, given data regarding the dimensions and locations of the buildings the model could easily be extended to take into account these buildings.

The Markov survivability model introduced in this thesis provides survivabilities of A/G weapons' trajectories by taking into account the directional radar cross-section of an A/G weapon and possible terrain shadow effects. Compared with the implementation of the Erlandsson model [11] used in this thesis, the Markov survivability model is more accurate, as the Erlandsson model does not treat the directional radar cross-section and shadows cast by the terrain. As the technical survivability model [34] is directly derived from technical requirements and working principles of radars and trackers, the relative survivabilities of the trajectories obtained with it should be closest to reality. However, as demonstrated in Chapter 6.3, these survivabilities are sensitive to uncertainties regarding the locations of S/A threat systems. On the other hand, the Markov survivability is robust, i.e., the relative survivabilities of the trajectories do not change even though uncertainty regarding the S/A threat systems' locations is varied. To summarise, the Markov survivability model gives credible relative survivabilities while being immune to increasing uncertainty regarding the locations of the threats.

Similar to the Erlandsson model, the Markov survivability model contains a set of parameters. The parameters are state transition intensities which are derived from the mean time needed for any given state transfer such as the time needed to form a track. These in turn can be defined by experts. The technical survivability model relies on more precise information regarding radars. This includes the track criterion on how many detections must be achieved to form a track and the track maintenance period during which at least one successful detection must be made to maintain an earlier track. These parameters have a large effect on the results of evaluations performed by the model. Furthermore, the Markov survivability model and the Erlandsson model can be extended to take into account infrared and optical sensors. The technical survivability model, on the other hand, is specifically derived from radar sensors, and thus a completely separate model must be constructed to

describe different types of sensors.

The Markov and Erlandsson survivability models rely on continuous-time Markov chains, and thus state probabilities are treated with differential equations. This can be useful in future endeavours when optimising the trajectories of A/G weapons. The same cannot be said of the technical survivability model in which the accumulation of risk is not defined in a similar elegant manner.

The motivation behind this thesis was the need to evaluate the relative survivabilities of alternative trajectories in situations where an A/G weapon traverses through airspace controlled by adverse air defence and the exact locations of S/A threat systems are not known. With the novel trajectory evaluation framework introduced in this thesis, the trajectories are evaluated which reveals the trajectory with the greatest survivability. The Markov survivability model used in the framework is well suitable for situations in which there is uncertainty regarding the locations of the S/A threat systems. With the spatial prediction model, intelligence information on the locations of the S/A threats is enhanced and probability maps that are applied with the Markov survivability model are produced.

The trajectory evaluation framework extends and complements the tool called Strike Aircraft Routing Software Suite presented in the master's thesis *Military aircraft routing with multi-objective network optimizations and simulation* [28]. The tool is used to create A/G mission scenarios that are analysed for determining optimal military aircraft routing. The spatial prediction and the Markov survivability models are implemented as subprograms within the tool. With the framework, the survivability of an A/G weapon can also be taken into account in military aircraft routing analysis.

Future research dealing with the grouping of S/A threats should take into account the interdependencies of the positioning of multiple S/A threat systems. In the trajectory evaluation framework, it is assumed that the S/A threat systems are located independently of each other. This assumption does not generally hold. The relations between the multiple systems and the effect of these relations on probability maps and trajectory evaluation should be studied. On the other hand, the Markov survivability model is only capable of handling radar sensors. It could be augmented to also treat different types of sensors such as infrared and optical sensors. Such sensors have a significant role in short range air defence and thus should not be disregarded.

Overall, the trajectory evaluation framework at hand is used to solve the trajectory planning problem of A/G weapons by identifying the trajectory with the

greatest survivability from a set of possible trajectories which penetrate into airspace defended by adverse air defence. The next step would be to properly optimise the trajectory of an A/G weapon using dynamic optimisation [5] or optimal control theory [22]. The solution of such a trajectory planning problem would provide the optimal trajectory which maximises the survivability of the A/G weapon.

# Bibliography

- [1] M. Austin. Spatial prediction of species distribution: an interface between ecological theory and statistical modelling. *Ecological modelling*, 157(2):101–118, 2002.
- [2] R. Beard, T. McLain, M. Goodrich, and E. Anderson. Coordinated target assignment and intercept for unmanned air vehicles. *IEEE Transactions on Robotics and Automation*, 18(6):911–922, 2002.
- [3] J. Benton and V. Subrahmanian. Using hybrid knowledge bases for missile siting problems. In *Proceedings of the Tenth Conference on Artificial Intelligence for Applications*, pages 141–148, 1994.
- [4] J. Berger, A. Boukhtouta, A. Benmoussa, and O. Kettani. A new mixed-integer linear programming model for rescue path planning in uncertain adversarial environment. *Computers & Operations Research*, 39(12):3420–3430, 2012.
- [5] D. Bertsekas. *Dynamic Programming and Optimal Control*. Athena Scientific, 2005.
- [6] A. Boukhtouta, A. Bedrouni, J. Berger, F. Bouak, and A. Guitouni. A survey of military planning systems. Technical report, Defense Research and Development Canada, 2004.
- [7] A. Brenning. Spatial prediction models for landslide hazards: review, comparison and evaluation. *Natural Hazards and Earth System Science*, 5(6):853–862, 2005.
- [8] E. Dijkstra. A note on two problems in connexion with graphs. *Numerische mathematik*, 1(1):269–271, 1959.
- [9] R. Durrett. *Essentials of Stochastic Processes*. Springer, 1999.

- [10] T. Erlandsson. Route planning for air missions in hostile environments. *The Journal of Defense Modeling and Simulation: Applications, Methodology, Technology*, 12(3):289–303, 2015.
- [11] T. Erlandsson and L. Niklasson. Automatic evaluation of air mission routes with respect to combat survival. *Information Fusion*, 20:88–98, 2014.
- [12] T. Erlandsson and L. Niklasson. An air-to-ground combat survivability model. *The Journal of Defense Modeling and Simulation: Applications, Methodology, Technology*, 12(3):273–287, 2015.
- [13] G. Espa, R. Benedetti, A. De Meo, U. Ricci, and S. Espa. Gis based models and estimation methods for the probability of archaeological site location. *Journal of Cultural Heritage*, 7(3):147–155, 2006.
- [14] M. Fischer and J. Wang. *Spatial data analysis: models, methods and techniques*. Springer Science & Business Media, 2011.
- [15] M. Fleming and R. Hoffer. Machine processing of landsat mss data and dma topographic data for forest cover type mapping. Technical report.
- [16] W. Franklin, C. Ray, and S. Mehta. Geometric algorithms for siting of air defense missile batteries. Technical report, Rensselaer Polytechnic Institute, 1994.
- [17] J. Hespanha, H. Kizilocak, and Y. Ateskan. Probabilistic map building for aircraft-tracking radars. In *Proceedings of the American Control Conference*, pages 4381–4386, 2001.
- [18] A. Hofmann, Š. Hošková-Mayerová, V. Talhofer, and V. Kovařík. Creation of models for calculation of coefficients of terrain passability. *Quality & Quantity*, 49(4):1679–1691, 2015.
- [19] K. Jones. A comparison of algorithms used to compute hill slope as a property of the dem. *Computers & Geosciences*, 24(4):315–323, 1998.
- [20] M. Jun and R. D’Andrea. Path planning for unmanned aerial vehicles in uncertain and adversarial environments. In *Cooperative Control: Models, Applications and Algorithms*, volume 1, pages 95–110. 2003.

- [21] P. Kabamba, S. Meerkov, and F. Zeitz. Optimal path planning for unmanned combat aerial vehicles to defeat radar tracking. *Journal of Guidance, Control, and Dynamics*, 29(2):279–288, 2006.
- [22] E. Kirk. *Optimal Control Theory, An Introduction*. Dover Publications, 1998.
- [23] A. Law. *Simulation Modeling & Analysis*. McGraw-Hill, 1998.
- [24] C. Lloyd. *Spatial Data Analysis - An Introduction for GIS users*. Oxford University Press, 2010.
- [25] J. Marcum. A statistical theory of target detection by pulsed radar. *IRE Transactions on Information Theory*, 6(2):59–267, 1960.
- [26] M. Pachter and J. Hebert. Optimal aircraft trajectories for radar exposure minimization. In *Proceedings of the 2001 American Control Conference*, pages 2365–2369, 2001.
- [27] Z. Peng, B. Li, X. Chen, and J. Wu. Online route planning for uav based on model predictive control and particle swarm optimization algorithm. In *10th World Congress on Intelligent Control and Automation (WCICA)*, pages 397–401, 2012.
- [28] H. Puustinen. Military aircraft routing with multi-objective network optimization and simulation. Master’s thesis, Aalto University, School of Science, 2013.
- [29] M. Richards, J. Scheer, and W. Holm. *Principles of Modern Radar, Volume I - Basic Principles*. SciTech Publishing, 2010.
- [30] P. Ritter. A vector-based slope and aspect generation algorithm. *Photogrammetric Engineering and Remote Sensing*, 53(8):1109–1111, 1987.
- [31] V. Roberge, M. Tarbouchi, and G. Labonte. Comparison of parallel genetic algorithm and particle swarm optimization for real-time uav path planning. *IEEE Transactions on Industrial Informatics*, 9(1):132–141, 2013.
- [32] R. Sheldon et al. *A first course in probability*. Pearson Prentice Hall, 9th edition, 2014.
- [33] S. Theodoridis and K. Koutroumbas. *Pattern Recognition*. Elsevier, 2009.
- [34] V. Väisänen to Riku Hyytiäinen. Memorandum. Ohjusilmatorjunnan mallinnus, Nov 2015.

- [35] C. Zheng, L. Li, F. Xu, F. Sun, and M. Ding. Evolutionary route planner for unmanned air vehicles. *IEEE Transactions on Robotics*, 21(4):609–620, 2005.

# Appendix A

## Probability of detection ( $P_D$ )

In each model discussed in this thesis, the capabilities of radar sensors to detect an A/G weapon play a vital role. Radar sensors include all sensors that transmit radio signals and by listening to the reflections of the transmitted signals determine whether there is a target in the vicinity. Only monostatic radars, i.e., radars in which the transmitter and receiver are co-located are considered. The capability of a sensor to detect the A/G weapon is measured with the probability of detection. The probability of detection  $P_D$  describes the probability whereby the sensor is able to detect a target in a given location. This appendix is written with reference to *Principles of Modern Radar* by M. Richards et. al. [29].

A radar sensor operates by transmitting short pulses of electromagnetic radiation and by listening to possible reflections or echoes from targets in the vicinity. The basic working principle of radar sensors is portrayed in Figure A.1. For a target to be successfully detected, the electromagnetic pulse radiated by the transmitter must reach the target and the radiation reflected from the target must reach the receiver with sufficient intensity, so that it can be distinguished from static noise. The different stages of target detection with a radar sensor will be considered separately in order to determine the performance capability of a radar sensor.

First, the incident power density at the target is determined. Given an isotropic transmitter, i.e., a transmitter that radiates electromagnetic radiation homogenously in all directions, the power density at distance  $R$  is

$$Q_i = \frac{P_t}{4\pi R^2}, \quad (\text{A.1})$$

where  $P_t$  is the power at which the radar is transmitting. This is because the power at which the radar is transmitting is evenly spread out on the surface of a sphere of

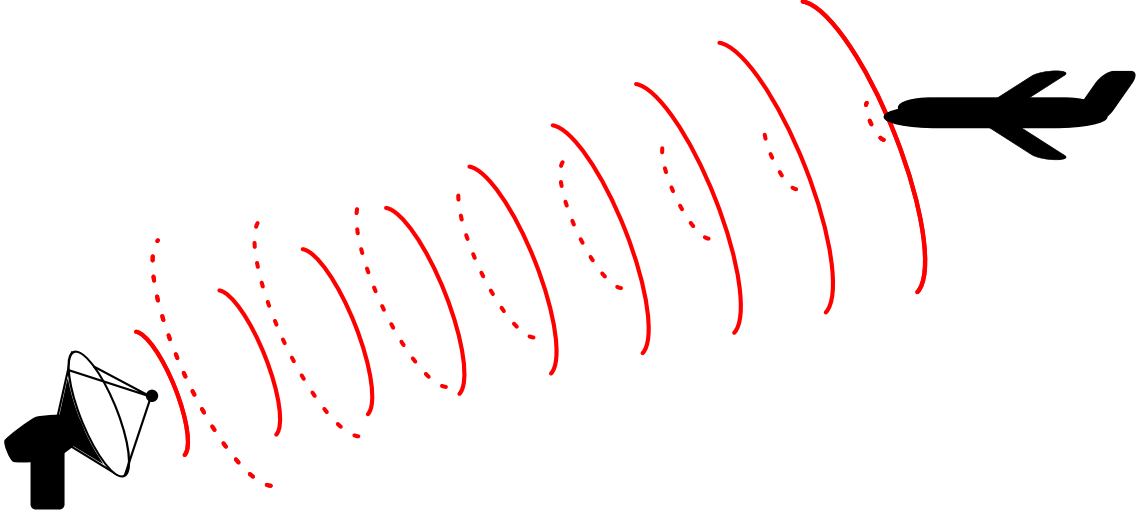


Figure A.1: The working principle of a radar sensor.

radius  $R$ . However, the electromagnetic radiation is usually directed to the assumed direction of a target. This is done with an antenna which is modeled mathematically by multiplying the Equation (A.1) with a transmitting gain coefficient  $G_t$ . Thus, the incident power density at the target is

$$Q_i = \frac{P_t G_t}{4\pi R^2}, \quad (\text{A.2})$$

where  $P_t$  is the power with which the radar is transmitting,  $G_t$  is the gain coefficient of the transmitting antenna and  $R$  is the distance of the target from the transmitter.

The electromagnetic radiation incident on the target is either reflected or absorbed by the target. The portion of the incident power which is reflected is represented by the radar cross-section  $\sigma$  of the target. The target is modeled to be an isotropic radiator radiating with power

$$P_{\text{refl}} = Q_i \sigma, \quad (\text{A.3})$$

where  $Q_i$  is the incident power density and is calculated with Equation (A.2). The reflected power is calculated by substituting  $Q_i$  in Equation (A.3) with Equation (A.2), i.e.,

$$P_{\text{refl}} = \frac{P_t G_t \sigma}{4\pi R^2}.$$

It is assumed that the reflected power is radiated isotropically, and thus the reflected

power density incident at the radar receiver is

$$Q_r = \frac{P_{\text{refl}}}{4\pi R^2} = \frac{P_t G_t \sigma}{(4\pi)^2 R^4}.$$

The power received by the receiver is calculated as

$$P_r = \frac{P_{\text{refl}} A_e}{4\pi R^2} = \frac{P_t G_t A_e \sigma}{(4\pi)^2 R^4}, \quad (\text{A.4})$$

where  $A_e$  is the efficient area of the receiver's antenna, i.e., the area of the antenna on which reflected radiation is incident to, taking into account possible inefficiencies. As shown in [29], the gain coefficient  $G$  of an antenna is dependent of the efficient area  $A_e$  of the antenna with relation

$$G = \frac{4\pi A_e}{\lambda^2}, \quad (\text{A.5})$$

where  $\lambda$  is the wavelength of the electromagnetic radiation used. Solving the efficient area  $A_e$  from Equation (A.5) and substituting that into Equation (A.4), the power received by the receiver is

$$P_r = \frac{P_t G_t G_r \lambda^2 \sigma}{(4\pi)^3 R^4}, \quad (\text{A.6})$$

where  $P_t$  is the power with which the radar is transmitting,  $G_t$  is the gain coefficient of the transmitting antenna,  $G_r$  is the gain coefficient of the receiving antenna,  $\lambda$  is the wavelength at which the radar is transmitting,  $\sigma$  is the radar cross-section of the target, and  $R$  is the distance of the target from the transmitter.

Up to this point all of the subsystems have been treated as ideal systems with no losses. In reality, the power received by the receiver is less than what Equation (A.6) predicts. Losses which are taken into account often include losses in the electrical components between the transmitter and the antenna, the attenuation of the electromagnetic signal while propagating in the atmosphere, losses in the electrical components connecting the antenna to the receiver, and losses related to signal processing. These losses are modeled with the system loss coefficient  $L_s$ . Taking into account all losses in the system, the final power at which the reflected signals are observed is

$$P_r = \frac{P_t G_t G_r \lambda^2 \sigma}{(4\pi)^3 R^4 L_s}.$$

Ideally, a radar could detect all objects which are not shadowed by the terrain or other obstructions. This is because even the weakest signals that are reflected from

objects very far away could, in an ideal system, be amplified until they are large enough to be registered. In practice, however, the signal is interfered by noise originating from different sources, and weak signals might be very difficult or impossible to distinguish from the noise. Noise entering the antenna can originate from multiple sources such as outer space, the sun, and the surface of the earth. However, it is often assumed that the thermal noise originating from electrical components within the receiver dominates over the noise entering the receiver through the antenna [29].

Thermal noise is caused by the random movement of electrons in the electrical components due to the ambient temperature in the receiver. Thermal noise can be characterised as white noise and as such its power spectral density is uniform, i.e., the noise power does not depend on the frequency or wave length at which the noise is being observed. The observed thermal noise power depends on the ambient temperature  $T_s$  of the receiver and the bandwidth  $B$  being observed, and is written as

$$P_n = kT_s B = kT_0 F B, \quad (\text{A.7})$$

where  $k$  is the Boltzmann constant,  $T_0$  is the standard temperature (290 K) and  $F$  is the noise figure of the receiver subsystem. The optimal bandwidth which should be observed to maximise the resulting signal-to-noise ratio is approximately the reciprocal of the pulse width  $\tau$  [29], i.e., the length of the pulse sent by the transmitter. The bandwidth in Equation (A.7) is substituted with  $B = 1/\tau$ :

$$P_n = \frac{kT_0 F}{\tau}.$$

The signal-to-noise ratio can now be calculated as the ratio of the received power and the thermal noise power:

$$\text{SNR} = \frac{P_t G_t G_r \lambda^2 \sigma \tau}{(4\pi)^3 R^4 L_s k T_0 F}.$$

When trying to determine whether there is a target in a given direction, it is common practice that multiple signal pulses are sent, and by combining the reflected signals of each of these pulses the likelihood that a target is in the given direction is determined. It is assumed that the signals are combined through a process called coherent integration, in which both the amplitude and phase of the signal are taken into account. By combining the signals by coherent integration, the signal-to-noise

ratio can be enhanced and the resulting signal-to-noise ratio is

$$\text{SNR}_c(n_p) = \frac{P_t G_t G_r \lambda^2 \sigma \tau n_p}{(4\pi)^3 R^4 L_s k T_0 F}, \quad (\text{A.8})$$

where  $P_t$  is the peak power at which the transmitter is transmitting,  $G_t$  is the gain of the transmitting antenna,  $G_r$  is the gain of the receiving antenna,  $\lambda$  is the wavelength whereby the transmitter is transmitting,  $\sigma$  is the radar cross-section of the target,  $\tau$  is the pulse width,  $n_p$  is the amount of pulses which are combined,  $R$  is the distance at which the target is,  $L_s$  is the loss coefficient of the complete system,  $k$  is the Boltzmann constant,  $T_0$  is the standard temperature, and  $F$  is the noise figure of the receiver.

Thermal noise is stochastic in nature and as such the identification of signals from within the noise is not trivial. This is demonstrated in Figure A.2 in which thermal noise is presented. The thermal noise is accompanied with signals with amplitude 0.8 V at bins 10, 20, 30, 40, 50, 60, 70, 80 and 90. A common scheme is to set a threshold voltage, so that every time a signal voltage greater than the threshold is observed at the sensor, a signal is interpreted as being present. A threshold voltage is also presented in Figure A.2. Every bin where the signal peaks above the threshold voltage is interpreted as containing a signal. However, due to the stochastic nature of the noise, it is possible that the voltage which is observed exceeds the threshold voltage even though there is no actual signal present. In Figure A.2, this is seen in bin 8, where there is no actual signal present but nevertheless the thermal noise voltage exceeds the threshold voltage. The probability of this happening is denoted with the probability of false alarm  $P_{\text{FA}}$ . On the other hand, it is possible that due to the stochastic thermal noise, an actual signal that without noise would be identified does not cause a great enough voltage at the sensor to exceed the threshold and thus goes unnoticed. This is seen in Figure A.2 at bins 50 and 90 where there is indeed a signal present, but due to the thermal noise the measured voltage does not exceed the threshold voltage. The probability that an actual signal caused by a target is successfully identified is denoted with the probability of detection  $P_D$ .

Radar systems can be characterised as either coherent or noncoherent systems. A noncoherent system only registers the amplitude of incoming signals and noise while coherent systems register both the amplitude and phase of a signal. Thus, the coherent systems effectively measure two components of a signal which are commonly denoted by in-phase component  $I$  and quadrature component  $Q$  [29]. The resultant voltage of a signal is  $v = \sqrt{I^2 + Q^2}$ . In thermal noise, both components of the

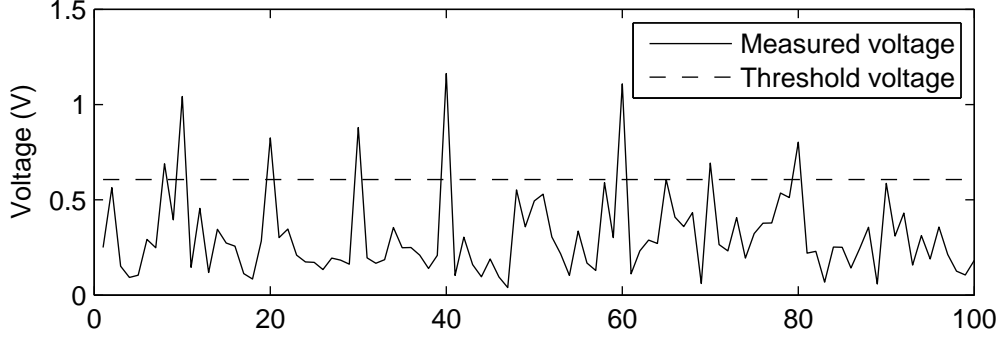


Figure A.2: Thermal noise accompanied with signals of amplitude 0.8 V in bins 10, 20, 30, 40, 50, 60, 70, 80, and 90.

signal  $I$  and  $Q$  are approximately normally distributed. Thus, the resultant voltage of thermal noise is stochastic and distributed according to the Rayleigh-distribution:

$$p_n(v) = \frac{v}{\sigma_n^2} \exp\left(-\frac{v^2}{2\sigma_n^2}\right), \quad (\text{A.9})$$

where  $\sigma_n^2$  is the variance of the resultant voltage, i.e., the mean square noise voltage. The mean square noise voltage is proportional to the thermal noise power. A probability density function for the measured voltage when there is only thermal noise present is shown in Figure A.3a. With Equation (A.9), the probability of false alarm  $P_{\text{FA}}$  is calculated for any given threshold voltage  $V_T$ :

$$P_{\text{FA}} = \int_{V_T}^{\infty} p_n(v) dv = -\exp\left(-\frac{V_T^2}{2\sigma_n^2}\right). \quad (\text{A.10})$$

Further, a minimum threshold voltage needed to achieve a probability of false alarm  $P_{\text{FA}}$  is determined by solving the threshold voltage  $V_T$  from Equation (A.10). The expression achieved for the threshold voltage needed to achieve a given probability of false alarm is

$$V_T = \sqrt{2\sigma_n^2 \ln(1/P_{\text{FA}})}. \quad (\text{A.11})$$

The threshold voltage for a false alarm rate of  $P_{\text{FA}} = 10^{-2}$  is plotted in Figure A.3. The shaded area to the right of the threshold voltage in Figure A.3a represents the probability of a false alarm, i.e., a signal is thought to be present even though no signal actually exists.

The resulting voltage that is achieved when thermal noise is accompanied with a signal of voltage  $v_s$  is represented with the Rician distribution [29]. The Rician

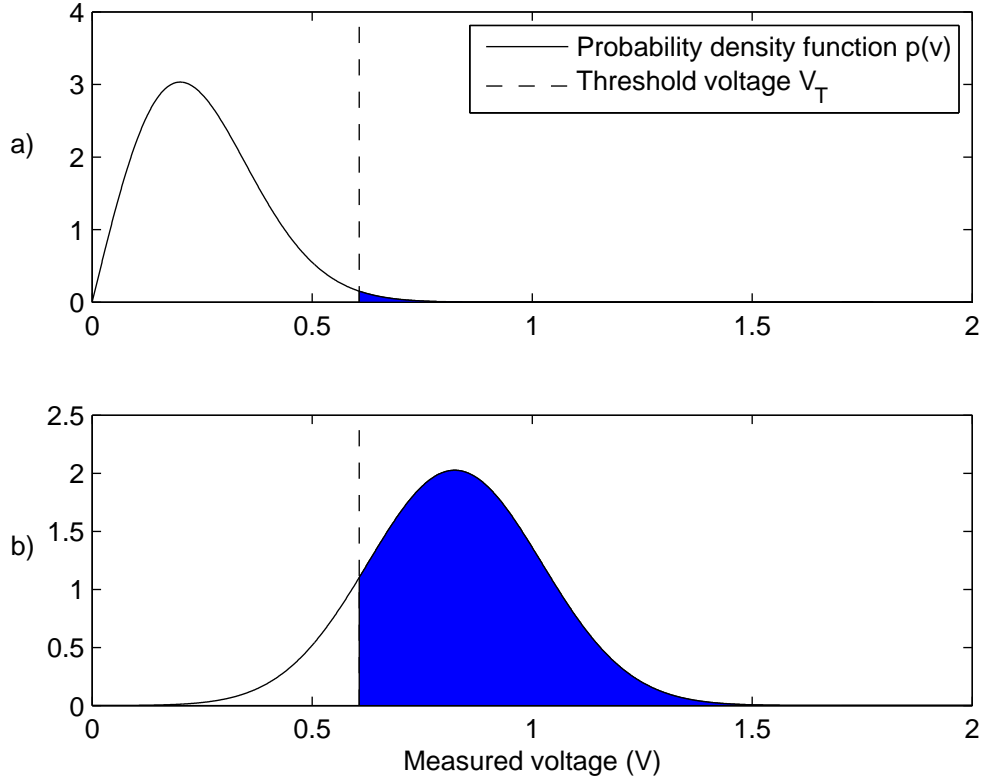


Figure A.3: The probability density function of measured voltage with a) only thermal noise and b) thermal noise and signal.

probability density function is

$$p_{s+n}(v) = \frac{v}{\sigma_n^2} \exp\left(-\frac{v^2 + v_s^2}{2\sigma_n^2}\right) I_0\left(\frac{vv_s}{\sigma_n^2}\right), \quad (\text{A.12})$$

where  $I_0$  is the modified Bessel function of the first kind and zero order. The probability density function of the resultant voltage when the thermal noise with mean square voltage  $(0.2 \text{ V})^2$  is accompanied with a signal of amplitude 0.8 V is given in Figure A.3b. The shaded area to the right of the threshold voltage represents the probability that the signal is detected. The probability of detection  $P_D$  is calculated by integrating the probability density function (A.12)

$$P_D = \int_{V_T}^{\infty} \frac{v}{\sigma_n^2} \exp\left(-\frac{v^2 + v_s^2}{2\sigma_n^2}\right) I_0\left(\frac{vv_s}{\sigma_n^2}\right) dv, \quad (\text{A.13})$$

which is not easily accomplished analytically. However, it can be calculated using

the generalised Marcum Q-function which is defined as

$$Q_M(a, b) = \int_b^\infty \frac{1}{a^{M-1}} x^M \exp\left(-\frac{x^2 + a^2}{2}\right) I_{M-1}(ax) dx, \quad (\text{A.14})$$

where  $I_{M-1}$  is the modified Bessel function of the first kind and order  $M - 1$ . Tools for the evaluation of the Marcum Q-function are readily available in most numerical computing environments such as MATLAB. By substituting  $v = \sigma_n x$  in Equation (A.13), the following form is achieved:

$$P_D = \int_{V_T/\sigma_n}^\infty x \exp\left(-\frac{x^2 + \left(\frac{v_s}{\sigma_n}\right)^2}{2}\right) I_0\left(\frac{xv_s}{\sigma_n}\right) dx. \quad (\text{A.15})$$

By comparing Equations (A.14) and (A.15), and by choosing  $a = v_s/\sigma_n$ ,  $b = V_T/\sigma_n$ , and  $M = 1$  the probability of detection  $P_D$  can be expressed with the Marcum Q-function as

$$P_D = Q_1\left(\frac{v_s}{\sigma_n}, \frac{V_T}{\sigma_n}\right). \quad (\text{A.16})$$

This can further be simplified by noting that the square of the signal voltage is proportional to the signal power received through the receiver, and the mean square voltage of the thermal noise is similarly proportional to the thermal noise power, i.e.,  $v_s/\sigma_n = \sqrt{\text{SNR}}$ . By substituting this and  $V_T$  from Equation (A.11) into Equation (A.16), the probability of detection  $P_D$  is written as

$$P_D = Q_1\left(\sqrt{\text{SNR}}, \sqrt{2 \ln(1/P_{\text{FA}})}\right), \quad (\text{A.17})$$

where SNR is the signal-to-noise ratio which is calculated with Equation (A.8) and  $P_{\text{FA}}$  is the probability of false alarm chosen by the radar operator. Probabilities of detection calculated with Equation (A.17) using different false alarm rates are presented in Figure A.4.

The signal-to-noise ratio is dependent of the geometry between the sensor and the target which the sensor is trying to detect as well as the target's orientation due to the directional radar cross-section. Thus, the probability of detection depends on the position of the sensor  $(x', y')$  as well as the location and orientation of the target  $(x, y, z, \phi, \theta, \psi)$ . Taking these into consideration, the probability of detection

is written as

$$P_D^{(x',y')}(x, y, z, \phi, \theta, \psi) = Q_1 \left( \sqrt{\text{SNR}(x', y', x, y, z, \phi, \theta, \psi)}, \sqrt{2 \ln(1/P_{\text{FA}})} \right), \quad (\text{A.18})$$

where  $x$ ,  $y$ , and  $z$  depict the coordinates of the target and  $\phi$  depicts the heading of the target,  $\theta$  depicts the pitch angle of the target, and  $\psi$  depicts the roll angle of the target.

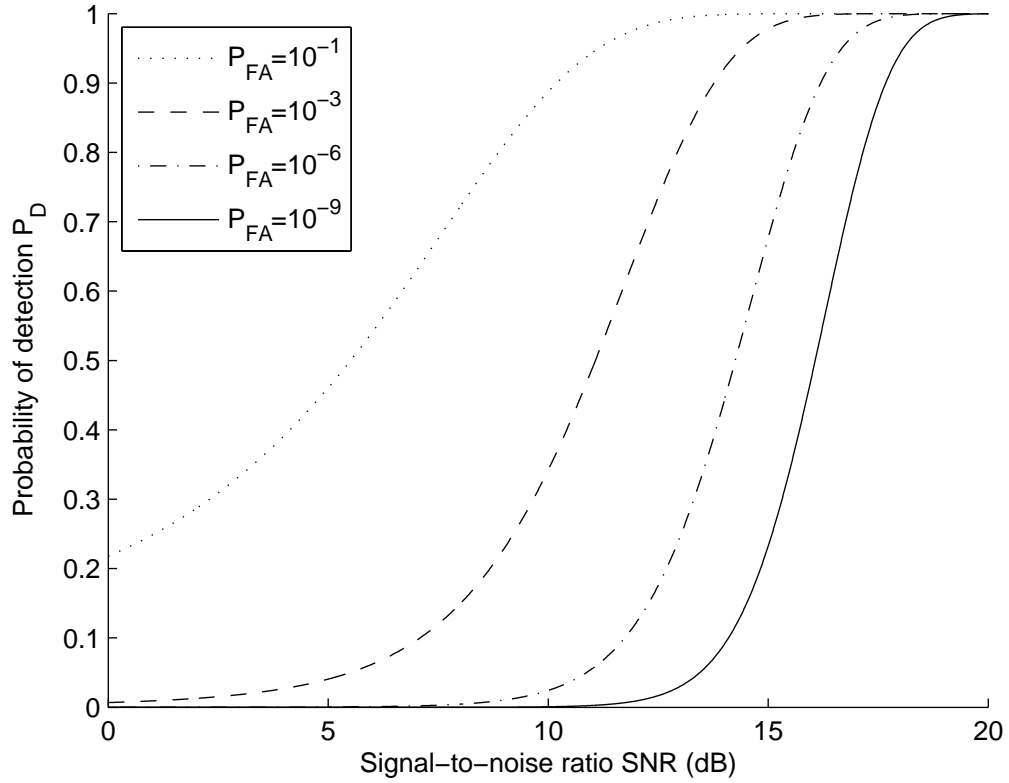


Figure A.4: Probability of detection with different rates of false alarm  $P_{\text{FA}}$ .

# Appendix B

## Continuous-time Markov chains

Two of the three survivability models discussed in this thesis are based on a class of stochastic models called Markov chains. Markov chains can be used to model finite state space systems, where the future states of the system depend on the current state and the rules governing the transitions from one state to another. The future states of a system described with a Markov chain do not depend on states visited prior to the current state, but only on the state which the system is in at a given time. This “memorylessness” is called the Markov property. As Markov chains are stochastic models, the evolution of the system’s state is captured by state probabilities which generally change over time. This appendix is written with reference to *Essentials of Stochastic Processes* by R. Durrett [9].

Markov chains can be grouped into discrete-time and continuous-time Markov chains. The models discussed in this thesis are based on continuous-time Markov chains, which are characterised with a state transition rate matrix  $\Lambda$  and are visualised as shown in Figure B.1. The state transition rate matrix  $\Lambda$  defines the Markov chain explicitly and is written as

$$\Lambda = \begin{bmatrix} -\nu_1 & \lambda_{1,2} & \lambda_{1,3} \\ \lambda_{2,1} & -\nu_2 & \lambda_{2,3} \\ \lambda_{3,1} & \lambda_{3,2} & -\nu_3 \end{bmatrix},$$

where  $\lambda_{i,j}$  is the transition rate from state  $i$  to state  $j$  and  $\nu_i = \sum_j \lambda_{i,j}$ , i.e., the rate at which the system leaves state  $i$ .

Given the knowledge that the system  $X$  is in the state  $i$  at time  $t$ , the probability that the system is in some other state  $j$  after an infinitesimal amount of time  $dt$  is

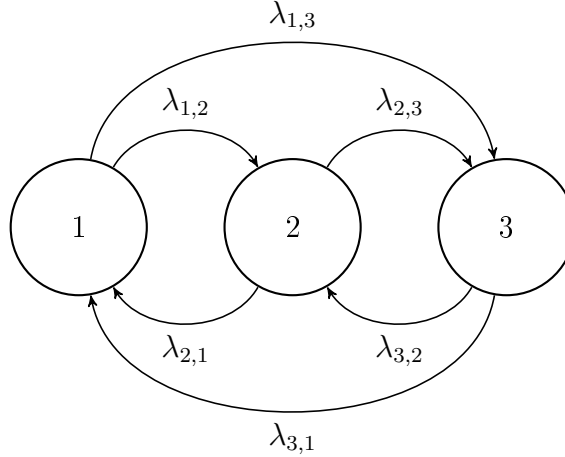


Figure B.1: A generic continuous-time Markov chain with three states.

calculated from the state transition rate  $\lambda_{i,j}$ :

$$P(X(t + dt) = j | X(t) = i) = \lambda_{i,j} dt.$$

Similarly, the probability that, given the knowledge of the system being in state  $i$  at time  $t$ , the system is still in the same state  $i$  after time  $dt$  is determined with

$$P(X(t + dt) = i | X(t) = i) = 1 - \nu_i dt.$$

Consequently the evolution of the state probabilities  $p_i(t) = P(X(t) = i)$  is described with the differential equation

$$\dot{\mathbf{p}}(t) = \Lambda^T \mathbf{p}(t), \tag{B.1}$$

where  $\mathbf{p}(t)$  is the state probability vector containing the probabilities that at time  $t$  the system is in each of the different states and  $\Lambda$  is the transition rate matrix of the Markov chain. The transitions between the states can also be characterised as Poisson processes and the time taken for the transition to happen is exponentially distributed with parameter  $\lambda_{i,j}$ . This is particularly useful when estimating parameters for models based on continuous-time Markov chains as the average time  $\tau_{i,j}$  needed for the transition from state  $i$  to state  $j$  is the reciprocal of the state transition rate, i.e.,

$$\tau_{i,j} = \frac{1}{\lambda_{i,j}}. \tag{B.2}$$

Each element in the state probability vector  $\mathbf{p}(t)$  corresponds to the probability of being in each of the states of the Markov chain at time  $t$ . With reference to the

Markov survivability model, the elements of  $\mathbf{p}(t)$  are the probabilities of an S/A threat unit portrayed by the Markov chain being in each of the states “Undetected”, “Tracked”, “Locked”, and “Hit” at time  $t$ . Similarly, in the Erlandsson survivability model, the elements of the vector  $\mathbf{p}(t)$  are the probabilities of S/A threat group depicted by the Markov chain being in each of the states “Undetected”, “Detected”, “Tracked”, “Engaged”, and “Hit” at time  $t$ .

Markov chains used in the Markov survivability model and the Erlandsson survivability model are inhomogenous time-continuous Markov chains. This means that state transition rates are not time-invariant, but can vary in time. Thus, the differential equation (B.1) is rewritten as

$$\dot{\mathbf{p}}(t) = \Lambda(t)^T \mathbf{p}(t). \tag{B.3}$$

# Appendix C

## Slope coefficient ( $C_{\text{slope}}$ )

In the spatial prediction model, the slope coefficient is defined as

$$C_{\text{slope}}(\phi) = \begin{cases} 1 & \text{if } |\phi| \leq \Phi_{\text{low}} \\ \frac{\Phi_{\text{high}} - |\phi|}{\Phi_{\text{high}} - \Phi_{\text{low}}} & \text{if } \Phi_{\text{low}} < |\phi| \leq \Phi_{\text{high}} \\ 0 & \text{if } |\phi| > \Phi_{\text{high}} \end{cases}, \quad (\text{C.1})$$

where the parameters  $\Phi_{\text{low}}$  and  $\Phi_{\text{high}}$  represent the slope angle values at which it begins to be hard for a threat system to operate and when it becomes impossible to operate a threat system. Furthermore,  $\phi$  depicts the terrain slope angle. It should be noted that if the two parameters  $\Phi_{\text{low}}$  and  $\Phi_{\text{high}}$  are set to be equal, the slope coefficient  $C_{\text{slope}}$  becomes a binary variable and evaluates to either 1 or 0.

Next, the terrain slope angle is calculated. As the digital elevation model used in the spatial prediction model is in raster form, i.e., the data consists of pixels of size  $d \times d$ , the terrain slope angle is calculated for each pixel separately. To do this, many known algorithms exist [19]. In the spatial prediction model, the method introduced by Fleming and Hoffer [15] and further developed by Ritter [30] is used. In this method, the terrain slope angle is calculated with each pixel's normal vector, which in turn is calculated with the elevation values of the pixel's four immediately adjacent pixels. The vectors are defined to be 3-dimensional and vector  $\mathbf{r}$  is represented by the triplet  $(i, j, k)$ , where  $i$  is the displacement in  $x$ -coordinates,  $j$  is the change in  $y$ -coordinates, and  $k$  represents the change in elevation. The pixel of interest's neighboring pixels are indexed beginning from the pixel's western neighbor and continuing clockwise  $P_1, P_2, P_3$  and  $P_4$  with elevations  $e_1, e_2, e_3$  and  $e_4$ , respectively.

The vectors that run through the pixel in the direction of  $x$ -axis and  $y$ -axis are

defined:

$$\mathbf{r}_x = (2d, 0, e_3 - e_1),$$

$$\mathbf{r}_y = (0, 2d, e_2 - e_4),$$

where  $d$  represents the width of one pixel. By taking the cross product of these two vectors, a vector which is perpendicular to both of these vectors and thus the normal vector of the pixel is obtained. That is

$$\begin{aligned} \mathbf{n} &= \mathbf{r}_x \times \mathbf{r}_y \\ &= (2d, 0, e_3 - e_1) \times (0, 2d, e_2 - e_4) \\ &= (-2d(e_3 - e_1), -2d(e_2 - e_4), 4d^2). \end{aligned}$$

The resulting normal vector is further simplified by dividing each term by  $2d$ , i.e.,

$$\mathbf{n} = (e_1 - e_3, e_4 - e_2, 2d).$$

To calculate the slope of the vector  $\mathbf{n}$ , the vector's horizontal and vertical components need to be differentiated. The vertical component is simply the third value of the triplet which represents the vector. The horizontal component, on the other hand, is the sum of the two first values. Only the length of the horizontal component is of interest. This is calculated with Pythagoras' theorem

$$|\mathbf{r}_h| = \sqrt{(e_1 - e_3)^2 + (e_4 - e_2)^2}.$$

Since the normal vector is perpendicular to the pixel of interest, the tangent of the pixel's slope angle is the multiplicative inverse of the normal vector's slope angle's tangent. Thus, the terrain slope angle is calculated with the inverse tangent function, i.e.,

$$\phi = \arctan \frac{\sqrt{(e_1 - e_3)^2 + (e_4 - e_2)^2}}{2d}.$$

# Appendix D

## Terrain coefficient ( $C_{\text{terrain}}$ )

The terrain coefficients used in example scenarios discussed in this thesis are listed in Table D.1.

Table D.1: The terrain coefficients ( $C_{\text{terrain}}$ ) which are used in the example scenarios.

<b>Description</b>	<b><math>C_{\text{terrain}}</math></b>
Continuous urban fabric	0.25
Discontinuous urban fabric	0.5
Industrial or commercial units	0.5
Road and rail networks and associated land	1
Port areas	0.75
Airports	1
Mineral extraction sites	0.0025
Cottage areas	0.125
Sport and leisure areas	0.125
Golf ranges	0.25
Track (horse racing)	0.25
Non-irrigated arable land (fields)	0.25
Non-irrigated arable land (other)	0.025
Pastures	0.125
Broad-leaved forest (mineral soil)	0.0125
Broad-leaved forest (peat soil)	0.005
Coniferous forest (mineral soil)	0.0125
Coniferous forest (peat soil)	0.005
Coniferous forest (rock)	0.005
Mixed forest (mineral soil)	0.0075
Mixed forest (peat soil)	0.005
Mixed forest (rock)	0.0025
Transitional woodland shrub (canopy cover < 10%)	0.025
Transitional woodland shrub (canopy cover 10-30%, mineral soil)	0.0125
Transitional woodland shrub (canopy cover 10-30%, peat soil)	0.005
Transitional woodland shrub (canopy cover 10-30%, rock)	0.0075
Transitional woodland shrub (disused agricultural land)	0.025
Beaches, dunes, sands	0.125
Bare rocks	0.025
Wetlands	0
Water bodies	0